

UNIVERSITY OF PADOVA  
Department of Industrial Engineering  
Doctoral Program in Industrial Engineering  
Curriculum: Electrical Engineering  
Cohort XXXVI

FEASIBILITY STUDY OF  
ELECTRIC DRIVES FOR AGRICULTURAL TRACTORS  
AND NUMERICAL TECHNIQUES  
FOR ELECTRIC MACHINE DESIGN.

Thesis for the degree of Doctor of Philosophy

Prof. Giulio Rosati, Course Coordinator  
Prof. Luigi Alberti, Candidate's Supervisor

Ph.D. Candidate: ELIA SCOLARO

Padua  
November 28, 2023





*Est modus in rebus.*

— Orazio



## ABSTRACT

---

Today, agriculture industry has a significant impact in global greenhouse gas emissions. A large amount of pollutants come from diesel internal combustion engines, widely used in agricultural machinery. Therefore, emission regulations are becoming tighter worldwide. Since mechanization in agriculture is fundamental to achieve a proper food production for a growing human population, changes are needed in common agriculture engineering to develop new farming machinery that could outperform conventional ones in terms of environmental impact, performance, productivity and safety. Electrification is a feasible solution.

A comprehensive review about agricultural machinery electrification is reported, with a particular focus on hybrid electric tractors and their implements. The introduction of electric drives in farming tractors is discussed in detail by looking at the main findings in literature and considering state-of-the-art technology.

A methodology to evaluate the economic feasibility of farming tractor electrification is developed. The method is based on an energetic model, input data from field measurements and life cycle cost analysis. A study is conducted on three tractor categories, which differs by power ratings and operating cycles. A parallel hybrid electric architecture is considered, although the approach can be extended to other powertrain configurations.

Besides investigations on a system level, also the design of specific components is conducted. Numerical techniques and fast simulation approaches are important for an effective design stage and to reduce R&D cost and time to market. The potentialities of harmonic balance method are investigated in simulating a basic electric generator front-end for a high-voltage automotive system. The case study comprises a six-pole three-phase surface-mounted permanent magnet generator connected to a six-pulse full-wave diode bridge rectifier. Simulations are performed at fixed generator speed in two operating cases: with an open-circuit DC bus and supplying a load resistance. Both main-stream time stepping and harmonic balance approaches are deeply discussed focusing on the model under study, along with relevant implementation details. Simulation results are commented in the end, together with an evaluation of computational performance.

The complete list of publications related to this dissertation is reported at the end.



# CONTENTS

---

<b>1</b>	<b>Introduction</b>	<b>1</b>
<b>2</b>	<b>Technology review</b>	<b>5</b>
2.1	Conventional powertrains . . . . .	5
2.1.1	Transmissions . . . . .	7
2.1.2	Diesel engine and auxiliaries . . . . .	8
2.1.3	Engine starting and electric system . . . . .	9
2.1.4	Hydraulic system . . . . .	10
2.2	Auxiliaries electrification . . . . .	11
2.3	Waste heat recovery . . . . .	12
2.4	Powertrain electrification . . . . .	14
2.4.1	Hybrid electric powertrains . . . . .	15
2.4.2	Full electric powertrains . . . . .	22
2.4.3	Industrial prototypes . . . . .	24
2.5	Implements electrification . . . . .	27
2.6	Main components for tractors electric drivetrains . . . . .	28
2.6.1	Energy storage systems . . . . .	28
2.6.2	Electric machines . . . . .	31
2.6.3	Power electronics converters . . . . .	33
<b>3</b>	<b>Life cycle cost analysis of hybrid electric tractors</b>	<b>35</b>
3.1	Conventional and hybrid electric powertrains under analysis .	35
3.2	Case studies and operating cycles . . . . .	36
3.3	System modeling . . . . .	39
3.3.1	Energy management strategy . . . . .	40
3.3.2	ICE and electric drive modeling . . . . .	40
3.3.3	Battery model . . . . .	42
3.3.4	Post processing stage . . . . .	43
3.4	Battery sizing and energy management tuning . . . . .	45
3.5	Life cycle cost analysis . . . . .	48
3.5.1	Powertrain components and energy pricing . . . . .	49
3.5.2	Powertrain components costs . . . . .	49
3.6	Results . . . . .	51
3.6.1	Main specifications and savings summary . . . . .	58
<b>4</b>	<b>Investigation on harmonic balance method</b>	<b>61</b>
4.1	Introduction . . . . .	61
4.2	Case study and modeling . . . . .	63
4.2.1	Non linearities . . . . .	67
4.2.2	2D AV formulation . . . . .	68
4.3	Methodology . . . . .	70

## CONTENTS

4.3.1	Time stepping approach . . . . .	70
4.3.2	Harmonic balance approach . . . . .	71
4.4	Numerical results . . . . .	73
4.5	Comments . . . . .	81
<b>5</b>	<b>Conclusions</b>	<b>83</b>
5.1	Key findings of the thesis . . . . .	83
5.2	Future developments . . . . .	84



## LIST OF FIGURES

---

2.1	Conventional powertrain of an agricultural tractor. . . . .	6
2.2	Hydrostatic transmissions. . . . .	7
2.3	Heavy-duty diesel engine with auxiliaries. . . . .	9
2.4	Conventional on-board electric system of agricultural tractors. . . . .	10
2.5	Example of on-board hydraulic system in agricultural tractors. . . . .	11
2.6	Waste heat recovery from engine exhaust gas. . . . .	13
2.7	Examples of tractors with series hybrid electric powertrains. . . . .	17
2.8	Example of a tractor with parallel hybrid electric powertrain. . . . .	21
2.9	Example of a tractor with power split hybrid electric powertrain. . . . .	22
2.10	Example of powertrain of a fuel cell electric tractor. . . . .	24
2.11	Ragone charts. . . . .	29
2.12	Example of overload ratings of different electric machines. . . . .	33
3.1	Outline of reference conventional powertrain. . . . .	36
3.2	Outline of reference parallel hybrid electric powertrain. . . . .	36
3.3	Load distribution in the three case studies. . . . .	38
3.4	Scheme of the hybrid tractor model for LCC evaluation. . . . .	39
3.5	Rule-based EMS in a demo operating cycle. Constant upper threshold torque limit is shown for sake of simplicity. . . . .	41
3.6	Battery capacity sizing iterative process. . . . .	45
3.7	EMS tuning: lower torque threshold $\mathcal{T}_{Lim}$ . . . . .	46
3.8	EMS tuning: upper torque threshold $\mathcal{T}_{Lim}$ . . . . .	46
3.9	Capex of hybrid electric specialized, row crop medium and heavy tractors. Percentage variations with regard to conventional counterparts are shown above bars. . . . .	52
3.10	LCC of hybrid electric specialized, row crop medium and heavy tractors. Percentage variations with regard to conventional counterparts are shown above bars. . . . .	55
3.11	Medium-duty row crop tractor: LCC variation with engine downsizing factor. . . . .	55
3.12	Heavy-duty row crop tractor: LCC variation with engine downsizing factor. . . . .	56
3.13	Payback time of specialized hybrid electric tractor as a function of ICE and battery price. . . . .	56
3.14	Payback time of row crop hybrid electric tractors as a function of ICE and battery price. . . . .	57
3.15	LCC behavior with varying diesel fuel price and fixed electric energy price (0.16 €/kWh). . . . .	57
3.16	LCC behavior with varying electric energy price and fixed diesel fuel price (0.9 €/L). . . . .	58

## LIST OF FIGURES

3.17	Total CO <sub>2</sub> emissions of hybrid electric specialized, row crop medium and heavy tractors. Percentage variations with regard to conventional counterparts are shown above bars. . . . .	58
4.1	2D finite-element model of the SPM generator. . . . .	65
4.2	Case study outline. . . . .	66
4.3	Modeling of non linearities. . . . .	67
4.4	Load AC phase current. . . . .	74
4.5	Load current through a diode. . . . .	75
4.6	Load voltage across a diode. . . . .	76
4.7	Load DC output current. . . . .	77
4.8	Open-circuit DC output voltage. . . . .	78
4.9	Graphical comparison between TS and HB computational performance on the case study under analysis. . . . .	80

## LIST OF TABLES

---

2.1	Classification of tractors with electrified powertrains . . . . .	14
2.2	Summary of electrified powertrains for agricultural tractors. . .	25
2.3	Prototypes of electrified tractors. . . . .	26
2.4	Prototypes of electrified implements. . . . .	27
3.1	Yearly time contribution and average power of each operation.	37
3.2	C-rate constraints. . . . .	43
3.3	Operating costs relative variation per cycle. . . . .	53
3.4	Fractions of useful work performed using electric energy. . .	54
3.5	Main electric specifications and summary of cost variations. .	59
4.1	SPM generator parameters and continuous ratings. . . . .	64
4.2	HB accuracy benchmarked with TS results. . . . .	79
4.3	TS and HB computational performance. . . . .	79



# 1 INTRODUCTION

---

Nowadays, agriculture is facing the transition to a new era. The welfare growth of countries has always benefit from the improvement of farming techniques. Yet, agriculture plays a key role now more than ever to feed a growing world population. Moreover, the adaptation to unusual harsher ambient conditions and extreme weather events needs to be addressed, as climate change is most likely unavoidable by now, and it has already begun to affect crop production significantly. Agriculture has longer been a human activity with an intimate contact with nature. Nevertheless, the responsibility of earth care has become of paramount importance today. A fundamental rethinking of the agricultural world is needed for a sustainable development of human kind. Path-breaking paradigms are gradually introducing changes in the conventional practices of farmers and stakeholders of agriculture industry.

Technology has longer been an enabling factor for the improvement of farming techniques. In particular, mechanization have dramatically increased crop productivity in the last century. Despite many new high-tech alternatives are emerging and old habits are being rediscovered, intensive field crop with agricultural machinery is still the mainstream farming practice world-wide. Nonetheless, today challenges are forcing changes also in conventional technologies and methods.

Agriculture sector is among the main contributors to global greenhouse gas emissions [1]. Although the larger part of this pollution is related to intensive animal farming and ground working [2], a considerable amount comes also from exhaust gas of diesel internal combustion engines (ICEs), which are the most widespread power sources in agriculture and forestry industry [3], both for moving self-propelled machinery and stationary standalone systems [4]. As a consequence, in Western countries, several regulators tightened the emissions limits of non-road mobile machinery (NRMM) [5, 6], to which agricultural vehicles belong. In order to meet new European Stage V and US Tier 4 standards [7], manufacturers are forced to equip the engines with additional exhaust gas aftertreatment devices. These components, in addition to an increased cost, make the diesel units bulkier, leading to a reduced power density. Whereas this issue may not be a major concern for high-power row crop vehicles, the design of narrow specialized tractors could become more challenging, due to stricter size constraints on the vehicle chassis.

Therefore, manufacturers are encouraging research on alternatives to powertrain architectures currently adopted in agricultural machinery. Among various proposals, one feasible solution is the electrification of conventional drivetrains, following the trend established in the automotive industry towards the development of hybrid electric and full-electric on-road vehicles [8].

## 1. INTRODUCTION

In recent years, electrification of agricultural machinery has gained attention from both industry and academia. Manufacturers are striving to maintain competitiveness while complying with emission regulations, which are becoming more and more tight. Thus, electrification is perceived as a promising path to improve energy and operational efficiency at the same time [9]. Indeed, the introduction of more electric drives in agricultural machinery has the potentialities to significantly reduce fuel consumption and increase performance, enabling new functionalities [10]. Nevertheless, it is still debated how to effectively exploit the advantages of electric drives in agriculture mechanization, in particular inside tractor drivetrains among other agricultural vehicles.

Tractor manufacturers are currently borrowing know-how and technologies from automotive companies, exploiting the experience in electrification of commercial vehicles and construction machinery. However, farming tractors have many peculiarities that distinguish them both from commercial on-road vehicles, as haul trucks, and other NRMM, as construction loaders, and make their electrification more challenging. Differently from road vehicles, traction effort is only a limited part of tractors workload. Agriculture operations often require the use of various external implements that may need to be supplied by tractor engine: power can be provided through mechanical power take offs (PTOs) or by means of hydraulic interfaces, in form of pressurized oil. Yet, the differences with road vehicles are not limited to additional main loads. Traction power demand is peculiar too: long periods at high torque and low speed during field operations are combined with shorter transportation tasks at lower torque and higher speed. Furthermore, traction effort of field operations has a wide variability because of unpaved soil conditions and implement towing requirements.

In terms of powertrain architecture, agricultural tractors have some similarities with other NRMM. However, the versatility of tractors distinguishes them from all other working vehicles. Indeed, agricultural machinery cover a wide power range, from a few tens of kW for small utility vehicles to more than 400 kW in case of row crop tractors. Moreover, the conventional powertrain presents a relevant amount of different arrangements, especially because of different ground drive transmissions.

Nevertheless, the main issue in tractor electrification is the lack of standard duty cycles. The identification of representative power demand profiles is not as easy as for road vehicles or other NRMM, because of the great variety of agricultural tasks. Thus, the assessment of new solutions and the choice of proper specifications are not straightforward.

Hybrid electric architectures seem the most promising solutions for an effective introduction of electric drives in agricultural tractors on a mid-term perspective [11]. Implements electrification is also perceived as a feasible path, with a focus on improved field efficiency, performance and new functionalities along with precision agriculture principles [12]. The availability of an electric

power take off (ePTO) and an increased automation are key enabling factor for implements electrification.

Despite the growing interest in this topic, electrification of agricultural machinery is still on a research stage. Feasibility evaluations and comparisons of hybrid electric drivetrains for agricultural tractors are based on few specific cases, missing generality purposes. Moreover, methodologies for the design of the main electrical components are also not well established. Most of the time, variable speed electric drives require the coupling of an electric machine and a power converter. Detailed simulations of drives steady-state behavior are conventionally carried out with time stepping (TS) numerical techniques. However, the computational time may be prohibitive, especially for systems with a relatively slow dynamic, as time stepping approach needs to go throughout all the initial transient. Thus, there is interest in faster numerical methods to reduce product development time, in particular for parametric sweep analyses and optimization processes. Harmonic Balance is a promising approach to simulate non-linear systems at steady state.

The main goal of this research is the proposal and validation of methods to design electric drives for agricultural machinery. This work aims at investigating the potentialities of electric drives in agriculture applications, with a particular focus on the development of hybrid electric farming tractors. This research has been developed in the frame of project PRIN “*Green SEED: Design of more electric tractors for a more sustainable agriculture*”, funded by the Italian Ministry of University and Research.

Field measurements and raw input data used in this thesis were collected at University of Bologna, thanks to the work of Prof. Michele Mattetti and his research group. Collaborations with researchers from University of Bolzano and University of Modena and Reggio Emilia were significant too. Moreover, insights on advanced simulation techniques for electric machines coupled with power converters have been investigated during a period abroad at Université Libre de Bruxelles, under the co-supervision of Prof. Johan Gyselinck and with the relevant participation of Prof. Ruth V. Sabariego of KU Leuven.

After a comprehensive review on tractor technology and powertrain electrification, a method to evaluate the feasibility of hybrid electric tractors based on life cycle cost is presented. Results are provided through simulations of three case studies. Then, harmonic balance and time-stepping approaches are compared in terms of results and computational performance in the simulation of a benchmark application, which features a three-phase permanent magnet generator connected to a full-bridge diode rectifier, the most simple configuration for the input generation set of an electromechanical continuously variable transmission in a hybrid electric drivetrain.

This dissertation is structured as follows: Chapter 2 reviews agricultural tractor technology and powertrain electrification; Chapter 3 presents a feasibility analysis of hybrid electric tractors based on life cycle cost; Chapter 4

## 1. INTRODUCTION

investigates harmonic balance numerical method applied to an electric generation set; in Chapter 5, the conclusions of this thesis are finally discussed.



## 2 TECHNOLOGY REVIEW

---

This chapter summarizes state-of-the-art technology in conventional powertrains of agricultural tractors and reviews up-to-date literature on the introduction of more electric drives in off-road heavy-duty vehicles, with a particular focus on agricultural machinery [13].

Feasible solutions for the electrification of auxiliaries, main drivetrains and implements are presented, highlighting potential advantages and drawbacks. Suitable energy management strategies are described for some of the electrified concepts, and their potentialities in agriculture operations are discussed. Low-level controls of electric drives and power converters are also mentioned, showing how they contribute to an effective operation of the entire system. Promising technologies are investigated for the main hardware components of electrified powertrains, namely energy storage devices, electric machines and power electronic converters, along with their most important features and design specifications [14]. Innovative proposals and prototypes both from academy and industry are considered.

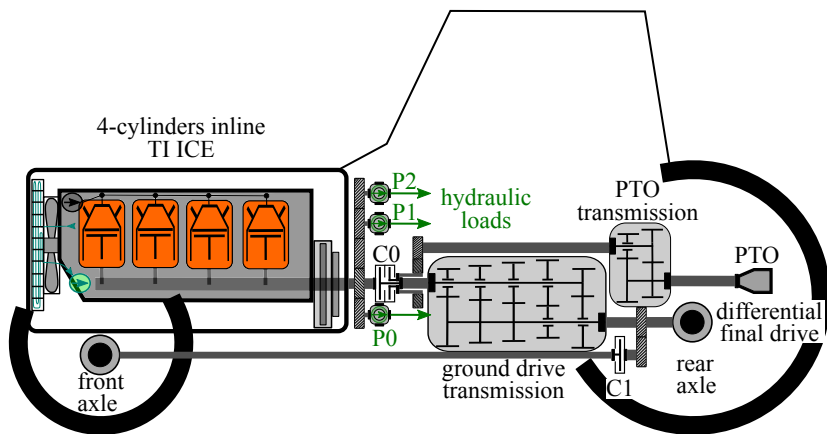
### 2.1 Conventional powertrains

The conventional powertrain of an agricultural tractor is outlined in Fig. 2.1. The only power source is a diesel turbocharged-intercooled (TI) internal combustion engine (ICE), which gradually burns the diesel fuel stored in an on-board tank (not shown). The chemical energy of fuel is firstly converted into thermal energy by a controlled combustion inside the cylinders, and then into mechanical rotation through pistons and crankshaft mechanism.

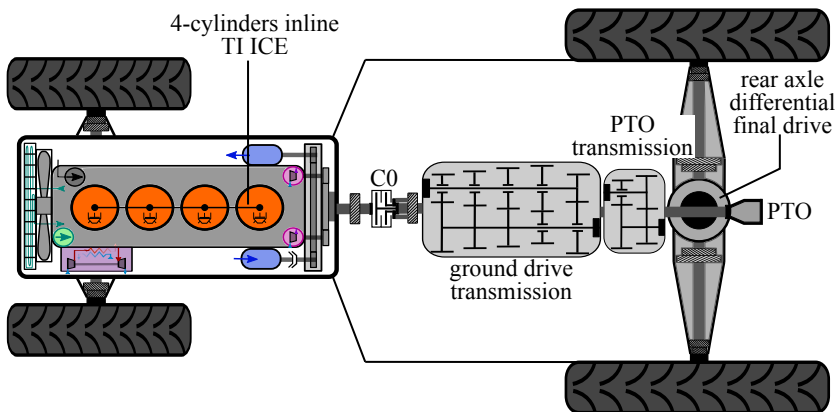
All the main loads are mechanically driven by the engine, as shown in Fig. 2.1a. The pumps P0-P2 are connected to engine shaft through speed reducer gearsets. The speed reduction ratios are usually equal to 1 or slightly different, with pumps rotating at the same engine speed or a bit faster, respectively. Pumps maintain rated pressure levels in on-board hydraulic circuits and supply hydraulic actuators with the needed flow rate of pressurized oil. A double clutch C0 allows an independent engagement of ground drive transmission and rear mechanical power take off (PTO): ground drive is engaged when the left side of C0 is closed, whereas the rear PTO engagement depends on the right side of C0. Thanks to this arrangement, the PTO can be operated even when the tractor is still, and conversely the tractor can move even with a still PTO. PTO transmission reduces input shaft speed (i.e. engine speed) to meet output standardized rated speed values, namely 540, 750 and 1000 rpm. Agricultural machinery industry has long adopted these values as reference to achieve an excellent trade-off between implements performance and fuel economy. These values are not to be intended as fixed steady states

## 2. TECHNOLOGY REVIEW

for the PTO, whose rotation is still constrained to ICE shaft, but they offer a standard for the reduction ratios of PTO transmission gearset. The ground drive transmission adapts the mechanical characteristic of the engine to torque and speed requirements of traction effort. Differently from PTO transmission, standard output speed values are impossible to define in this case due to the great variability of traction load. Transmission output shaft is connected to the rear transaxle, that integrates both differential and final drive, as shown in Fig. 2.1b. A single clutch C1 allows the mechanical engagement of the front axle for a four wheel drive configuration at the need. This solution, known as mechanical front wheel drive (MFWD), is currently the most implemented in agricultural tractors, thanks to its versatility in switching between two rear wheel drive (2WD) and four wheel drive (4WD) configurations. Moreover, the 4WD arrangement is possible even with smaller front wheels.



(a) Lateral view section.



(b) Top view section.

Figure 2.1: Conventional powertrain of an agricultural tractor.

### 2.1.1 Transmissions

Since agricultural tractors come in a great variety of layouts, the powertrain in Fig. 2.1 has many conventional variants. In particular, the clutch C1 and the MFWD connection are absent in 2WD architectures and in isodiametric 4WD tractors. Nowadays, the former configuration is implemented only in low power and low-tech machinery, i.e. below 50 kW (70 hp), while the latter is a well-known high-performance solution for specialized vehicles and high-power row crop machinery. However, isodiametric configuration is not so common, due to its mechanical complexity.

The ground drive transmission exhibits an even greater variability, due to its key role in the whole drivetrain: indeed, both tractor performance and fuel economy strongly depend on transmission features. Stepped geared transmissions are the most widespread in the whole power range of agricultural machinery, with both hydraulic-actuated automatic and power shifting widely exploited above 150 kW (200 hp). Many different arrangements can be adopted, the number of gears ranging from a minimum of 10 to a maximum of 40, considering both forward and reverse.

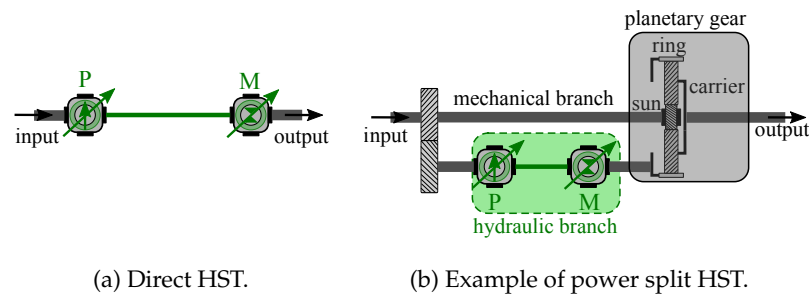


Figure 2.2: Hydrostatic transmissions.

Continuously variable transmissions (CVTs) are used almost exclusively in medium-to-high power high-tech tractors, i.e. above 150 kW, due to cost-related reasons. Among them, hydrostatic transmissions (HSTs) are the state-of-the-art architectures, both in direct and power split configurations [15]. HSTs are outlined in Fig. 2.2. In a direct HST (Fig. 2.2a), the input shaft drives a variable-displacement pump (P), which supplies a variable-displacement hydraulic actuator (M), that finally powers the output shaft. Since the oil flow rate in the circuit can be controlled according to pressure drop, the output shaft speed can be continuously regulated whatever the input shaft speed, in the entire operating range of the transmission. In a power split HST (Fig. 2.2b), the power path is divided between a mechanical and a hydraulic branch, thanks to the use of a planetary gear. This configuration has the advantage of requiring smaller pumps and motors, as they are sized only for a part of the entire power, while maintaining the continuous speed regulation of a CVT

## 2. TECHNOLOGY REVIEW

solution. Different power split layouts can be arranged depending on how the mechanical and hydraulic branches are connected to the planetary gear parts, i.e. sun, planets carrier and ring, and on how many planetary gears are used. Every ground drive CVT decouples wheel speed both from engine and PTO speed.

The PTO transmission is far more standardized than ground drive transmission, thanks to widely adopted reference speed values. Usually, it consists of a two-speed stepped gearbox with manual shifting, that allows two speed range, one with a 540 rpm reference (PTO 540), and the other with a 1000 rpm reference (PTO 1000). In many high-power tractors, an additional gear shift makes available a third speed range around the standard 750 rpm. This arrangement is called PTO 750 or PTO ECO mode, as it is specifically designed to improve fuel economy. Sometimes, a single-speed front PTO is also available, provided that the engine has a proper front mechanical connection.

### 2.1.2 Diesel engine and auxiliaries

Diesel units of off-road vehicles are also quite standardized. Fig. 2.3 shows a schematic outline of a heavy-duty diesel engine suitable for agriculture applications (Fig. 2.3a), and the front and render view of the unit (Fig. 2.3b), with highlighted auxiliary components.

Turbocharging is common practice in this type of engines, as it allows a higher torque output: air is drawn and compressed by a charging compressor (CC); since the compressed air is too hot for an efficient combustion, it is cooled by a heat exchanger, called intercooler (IC); the compressor is driven by a charge turbine (CT) that processes exhaust gas coming from the cylinders. The fuel injection system comprises a fuel pump (FP) and a common rail device for a calibrated fuel dosing.

Both forced air and liquid cooling are exploited to dissipate exhaust heat and maintain the engine at working temperature. The cooling system includes a coolant pump (CP), a radiator and a fan. Pumps and fan are mechanically driven by engine shaft. A flywheel dampens crankshaft oscillation, producing a smoother torque output. Moreover, it mechanically links the engine shaft with the brake compressor (BC) and the compressor for heating, ventilation and air conditioning (HVAC) of the cabin. Alternator (ALT) and starting group, comprising a motor (START) and a solenoid electromechanical actuator (S), complete engine auxiliaries.

Since the enforcement of tighter emission regulations, additional aftertreatment devices have become unavoidable in diesel engines of off-road machinery above 56 kW. These components are usually placed before the exhaust gas outlet and they filter pollutants by various mechanical and chemical actions. Selective catalytic reducers, diesel particulate filters and fluid tanks are commonly used for this purpose. Aftertreatment devices are not reported in

Fig. 2.3, although they have a relevant impact on engine overall displacement and weight.

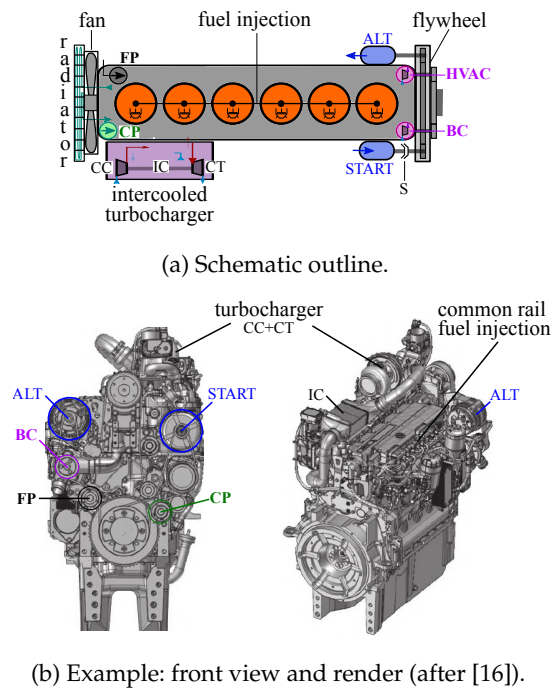


Figure 2.3: Heavy-duty diesel engine with auxiliaries.

### 2.1.3 Engine starting and electric system

It is well known that ICEs do not start on their own. Heavy-duty diesel engines for agricultural tractors take advantage of electric starting: the starter group comprises a naturally air cooled DC motor (START) and a solenoid (S), that electromechanically engages ICE shaft when subjected to a current flow. Cold cranking current ranges between 300 and 2500 A, depending on ICE displacement. The starter motor is designed to work intermittently in extreme overload conditions, in order to minimize its size and weight. Reduction gear starters further increase power density, when compared to direct drive solutions.

The battery must be designed to sustain the required cranking current just for tens of second without a complete discharge. Lead acid batteries are the standard choice, as in the majority of automotive applications. Besides the starting systems, the battery needs to supply all the low-voltage electric loads, such as lights, cabin ventilation, electronic boards, automatic shifting mechanisms. The battery is charged exclusively by the alternator (ALT), which is driven by ICE shaft. The alternator is commonly a single-phase or three-phase wound-field salient-pole synchronous generator. The machine is self

## 2. TECHNOLOGY REVIEW

ventilated and designed to keep a fixed output voltage continuously at a variable speed.

AC-DC power conversion is performed by a diode rectifier: both half and full bridge configurations can be exploited. The system can be rated at 12 or 24 V, even though the actual voltage can vary of  $\pm 10\%$  due to the switching on and off of the alternator. It is worthwhile to notice that the voltage regulation of the system entirely relies on the excitation control of the alternator, as no other active power components are used in the system. The on-board electric system of a conventional agricultural tractor is shown in Fig. 2.4.

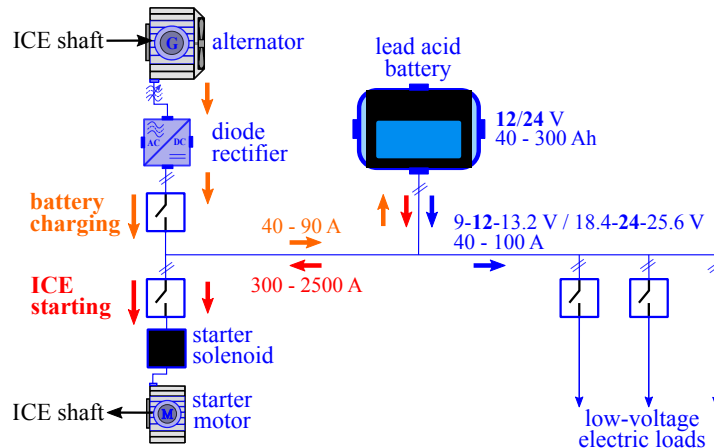


Figure 2.4: Conventional on-board electric system of agricultural tractors.

### 2.1.4 Hydraulic system

Last but not least, hydraulic systems come in a great variety of layouts in agricultural tractors. An example is shown in Fig. 2.5, where three separate circuits are used to supply loads on implements, hydraulic motors (HM1-HM2) of front and rear hitch lifters and front loaders (when present), power steering and transmission. Hydraulic actuators on implements can be supplied in two ways:

- through a selective valve distributor placed on the back of the tractor, to control the oil flow rate when there are no valves on the implement;
- in power beyond mode, bypassing the distributor, when dedicated flow rate control devices are present on the implement.

Pressure values range from 140 to 200 bar while typical flow rates are in between 40 and 160 L min<sup>-1</sup>. Axial-pistons swash plate variable-displacement pumps with bent axis can be used instead of fixed-displacement gear units to reduce hydraulic losses, together with pressure control and load sensing systems.

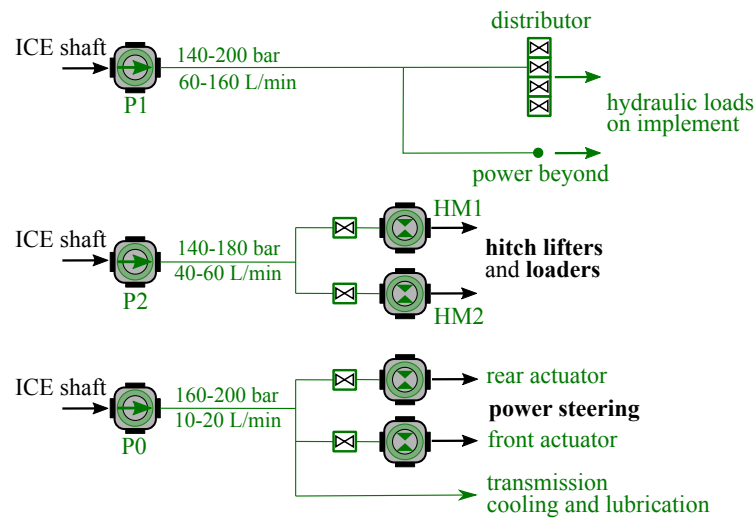


Figure 2.5: Example of on-board hydraulic system in agricultural tractors.

## 2.2 Auxiliaries electrification

A first step in tractors electrification is the introduction of electrically-driven engine auxiliaries, namely radiator fan, coolant pump, HVAC and brake compressor. In conventional layouts, ICE auxiliaries require up to 35 % and 25 % of engine power when the tractor is idling and operating on field, respectively [17]. If auxiliaries are driven by electric motors, the alternator must be resized to supply the increased electric load. Electrically-driven auxiliaries can be switched on and off at the need, and their speed can be controlled independently from ICE speed. This easier and less constrained control, if it is well exploited, can compensate the losses arising from the double energy conversion, i.e. from mechanical to electrical (alternator) and then back to mechanical (auxiliary electric drive), finally improving fuel economy. An average 5 % reduction in fuel consumption and a 4 % increase of engine net torque are expected by adopting only an electrically-driven radiator fan [18].

Moreover, the decoupling of each auxiliary from shaft speed, in addition to efficiency improvements, enables new functionalities. As instance, an independent fan can produce a higher air flow when ICE works at high load and low speed, improving cooling, and a lower air flow when ICE operates in low-load high-speed conditions, reducing fuel consumption [19]. Furthermore, fan rotation can be easily reversed to clean the radiator [20]. Some of these functionalities can be achieved even with engine-driven cooling fans, but in this case the use of variable pitch fans or variable speed transmissions is needed, thus increasing machine overall dimensions, mechanical complexity and maintenance requirements.

Temperature control and cooling performance can be further improved

## 2. TECHNOLOGY REVIEW

with an electrically-driven coolant pump, which can provide a flow rate for some minutes after ICE shutdown, avoiding over-temperatures both in the engine block and turbocharger [21, 22]. In addition, high reference working temperatures are possible, with a consequent increase of ICE efficiency.

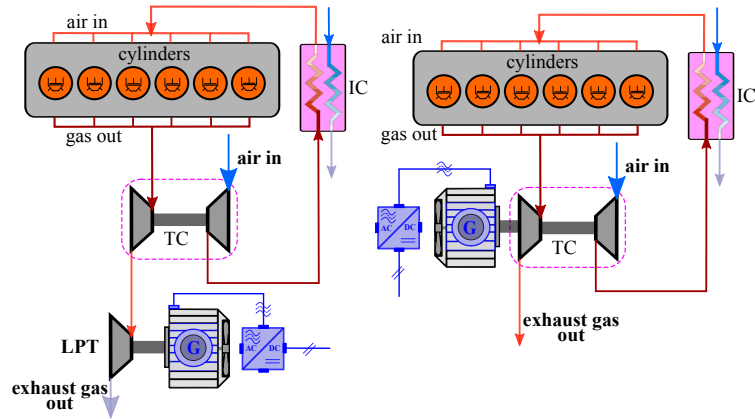
Farming tractors manufacturers early moved to electrify ICE auxiliaries. Two tractors with electrically-driven auxiliaries were launched by John Deere in 2007: the 7430 and 7530 E-Premium [23]. The standard 2.4 kW alternator was replaced by a 20 kW machine integrated in engine flywheel. The new generator was able to supply several auxiliaries driven by electric motors, such as brake compressor, radiator fan, coolant pump and HVAC compressor, allowing maximum cabin cooling even with ICE at idle. In the 7530 E-Premium, as a further upgrade, an on-board AC power socket was also included to supply external portable working equipment, such as welding, drilling and cutting tools, at a line-to-line rated voltage of 380 V (both one-phase and three-phase supply available), and up to 5 kW power. This AC socket was the first example of electric PTO (e-PTO) ever implemented in a tractor. According to a tests on the 7530 conventional and electrified variants, a 4 % and 16 % fuel consumption reduction was achieved, respectively in harrowing and road transport tasks. Nevertheless, the electrified versions were discontinued, perhaps due to an unsuccessful market demand.

### 2.3 Waste heat recovery

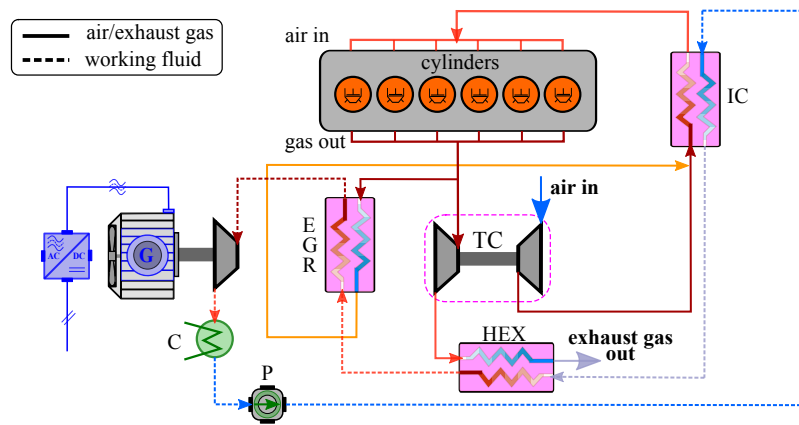
Waste heat recovery can potentially increase efficiency up to 55 % in high-power heavy-duty diesel engines above 200 kW (270 hp), leading to significant reduction in specific fuel consumption (SFC). In recent years, exhaust gas energy recovery has been the topic of several studies, although few of them have investigated applications in agricultural machinery [24]. Despite the focus have been mainly on long-range trucks [25], power plants and marine generation sets [26], the outcomes of these studies can be extended also to off-road vehicles in general, and to agricultural machinery in particular.

Fig. 2.6 shows the three most promising systems that have been proposed to harness energy from exhaust gas of heavy-duty diesel engines: a low pressure turbine (LPT) after the turbocharger [27]; electric turbocompounding [28]; steam or organic Rankine cycle (ORC). The harvested power can be used to drive an electric generator (G) or can be fed to the crankshaft through a gear train, with the former case being relevant for auxiliaries and powertrain electrification. LPT system shown in Fig. 2.6a provides the higher potentialities: if properly sized, it can harness up to 10 % of net output power at medium-to-high speed and high load, and up to 6 % at low speed and partial load, leading to 5 - 8 % reduction of SFC. However, this system is sensitive to LPT sizing, which must be properly performed to avoid undesired back-pressure. Electric turbocompounding consists in a generator driven by the turbine of the





(a) Generator on low pressure turbine. (b) Generator on turbocharger.



(c) Rankine cycle.

Figure 2.6: Waste heat recovery from engine exhaust gas.

turbocharger group, as outlined in Fig. 2.6b. Since no additional turbines or heat exchangers are needed, electric turbocompounding is the most compact layout for energy harvesting. Furthermore, the high speed of the turbocharger leads to a more compact design of the generator. However, the performance are lower than LPT both in terms of recovered power and SFC reduction, as gas expansion in the turbine takes place in a single stage and the pressure cannot be too high, in order to avoid excessive back-pressure. Moreover, generator design is not straightforward, because the turbocharger speed is far beyond the common range for electric machines, i.e. up to 250 krpm. Steam and organic Rankine cycles recover even lower amount of power, although they allow a higher SFC reduction than LPT at high speed and high load, the best performance obtained with organic fluids (ORC). Besides, system weight and volume are considerably higher than both turbocompounding and LPT, because many additional components are needed, namely a condenser

## 2. TECHNOLOGY REVIEW

(C), a pump (P), an exhaust gas heat exchanger (HEX) and an exhaust gas recirculation cooler (EGR). Rankine cycle system is depicted in Fig. 2.6c. Air-Brayton cycles have also been investigated. However, their performance do not compete with none of the previous solutions, as the charging compressor is shared with the engine, thus limiting the mass flow rate.

From the reviewed literature, it emerges that in all the proposed systems the higher the speed and the engine load, the higher the percentage of recovered power and the SFC reduction. In conclusion, in heavy-duty off-highway vehicles with engine power above 150 kW (200 hp), once a DC bus is available, it could be worthwhile to recover waste heat from the exhaust gases [29]. This power range corresponds to row crop tractors and combines, which usually do not perform as many low-power duties as specialized tractors (for example precision operations in vineyards, as shoot tipping). Thus, a high amount of exhaust energy is often available, and it could be beneficial to adopt some sort of waste heat recovery.

Thermoelectric generators based on Seebeck effect have also been proposed for engines waste heat recovery. However, they are currently not attractive for automotive applications due to relatively low efficiency and high cost. Nevertheless, research on these devices is still pursued by companies and universities.

### 2.4 Powertrain electrification

Table 2.1: Classification of tractors with electrified powertrains

Hybrid electric tractors (HETs)	Full electric tractors
Series (direct e-CVTs)	Battery electric tractors (BETs)
Parallel	Fuel cell electric tractors (FCETs)
Power split (e-CVTs)	

Powertrain electrification regards the introduction of electric drives in the specific drivetrains of the main loads of a vehicle. Main loads refer to machinery primary tasks. In the case of agricultural tractors, main loads do not comprise only the traction effort, as it happens in on-road vehicles, but they include also mechanical PTOs, hydraulic remotes on implements and hydraulic actuators of hitch lifters and loaders. On the contrary, the driving systems, such as steering and braking actuators, engine auxiliaries, cabin cooling and air conditioning, and all the other systems that are functional to driver comfort and vehicle driveability are not considered as main loads, even though some of them may have a relevant power demand.

Tab. 2.1 reports the classification adopted hereafter for farming tractors with electrified powertrains. Powertrain electrification can result in hybrid

electric architectures or full electric drivetrains [30]. In the former the ICE is still the main power source, whereas in the latter the whole vehicle is powered by electric sources.

In both solutions, high-voltage systems are exploited to achieve competitive performance in comparison with conventional powertrains. In automotive electric power systems, the term *high voltage* indicates a DC bus rated voltage higher than 60 V. Below this threshold, the systems are classified as *low voltage*. In vehicles, standard low-voltage levels are 12, 24 and 48 V, because these values can be easily obtained with lead acid batteries. On the contrary, standard high-voltage levels have not been defined yet, even for on-road vehicles, due to the great flexibility of lithium-ion (Li-ion) modules in terms of electrical specifications, and thanks to the versatility of power converters in regulating voltage. It is worthwhile to mention that in most of the hybrid and full electric vehicles a low-voltage system is still present, together with a high-voltage part. Usually, the two voltage levels are insulated between each other and two different batteries are used.

In addition to low-level controls of power converters and drives, electrified powertrains need suitable high-level energy management strategies (EMSs), that coordinate the working set points of the main drives and converters to obtain an effective and efficient operation of the overall system. EMSs are usually programmed in on-board CPUs that supervises power converter microcontrollers through CAN-bus standard communication protocols. ICE CPU is also networked together with the other controllers.

Powertrain electrification of road vehicles, passenger cars in particular, is commonly quantified looking at the so-called degree of hybridization (DoH), also known as hybridization factor ( $H$ ) [31]. In non-road mobile machinery (NRMM), the definition of this index is modified to account for the additional main tasks of these vehicles [32]. DoH of NRMM is defined as follows:

$$H = \frac{1}{2} \left( \frac{P_{eT}}{P_{eT} + P_{ICE}} + \frac{P_{eL}}{P_{eL} + P_{ICE}} \right) ; \quad (2.1)$$

where  $P_{ICE}$  is the rated engine power, while  $P_{eT}$  is the maximum power of electric motors in the traction drive and  $P_{eL}$  is the maximum power of e-PTO and electrically-driven main loads. The definition is the arithmetic mean between the hybridization factor of traction drivetrain and the DoH of PTO and hydraulic powertrains. From (2.1), it derives that conventional powertrains have DoH equal to 0, while  $H$  is equal to 1 for full electric powertrains, and hybrid electric architectures lay in between.

### 2.4.1 Hybrid electric powertrains

Hybrid electric tractors (HETs) are currently the most promising and feasible solution toward more electric agricultural machinery, in particular for high-

## 2. TECHNOLOGY REVIEW

power row crop vehicles. HETs can be classified into three basic architectures, also called power flow topologies: series, parallel and power split. In all these configurations, a diesel engine remains the primary power source.

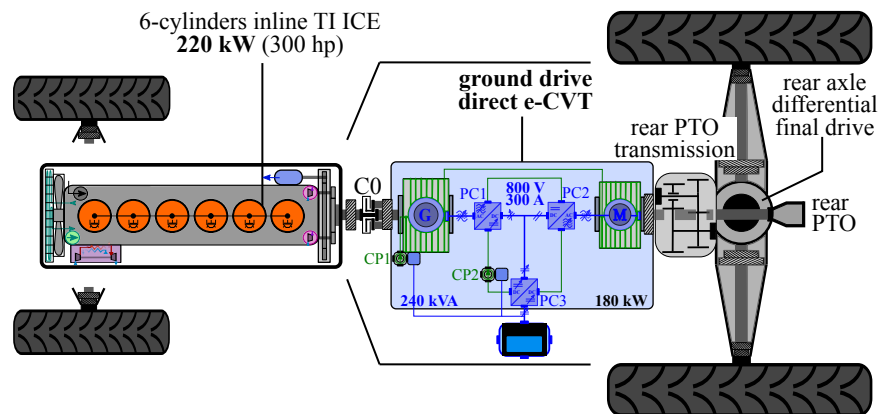
Series and power split topologies result in electromechanical continuously variable transmissions (e-CVTs). The operating principles are similar to HSTs presented in Section 2.1.1: hydraulic branches are substituted by high-voltage electric systems with a common DC bus, while hydraulic pumps and actuators are replaced by electric generators and motors, respectively. Additional electric storage devices are not mandatory, although their use increase e-CVTs performance significantly. Storage systems help in regulating DC bus voltage through DC-DC bidirectional converters by supplying or absorbing power during fast transients and peak demands. Both lead acid and lithium-based battery technologies or supercapacitor banks are suitable for this power buffering task. When storage devices are absent or they perform only power buffering, the hybrid powertrain works in the so-called diesel electric mode. In this modality, the storage device can be recharged only by ICE surplus power or regenerative braking. However, storage devices can be sized to achieve also a full electric driving mode during low-power operations, and plug-in designs can be implemented to allow recharging from an external power supply. As a consequence, more degrees of freedom are available in energy management strategy, leading to further potential reductions of fuel consumption.

These solutions are almost mandatory in parallel topologies, where ICE and electric drives power outputs are summed together. Indeed, in these architectures diesel electric mode is not feasible, as there are no e-CVTs. Thus, batteries have a key role in the operation of these powertrains and lithium-based technologies are currently the best choices. Moreover, plug-in layouts are of primary importance, since battery charging by ICE surplus power should be limited due to efficiency reasons and regenerative braking has been proved to be insufficient in agricultural field operations, due to very low speed and viscous soil.

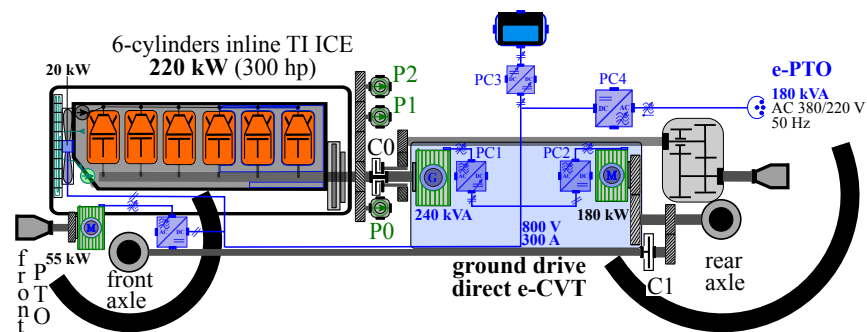
### **Series architectures**

Fig. 2.7 shows two examples of series hybrid electric powertrains proposed for row crop tractors. Minsk Tractor Works presented these concepts in 2009 with its 300 hp Belarus 3023 prototype [33].

Fig. 2.7a outlines the basic configuration, where the conventional ground drive stepped transmission is replaced by a direct e-CVT. In this layout, only traction is electrified, while all the other main loads are still driven by engine shaft, as in conventional powertrain. The direct e-CVT features two three-phase liquid-cooled double-cage induction machines: a 240 kVA machine working mainly as a generator (G) and a 180 kW traction motor (M). G supplies a 800 V-rated DC bus through a full-bridge 6-pulse active rectifier (PC1),



(a) Ground drive direct e-CVT.



(b) Ground drive e-CVT, e-PTO, electrically-driven front PTO and engine fan.

Figure 2.7: Examples of tractors with series hybrid electric powertrains.

which regulates DC bus voltage and power factor on generator AC side at the same time. The traction inverter (PC2) converts high-voltage DC power into AC regulated power, modulating both frequency and amplitude of voltage waveforms according to traction needs. The e-CVT works in diesel electric mode. A lead acid battery is connected to the high-voltage DC bus through a bidirectional DC-DC power converter (PC3), which regulates battery current during power buffering. PC3 has an isolated resonant topology to meet the particular requirements of this application. The battery supplies also the two low-voltage electrically-driven coolant pumps (CP1 and CP2), responsible of electric machines and power converters cooling. Moreover, the same battery is used for engine starting. Thus, PC3 must sustain also the cold cranking current. Since double-cage induction machines cannot be directly started as generators, G is used also as starting motor for ICE cranking, with PC1 operating as inverter. It is worthwhile to notice that engine alternator still supplies the conventional low-voltage system of the vehicle, whereas the starter motor is no more needed.

## 2. TECHNOLOGY REVIEW

An upgraded configuration is shown in Fig. 2.7b. The high-voltage DC bus now supplies also a 55 kW front PTO and a 20 kW engine fan, both electrically-driven by liquid-cooled squirrel-cage induction motors. Moreover, the tractor is equipped with a 180 kVA power socket (e-PTO) at standard 50 Hz three-phase or single-phase industrial low voltage (380 V line-to-line, 220 V line-to-neutral). The output voltage is regulated by an inverter (PC4) with an isolated topology.

In series architectures, engine speed is decoupled from electrified loads. Furthermore, electrified loads are also decoupled from each other and from conventional drivetrains. Thus, even without power buffering and neglecting speed constraints given by non electrified drivetrains, the energy management control can operate ICE along its optimal consumption line at given power, i.e. those speed values that minimize specific fuel consumption at given power output [34]. In practice, EMS sets the engine speed that minimizes fuel consumption at the required load power, considering also speed dynamic change. As a consequence, engine speed is usually kept constant most of the time, to avoid fuel consumption arising from transient dynamics during speed variations. The adoption of storage devices properly sized allows a further improvement of fuel economy. Indeed, a finely-tuned power buffering can maintain ICE always close to its optimum operating point [35]. When using large-capacity lithium-based batteries, series architectures can go beyond diesel electric mode. In these cases, the battery can supply all the electrified loads and ICE can be switched off when long-lasting low power demands occur.

An average 18 % reduction in fuel consumption was observed during various plowing tests on the Belarus 3023 prototype in comparison with the related conventional tractor. Up to 63 % fuel savings have been obtained in simulations of a diesel electric backhoe loader for construction applications during standard reference duty cycles [36]. The model featured a series architecture with electrified hydraulic loads only: in particular, it considered a conventional ground drive transmission; an electrically-driven pumps for main hydraulic circuits, i.e. front and rear loaders and power steering, and a supercapacitor bank for power buffering.

The main drawback of series architectures is an increased volume and weight of the powertrain. Indeed, the generator must be sized to ICE full rated power and the motors must provide the entire load power. Thus, a high power density is a key requirement for electric drives in this application. Moreover, components must exhibit outstanding efficiencies to compensate the losses arising from double energy conversion, i.e. from mechanical to electric (generator) and then back to mechanical (motors). As a consequence, liquid cooling becomes mandatory for both machines and power converters. A high-voltage DC bus helps in reducing conduction Joule losses among all components, and high-speed geared drives may be a better choice than direct drive solutions

to reduce machines weight. On the other hand, higher voltage levels and higher machine speeds make converters design more challenging and need additional safety expediences. Converters integrated with machines can be used to achieve higher compactness and generators are sometimes integrated in engine flywheels, assembling more compact diesel generation sets. Despite these solutions, reducing electric machines weight remains a challenge. An heavier vehicle requires more traction power, therefore fuel consumption reduction must be carefully estimated during design stage. Besides, in the case of agricultural machinery a weight marginal increase causes a higher soil compaction, leading to faster soil depletion, although it may not be a relevant issue in some other heavy-duty vehicles.

### Parallel architectures

Fig. 2.8 outlines the powertrain of a plug-in HET with parallel architecture. A conventional specialized tractor for orchards and vineyards is converted to a parallel hybrid electric configuration by downsizing the diesel engine from an original 4-cylinder 77 kW (100 hp) unit to a new 3-cylinder 55.4 kW unit, the key expedient to comply with Stage V European regulation in an easier way [37]. The additional room that is obtained through the cylinder removal is exploited to insert a liquid-cooled surface-mounted permanent magnet machine (M), so that the vehicle wheelbase does not need to be increased. The electric machine is mechanically coupled to ICE shaft through a direct drive flange connection and it works mainly as a motor, performing engine starting and torque boosting. Machine design prioritizes overload capability to reduce volume and weight: maximum peak power (40 kW) and torque (150 N m) are almost 4 times the continuous ratings. Machine AC current is regulated by an inverter linked to a 700 V-rated DC bus. Pumps (P0-P2) of main hydraulic loads are electrically-driven, and their drives are also fed by the common DC bus. A 25 kWh battery pack is sufficient to have autonomy for a 8 h working day with the implemented EMS, considering a typical mix of light and heavy vineyard operations. LiFePo technology is chosen because of its high thermal stability and safety in case of perforation or crash. A resonant DC-DC converter links battery pack to DC bus.

In parallel architectures, the EMS can exploit electric drives to perform a load point shifting of engine output [38]. The working point can remain below, or close to, the optimal consumption line at given speed, i.e. those torque values that minimize SFC at imposed speed. Battery charging is necessary to keep the engine close to the optimal trajectory when load demand is far below the optimal value, with the electric machine operating as generator, thus adding additional load torque to engine shaft. However, this battery charging modality is very inefficient. By consequence, it should be limited to situations wisely identified to achieve a better overall fuel economy, or

## 2. TECHNOLOGY REVIEW

definitely avoided. Therefore, electric drives usually perform torque boosting most of the time, when load demand exceed the optimal value at imposed speed. The additional clutch C2 allows disengagement between ICE and M during long-lasting low-power operations. In this condition, ICE can be shut down and a full electric driving mode can be achieved to significantly reduce fuel consumption.

Parallel configurations are the most inexpensive hybrid architectures, and in many cases the easiest to implement for the powertrain electrification of an existing vehicle [39]. Indeed, only one electric machine is needed in a basic layout, and the engine can be significantly downsized, thanks to the possibility of torque boosting. Moreover, power density and efficiency of electric drives are not so concerning as in series architectures.

On the other hand, battery recharging through ICE surplus power is very inefficient, and it is usually limited. Therefore, the battery must have enough capacity to guarantee a sufficient autonomy and it must have outstanding discharge specifications. Thus, expensive lithium-based modules are a mandatory choice, as well as on-board chargers for plug-in designs. Nevertheless, the major drawback is that the engine is still mechanically connected to the loads, which are still coupled between each other. As a consequence, ICE cannot work always close to its lowest SFC point and new functionalities are strongly limited, due to speed inter-dependencies. Besides, mechanical transmissions are still needed, so no gain in maintenance requirements can be obtained. Reductions of transmission gears and loads decoupling may be improved by adopting an electric drive mechanically connected to each main load shaft, instead of a single machine on ICE shaft. Furthermore, the lack of an electric machine working mainly as generator is a relevant disadvantage in agricultural machinery, although it leads to cheaper and less complex layouts. Yet, the implementation of e-PTO relies entirely on battery capabilities, making the supply of electrified implements challenging and potentially unreliable. The electric machine can work as generator for a more effective e-PTO implementation. However, when feeding electric implements, torque boosting is unavailable and engine load point shifting is strongly limited.

### **Power split architectures**

Power split e-CVTs can be arranged in different layouts, depending on how the electric drives are connected to planetary gear parts, i.e. sun, planets carrier and ring. The various configurations can be classified into three main categories, namely input-coupled output-split, input-split output-coupled and compound coupled [40].

Fig. 2.9 represents an example of power split hybrid electric powertrain for a specialized 85 kW agricultural tractor [41]. Only traction is electrified, whereas the other main loads and the auxiliaries have still conventional driv-



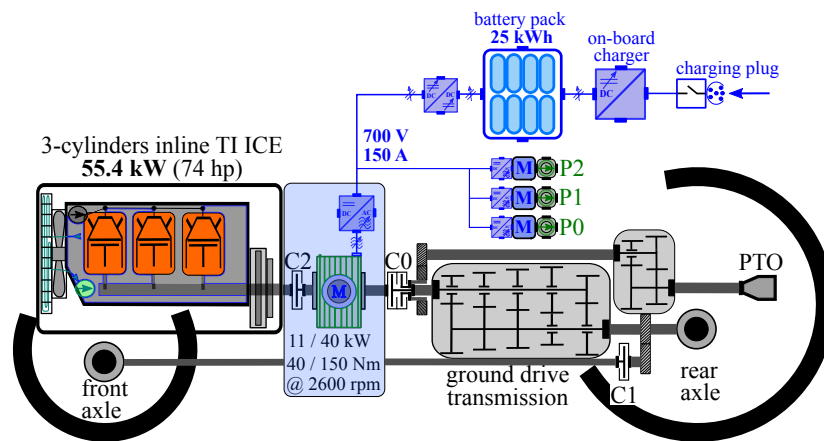


Figure 2.8: Example of a tractor with parallel hybrid electric powertrain.

etrains. Ground drive transmission is substituted by a power split e-CVT of the input-split output-coupled type. The layout features two liquid cooled electric machines with the associated bidirectional power converters, i.e. active rectifier and inverter: a 25 kVA surface-mounted permanent magnet machine working mainly as generator (G) is connected to the sun (S) of the planetary gear, while a 26 kW-rated induction motor (M) is linked to the ring (R). Engine shaft drives the planets carrier (C). A 140 V-rated DC bus links both electric drives and a bidirectional DC-DC bus interfacing a 15 kW LiFePo battery pack. G is designed to work most of the time at continuous rating. Overload operation is planned only during engine cranking. On the contrary, M has a discrete overload capability, i.e. 65 kW of maximum power, to fulfill traction peak demands. Clutch C0 allows disengagement and shut down of ICE for full electric driving mode. In this modality, both machine work as motors and they are fed exclusively by battery: G drives hydraulic pumps (P0-P2), auxiliaries and rear PTO (if engaged through clutch C2), while M is responsible of traction load. G can be switched off when the sun of the planetary gear is locked to vehicle frame by closing clutch C3, with C0 also closed. This expedient allows a parallel configuration, with M that shifts engine load point, or, alternatively, a conventional combustion-only mode if M is also switched off. Diesel electric mode is arranged with C0 closed and C3 open, with battery pack performing power buffering in power split configuration. An integrated compact solution have been proposed for the e-CVT, exploiting a coaxial and concentric arrangement of the electric machines. In particular, the inrunner permanent magnet machine (G) can be inserted inside the stator of an outer-rotor induction motor (M).

Power split architectures overcome the drawbacks of series and parallel layouts. The EMS can combine the features of series and parallel configurations, leading to more degrees of freedom in the high-level control [42]. Loads

## 2. TECHNOLOGY REVIEW

are decoupled from engine speed and between each others and there is the possibility of ICE downsizing. The presence of an electric machine working mainly as generator makes e-PTO more reliable. Moreover, electric drives do not need to be sized to the entire engine rating, thanks to the parallel power flow on the mechanical branch.

The main disadvantages of power split architectures are an increase mechanical complexity and the need of at least two electric machines. Moreover, in the EMS design a particular care must be taken to avoid circular power flows in the electric branch, that cause useless double energy conversions. In addition, power density and efficiency of electric drives are still crucial requirements.

Despite the higher complexity of hardware and control, power split architectures offer significant potentialities. However, fuel savings and performance have not been deeply investigated yet in agricultural machinery.

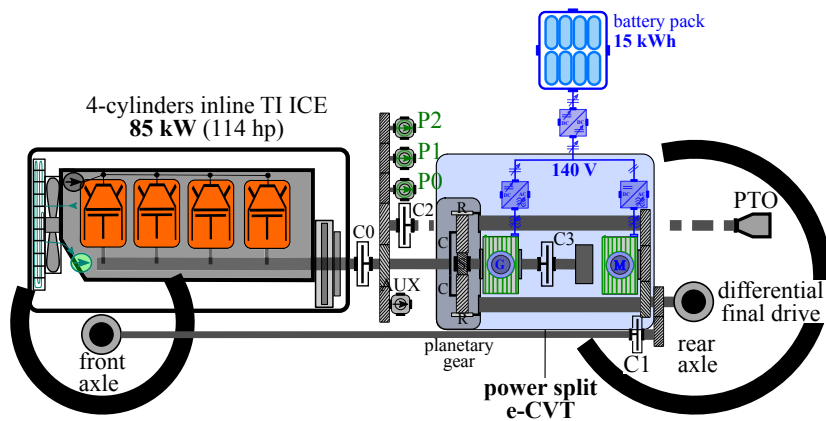


Figure 2.9: Example of a tractor with power split hybrid electric powertrain.

### 2.4.2 Full electric powertrains

In a full-electric powertrain, the entire energy demand is provided by electric sources. The two main configurations in automotive applications consist in drivetrains completely powered by a rechargeable battery pack, commonly of lithium-based technology, or in hydrogen-propelled powertrains, where fuel cell stacks are usually electrically coupled with a high-power battery module or a supercapacitor bank to increase the dynamic performance and improve efficiency. These two concepts have been proposed also for agricultural machinery, resulting in battery electric tractors (BETs) and fuel cell electric tractors (FCETs).

### Battery electric tractors

Full electrification by on-board batteries is currently unfeasible for row crop tractors and agricultural machinery beyond 120 kW (160 hp) because of the insufficient energy and power density of state-of-the-art lithium-based batteries. In general, BETs are unsuitable when a relevant part of the work comprises heavy-duty operations, for instance plowing and other soil tillage. In these situations, the total amount of energy required for a 8 h working day may vary between 600 and 900 kWh. This capacity would require a battery pack with a weight of  $4.0 - 5.3 \times 10^3$  kg and a volume of  $2.0 - 2.7 \text{ m}^3$ , considering a specific energy of  $0.15 \text{ kW h kg}^{-1}$  and an energy density of  $0.30 \text{ kW h L}^{-1}$ , typical values for LiFePo cells. Both volume and weight lead to unfeasible designs, even though engine, transmission and fuel tank are no more needed. Indeed, the replaced parts together usually weight  $1.5 - 3.0 \times 10^3$  kg and have a volume of  $0.8 - 1.3 \text{ m}^3$  for high-power row crop tractors. In particular, the additional weight is the main reason of BETs unsuitability beyond a certain power. Performance would be insufficient as vehicle weight would increase at least of 30 % with respect to conventional tractors, and battery would be more than half of the overall vehicle weight. Moreover, soil compaction would increase unacceptably.

Nevertheless, BETs deserve attention for small scale family farming [43], low-power operations and specialized tasks. Manufacturers have also proposed proofs of concept and prototypes of battery-powered utility tractors below 120 kW. It is interesting to mention that a conventional high-power tractor may be substituted by a couple of unmanned low-power BETs with battery capacities around 110 kWh by rescheduling and rethinking agricultural tasks in a farm [44]. The total cost of operations may decrease of 15 %, while the energy consumption and the greenhouse gas emissions may be reduced of 58 % and 92 %, respectively, if compared to conventional diesel, when energy consumption and emissions from battery manufacturing are taken into account.

However, BETs highly rely on the availability of a fast charging infrastructure near the farmland, which is currently unavailable most of the time. The exploitation of in-site renewable power plants can help in building charging infrastructure in remote farmlands, thus spreading BETs use.

### Fuel cell electric tractors

Fuel cells seem a more promising alternative for high-power heavy-duty vehicles, thanks to the higher energy density of pressurized hydrogen with respect to batteries and the faster refueling. Thus, FCETs may be feasible solutions in the whole power range of agricultural applications. Fig. 2.10 outlines the powertrain of the prototype New Holland NH2™ fuel cell electric tractor, presented by CNH in 2011 [45]. It is equipped with two 124 kW PEM

## 2. TECHNOLOGY REVIEW

(Proton Exchange Membrane) fuel cell stacks, fueled by a tank that can hold 8.2 kg of hydrogen gas at a pressure of 350 bar. Fuel cell stacks supply two 100 kW liquid-cooled electric motors driven by independent inverters, one for traction and one for PTO, hydraulic pumps and auxiliaries. Low-voltage electric loads are supplied by a DC-DC converter with isolated buck topology. A Li-ion battery pack with a capacity of 12 kWh and a peak power of 50 kW is connected to the 600 V DC link to improve system efficiency and dynamic performance of the tractor, while preserving fuel cell stacks life. DC bus voltage is regulated by boost DC-DC converters connected to the fuel cell stacks and by battery bidirectional DC-DC converter.

FCETs have great potentialities: equivalent energy consumption can be reduced by at least a third if compared to conventional diesel-fueled vehicles [46], and emissions can also be highly limited, even considering hydrogen production and transportation. However, the successful introduction of FCETs strongly depends on an effective infrastructure for hydrogen production and transportation, which is currently missing and it requires a long time of development and deployment. Moreover, hydrogen fuel cells are currently the most expensive electrochemical technology.

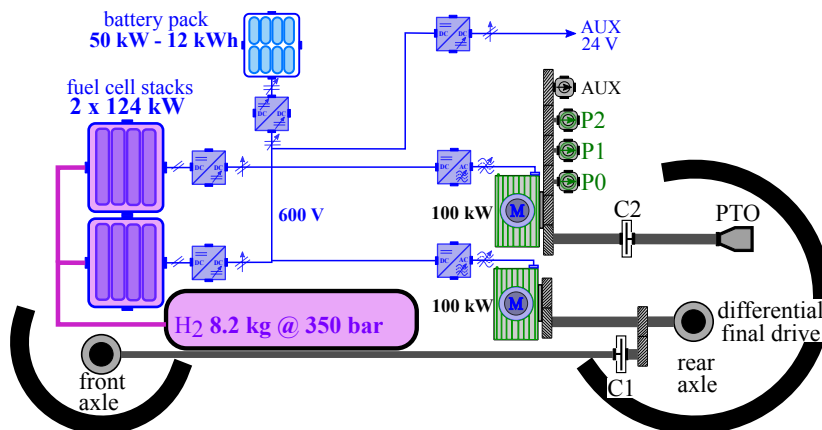


Figure 2.10: Example of powertrain of a fuel cell electric tractor.

### 2.4.3 Industrial prototypes

Tab. 2.2 summarizes the main advantages and disadvantages of each powertrain configuration for farming tractors electrification previously discussed. Potentialities and performance are quantified as percentage with respect to equivalent conventional powertrains. Only best values that can be obtained in a relatively short-term perspective are reported, considering the power range and tractor types more suitable for every architecture, i.e. row crop vehicles above 150 kW for series HETs and FCETs; utility and specialized tractors

Table 2.2: Summary of electrified powertrains for agricultural tractors.

Configuration	HETs			BETs	FCETs
	series	parallel	power split		
e-CVTs	Yes	No	Yes	/	/
e-PTO	Yes	Limited	Yes	Limited	Limited
Speed decoupling	Yes	Partial	Yes	Yes	Yes
Load point shifting	Yes	Yes	Yes	/	/
Power-to-weight ratio	+3 %	+6 %	+8 %	+9 %	+12 %
Fuel economy	+20 %	+12 %	+30 %	+100 %	+100 %
Overall emissions	-12 %	-8 %	-21 %	-92 %	-61 %
Initial cost	+45 %	+32 %	+56 %	+100 %	+134 %

below 120 kW for parallel and power split HETs and BETs.

Industry interest on agricultural machinery electrification has increased in recent years. Despite the development of HETs and full-electric tractors is still on a research stage, more electric drives are expected to be integrated inside machinery available on market in the incoming years.

Tab. 2.3 reports and compares relevant prototypes of electrified tractors presented by manufacturers until now [47, 48, 49, 50]. Concepts of HETs, BETs and FCETs described so far are included, highlighting the rated maximum continuous power of the whole vehicle, i.e. the continuous rating of the primary power source. Prototypes with electrified engine auxiliaries (e-aux.) are also considered, and the rated power of auxiliary electric drives is indicated. e-PTO and ground drive e-CVTs continuous capabilities are reported as well, when available. It is worth remembering that e-PTO refers to an electric interface between tractor and implements, while ground drive e-CVT means the presence of a diesel generator set supplying one or more traction motors in a series or power split configuration. PTO and hydraulic e-CVTs are not explicitly indicated, as well as overload capabilities, that may be significantly higher than continuous ratings.

Prototypes are characterized by the degree of hybridization (DoH) defined in (2.1), where 0 % DoH means a conventional diesel-fueled powertrain, potentially with electrified ICE auxiliaries, whereas a 100 % DoH refers to full-electric powertrains, namely BETs or FCETs. HETs have a DoH between these two limit values.

From Tab. 2.3 it can be seen that interest toward electrification in agriculture arose at the beginning of this century, as proved by some early prototypes unveiled between 2007 and 2011. Then, the topic lost interest for almost ten years, maybe due to an insufficient market demand. Nevertheless, now industry interest toward electrification is increasing again, as demonstrated by many prototypes presented in recent years (2018-2022). Among them, in

## 2. TECHNOLOGY REVIEW

Table 2.3: Prototypes of electrified tractors.

Company	Model Year	Power (kW)	e-aux. (kW)	e-PTO (kW)	e-CVT (kW)	DoH (%)
John Deere	7430 E-Premium 2007	135	20	/	/	0
John Deere	7530 E-Premium 2007	135	20	5	/	1.8
Minsk Tractor Work	Belarus 3023 2009	220	20	180	180	45
Rigitrac	EWD120 2011	91	/	80	90	48
CNH Industrial	New Holland NH2™ 2011	200	/	/	/	100
AGCO	Fendt e100 Vario 2018	75	/	75	/	100
AGCO	Fendt X-Concept 2019	150	/	130	/	23
CNH Industrial	Steyr Konzept 2019	150	/	150	150	50
Rigitrac	SKE50 Electric 2019	50	/	/	/	100
Argo Tractors	Landini Rex4 Electra 2020	82	/	/	20	10
Rigitrac	SKE40 Electric 2021	40	/	/	/	100
Kubota	LXe-261 2022	20	/	/	/	100
CNH Industrial	New Holland T4 Electric Power 2022	55	/	5.8	/	100

In addition to the concepts reported in Tab. 2.3, a mention is deserved by Carraro hybrid electric solutions [51], ZF e-CVTs, Soletrac BETs and the prototype HET of AUGA Group. John Deere has also kept pursuing electrification after the first E-Premium platforms, mainly focusing on hybrid layouts for row crop tractors: a power split e-CVT for PTO with an additional electric interface to implements is now an available option in some John Deere high-power tractors. Furthermore, many startups and spin-offs are actively developing technology for agriculture electrification and testing market potentialities.

## 2.5 Implements electrification

Table 2.4: Prototypes of electrified implements.

Company	Year	Implement	Electrified elements
Amazone	2007	Trailed fertilizer spreader	Disk motors
		Precision air seeder	Pneumatic transport fans Singling drives
		Trailed sprayer	Piston spray pump Auxiliary pumps
John Deere	2008	Trailed sprayer	Centrifugal spray pump
Reuch	2008	Fertilizer spreader	Disk motors
IAV and Krone	2019	Mower	PTO-driven generator Conditioner roller Cross conveyor belt
Joskin and John Deere	2019	Slurry tanker	Traction motor

Market acceptability of HETs and full electric tractors can be highly supported by a sufficient availability of electric implements, that can be totally or partially supplied by e-PTO. Powertrains and implements electrification should proceed in parallel for a successful market penetration. Indeed, implements electrification was early investigated through joint projects between agricultural machinery companies [52], and currently tractor industry is encouraging implement manufacturers in the development of electrified products. Relevant prototypes of partially-electric implements presented until now are reported in Tab. 2.4.

Implements electrification has several advantages. Both fuel economy and field efficiency can be significantly increased by performance improvement and new functionalities, especially when precision and automation agriculture principles are exploited. In particular, implements electrification can lead to fuel savings thanks to a more efficient power transfer, while allowing faster and more accurate controls [53]. As an example, chemicals and seeds dosing can be enhanced with trailed atomizers, air seeders and fertilizer spreader where hydraulic actuators are substituted by electric drives [54]. These systems show an up to 30% efficiency increase during field tests when compared with their hydraulic counterparts [55]. Electric drives outperform conventional hydraulic circuits especially at partial loads. In addition, maintenance requirements are lower. Further improvements in traction and steering can be obtained by electrification of mechanically-driven implements. As instance,

## 2. TECHNOLOGY REVIEW

trailed tankers with electric motors integrated in the driving axles can be towed by smaller tractors, enabling a tighter steering clearance [56]. Moreover, operators safety is highly enhanced when avoiding the use of mechanical PTO, and maintenance is less concerning also in these cases.

Despite the higher efficiency, fuel savings remain limited between 2 and 14%, due to the higher weight of electric drives, which often requires more traction effort [57]. Therefore, the main focus of implements electrification should be on increased functionalities along with automation and precision agriculture principles, because the potential fuel savings do not, themselves, justify the higher cost of electric drives. Nevertheless, PTO and implements electrification is gaining interest and an international standard (ISO/CD 23316) is now under development to define a high voltage electric interface between tractors and implements.

### 2.6 Main components for tractors electric drivetrains

The design and manufacturing of the main components for electric drivetrains of heavy-duty off-highway vehicles is still an open issue. In particular, the identification of proper design specifications, requirements and constraints is challenging, and an optimal choice of hardware devices and system settings is not straightforward. In this section, feasible proposals about the design and specifications of main components for agricultural machinery electrification will be covered. Device features and requirements will be presented, highlighting advantages and drawbacks.

#### 2.6.1 Energy storage systems

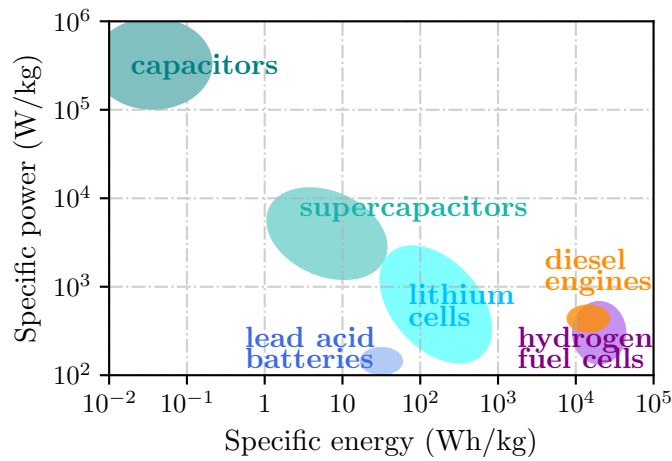
The choice of energy storage system and primary power source is the first step in the design of a hybrid or full electric powertrain. Different devices suitable for automotive applications can be compared in terms of power and energy density, as depicted in Fig. 2.11.

Lead acid batteries are commonly used in low-voltage systems up to 48 V, while lithium-based cells are the state-of-the-art technology for high voltage levels. Lithium-ion is expected to become the dominating battery technology for automotive applications in the next years, thanks to its energy and power density, that are higher than any other battery type both in terms of mass and volume. However, its storage capability is far from any liquid or gaseous fuel. As instance, lithium cells have a specific energy per unit of mass 100 times lower than diesel fuel, and an energy density per unit of volume 50 times lower. Therefore, the complete replacement of diesel engines as primary power source in heavy-duty off-road vehicles is not expected.

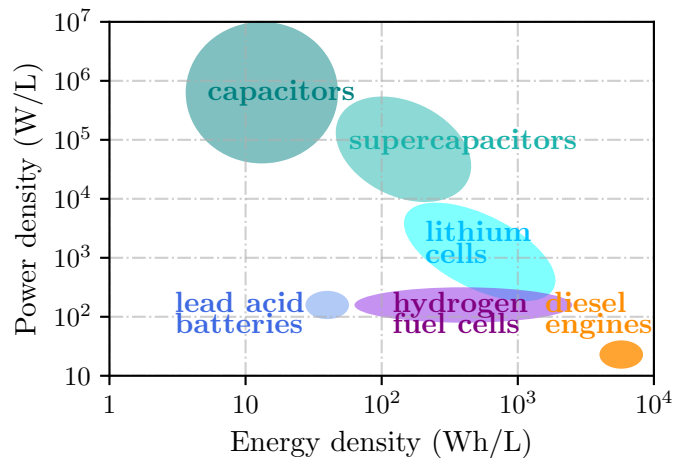
Common capacitors have the highest specific power, but their specific energy is insufficient for power tasks in automotive applications, as it can



## 2.6. MAIN COMPONENTS FOR TRACTORS ELECTRIC DRIVETRAINS



(a) Gravimetric density, i.e. per unit of mass.



(b) Volumetric density, i.e. per unit of volume.

Figure 2.11: Ragone charts.

be seen from Fig. 2.11a. Supercapacitors exhibit a sufficient specific energy and their specific power is higher than lithium cells, even though their power capability is still lower than any common capacitor [58]. Therefore, supercapacitors are the most suitable choice to fulfill fast-changing duty cycles, peak power demands and to recover braking kinetic energy more effectively. On the contrary, Li-ion batteries work as energy storage devices at first instance. In particular, Fig. 2.11b shows that supercapacitors are a more appropriate choice than batteries when power specifications have priority over energy requirements, due to the higher power density per unit of volume. Systems that combine batteries and supercapacitors can be implemented in order to exploit the advantages of both technologies at the same time [59, 60]. Hybrid battery-supercapacitors systems could be beneficial to sustain fast discharges during agricultural field operations. For the same reason, power-oriented

## 2. TECHNOLOGY REVIEW

Li-ion modules should be preferred than energy-oriented ones, especially in HETs, where torque boosting and power buffering are needed.

Battery charging is the most important technology bottleneck, together with energy density. BETs and HETs with rechargeable batteries are unattractive for end users without an effective charging infrastructure. High-voltage wired DC charging is currently the most feasible solution for agricultural machinery [61], as it allows a complete recharge of large capacity batteries in an acceptable working time [62, 63]. High-voltage levels can be available close to farmlands taking advantage of in-site renewable power plants, such as photovoltaic or bio-gas installations [64]. Moreover, the DC-DC charger can be installed in the farm, thus removing a component from the vehicles. Battery exchange could be more competitive than wired charging in agricultural applications [65], provided that a standard is defined and widely adopted for this solution. Wireless systems could be promising in a long-term perspective [66].

Hydrogen fuel cells seem more suitable than batteries for electrification of off-road heavy vehicles [67], despite only few studies have investigated this technology in agricultural applications. Hydrogen specific energy is higher with diesel fuel and engine power-to-weight ratio is comparable with fuel cells, as shown in Fig. 2.11a. Moreover, refueling is faster and easier than battery charging.

Among present technology, PEM and SO (solid oxide) fuel cells are the most promising technologies for mobile high-power applications [68]. However, they have poor dynamic performances due to the slowness of their chemical reactions. Therefore, auxiliary batteries or supercapacitor banks are mandatory to fulfill power peaks and fast transients typical of automotive applications, causing an increase in the overall system cost.

Furthermore, hydrogen storage is complicated and expensive: high-pressure tanks and cooling systems are needed to obtain a sufficient energy density per unit of volume. Besides, the best value, given by liquid hydrogen storage, is still lower than a diesel fuel tank. Then, safety issues are major concerns due to extreme flammability of hydrogen, although some studies have already proven that both pressurized gas hydrogen and liquid hydrogen storage have an explosion risk comparable to gasoline fueled vehicles, thanks to hydrogen volatility in the former case [69], and when proper tanks are used in the latter solution [70]. A further safer option is metal hydride storage [71], which allows an energy density comparable with pressurized hydrogen with no risk either of inflammability nor explosions. On the other hand, the weight increases significantly, thus reducing gravimetric energy density.

Nevertheless, a successful introduction of hydrogen propulsion in off-road applications is strictly related to the development of a reliable and widespread infrastructure for hydrogen production, transportation and refueling, which is currently missing and it requires a long deployment time.

### 2.6.2 Electric machines

The design of electric machines (EMs) seems particularly challenging for HETs rather than for full electric tractors, due to the coexistence of high-power electric components and a diesel unit in a limited space, even though some issues are shared by both configurations.

The development of an effective HET can be performed through a conversion of existing conventional platforms. Yet, at these conditions, there are strict size constraints for EMs, which must fit in the volume cleared by ICE displacement reduction, or by the removal of mechanical components. Therefore, EMs for agricultural tractors must exhibit a high power density. Since speed values in agricultural machinery are relatively low, power density can be often translated with torque density. This requirement is quite important also to make electric drives more competitive with their hydraulic counterparts, widely used in tractors. Indeed, state-of-the-art EMs have a lower torque density than hydraulic actuators, although they allow an easier and more accurate control. Thus, sometimes the higher efficiency of electric drives may not be exploited due to an increased weight of the machinery, which may lead to an insufficient overall efficiency to justify the higher initial costs.

Electric loading, i.e. the current density in the armature winding, should be maximized to achieve a high torque density. As a consequence, a higher thermal load must be dissipated to avoid over-temperatures in slot insulation. Therefore, liquid cooling is often mandatory, instead of air-cooled self-ventilated machines. The use of hair-pins for armature winding can be beneficial to further improve torque density and heat dissipation [72].

An effective cooling is of paramount importance also to achieve lower operating temperatures, thus reducing Joule losses [73]. Efficiency may not seem a critical aspect in EMs. However, the highest efficiency region is usually placed at high speed, whereas farming tractors often works at low speed during field operations [74].

The major challenge in EMs design is the identification of proper specifications. In particular, the choice of torque requirements is not straightforward. The maximum power demand may not be a cost-effective option, or it may lead easily out of size constraints. Since in many agricultural working conditions EMs are subjected to a highly-varying torque demand, it can be a proper choice to set a lower rated torque, while peaks can be covered in overload operation [75]. Following this criteria, the EM must have a proper overload capability, in order to fulfill peak torque demands for enough time, without incurring in electromagnetic or thermal damages, namely demagnetization of permanent magnets and degradation of insulation inside slots.

The choice of electric machine type is not straightforward too. Overload characteristics and speed ranges are represented in Fig. 2.12 for four different types of EMs suitable for automotive applications [76], namely

## 2. TECHNOLOGY REVIEW

asynchronous induction machines (IM), wound-rotor synchronous machines (WRM), surface-mounted permanent magnets (SPM), interior permanent magnets (IPM), both in terms of torque (Fig. 2.12a) and power (Fig. 2.12b). Quantities are reported in per units, where base values are rated speed, torque and power. Reference continuous curves are depicted in black dashed lines.

Generally, permanent magnet synchronous motors, both SPM and IPM, have the highest torque density. SPMs are a suitable solution for low-to-medium speed applications when a high torque is needed in the whole speed range. The machine is mainly controlled in maximum-torque-per-ampere mode (MTPA). On the other hand, IPMs are preferred when a constant power is required in a wide speed range, thanks to their flux-weakening capabilities [77]. The use of rare-earth magnets seems to be mandatory to fulfill the power density requirement of agricultural applications. Thus, both SPMs and IPMs are more expensive than WRMs and IMs. Yet, automotive industry is now greatly interested in the complete replacement or significant reduction of rare-earth magnets, especially of high-grade ones [78], due to unreliable supply chains, price instability and geopolitical reasons [79]. Furthermore, high temperature class magnets must be used to achieve the needed overload capabilities, and a particular care must be given not to demagnetize them. On the contrary, WRMs and IMs do not suffer from demagnetization problems, and the thermal issues are limited only to slot insulation. Thus, they can exhibit better overload capabilities. However, their torque density is lower.

The choice of machine type is strongly related to powertrain architecture, especially on how the EM is mechanically connected to the load. When direct drive low-speed solutions are adopted, i.e. EM is installed on engine crankshaft, as instance in a parallel configuration or the generator in a series architecture, then high speed is not required (speed values below 3000 rpm). Therefore, SPMs are proper choices. On the other hand, when EM is mechanically coupled through speed reducers or gear trains, as instance in power split configurations, then a wide speed range at constant power is needed, thus IPMs or IMs are better choices.

When some strict size constraints occur, it may be possible that a very low aspect ratio is needed, i.e. diameter greater than length. In these cases, axial flux machines should be considered as well [80, 81], and they could be preferred to their radial flux counterparts in some situations [82, 83]. Other special machines could be suitable for this challenging application too, with several advantages if compared to conventional types. For instance, double-rotor radial flux machines can make integrated power split e-CVTs [84], while double-stator machines can be used as wheel motors or double generators [85]. As another significant example, hybrid excitation permanent magnet machines, both radial flux [86] and axial flux types [87, 88], have great potentials for heavy-duty off-highway vehicles, thanks to their increased torque capability and wide speed range.

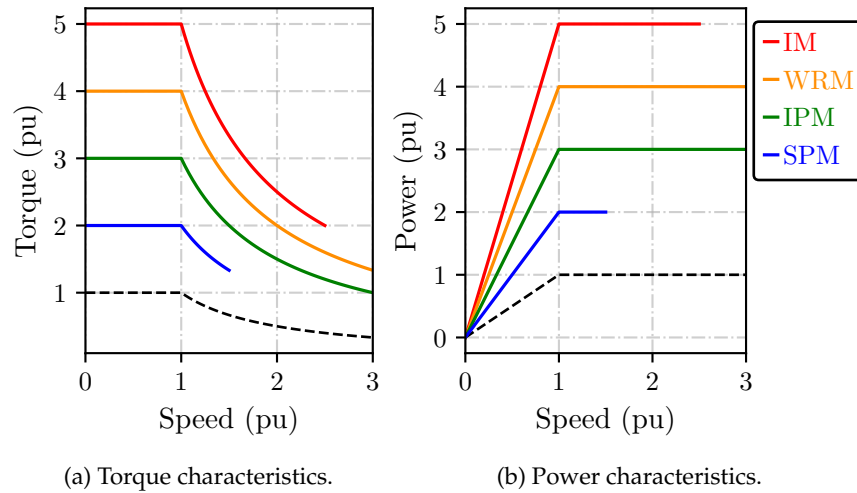


Figure 2.12: Example of overload ratings of different electric machines.

### 2.6.3 Power electronics converters

The choice of power electronics converters (PE) for electric drivetrains of tractors is mainly driven by the same demanding requirements already described for EMs, although some considerations should be drawn as there are peculiarities which applies specifically to this drive component.

As happens for EMs, there is a need to minimize volume and weight of the electric power unit too, which again results in challenging requests in term of power density and efficiency. However, differently from EMs, where working cycle can be used to properly design the machine and avoid oversizing, inverters are usually sized considering the maximum current supplying at full load to the electric machine, being their thermal responsiveness much greater than the EM one (i.e. they heat up more quickly).

Liquid cooling is preferred to convection or forced air cooling also for PE. Moreover, in hybrid solutions where the level of integration is high, there is a tendency in using the same coolant for the engine and the electric drive. As the optimal coolant temperature for ICE is around  $90^{\circ}\text{C}$ , this results in demanding requirements for the EM and very challenging design constraints for PE [89].

At the moment, the most used switching power device for automotive systems, in the range of power and voltage relevant for agricultural applications, is the Silicon IGBT, which, however, is known for rapidly decreasing its performance when operating at high temperature [90]. Requirements of demanding temperature environment are usually fulfilled by selecting devices with superior current rating, or by oversizing the converter heatsink. Nevertheless, the recent advent into the market of the so-called wide-bandgap devices (WBG), Silicon Carbide (SiC) and Gallium Nitride (GaN), can pave the

## 2. TECHNOLOGY REVIEW

way for lighter and more efficient power converters. WBG-based converters are characterized by lower switching losses and higher switching frequencies. Furthermore, they can operate efficiently at higher temperatures than their silicon counterpart. In addition, they are suitable in case of partial load operation, with working cycles subjected to frequent current variations.

As farming tractors often work at high torque and low speed, conduction losses are expected to be the prominent source of power losses for PE. Therefore, converter architectures that minimize the number of switching devices in series are preferred. Thus, voltage source inverters are advantaged compared to other options. In particular, modular interleaved parallel solutions are beneficial [91].

Nevertheless, as the requirements are becoming more and more demanding, it is expected that power electronics and electric machines will be no longer designed separately, but a cooperative design process will be preferred [92], which involves a high level of integration. In case of high efficiency required in the low speed high torque region, multi-phase segmented integrated architectures represent a promising solution [93].

## 3 LIFE CYCLE COST ANALYSIS OF HYBRID ELECTRIC TRACTORS

---

This chapter presents a method to evaluate the economic feasibility of tractor powertrain electrification based on life cycle cost analysis. For a parallel hybrid electric architecture, the best combustion engine downsizing is evaluated among some discrete values. The methodology is applied to three case studies with different power levels and operating cycles: a 76 kW orchard tractor, a 175 kW row crop tractor with medium duty use, and a 210 kW row crop tractor with heavy duty use. Fuel and electrical energy consumption are estimated through simulation. A range of prices for main powertrain components, diesel fuel and electrical energy is taken into account from tractor manufacturer and end-user point of view, in order to cover price uncertainty and analyze its effects. The results show that operating cost savings decrease when more power-intensive operations are performed. The operating cost savings, respectively for orchard, row crop medium duty, and row crop heavy duty, are approximately 8 %, 3 %, and 0.5 %, which result in 6 %, 1 %, and 0.1 % life cycle cost savings. Thus, parallel hybrid electric powertrains should probably be avoided in high-power tractors, whereas they could be beneficial for specialized orchard and vineyard vehicles.

### 3.1 Conventional and hybrid electric powertrains under analysis

The conventional tractor powertrain taken as reference for this study is outlined in Fig. 3.1. Conventional state-of-the-art drivetrains for agricultural tractors are deeply covered in the previous chapter. A diesel internal combustion engine (ICE) is the only power source. Its mechanical power is used for traction, power take-off (PTO), hydraulic pumps for implement and three-point linkage operation, as well as for a variety of systems that are not strictly fundamental for the performed tasks, e.g. engine auxiliaries or cabin air conditioning. Power is transmitted to the wheels through a stepped mechanical transmission, or through a continuously variable transmission (CVT, splitting the power between a fixed mechanical path and a variable path, usually hydrostatic), whereas PTO and hydraulic pumps are commonly powered using *live* shafts, bypassing the ground drive transmission, so that they can be driven while the wheels are not moving.

Various configurations are possible for powertrain electrification of agricultural tractors. An exhaustive discussion is reported in the previous chapter. In this work, a plug-in parallel hybrid architecture is adopted, due to its easier

### 3. LIFE CYCLE COST ANALYSIS OF HYBRID ELECTRIC TRACTORS

and cheaper implementation compared to other layouts. The configuration chosen as reference for the hybrid electric tractor is outlined in Fig. 3.2. A Li-ion battery pack is selected due to its high energy density. More advanced hybrid storage systems that combine batteries and supercapacitors are also suitable for this application [94], and their use could be beneficial, as they exploit the advantages of both technologies. However, these hybrid storage systems are not considered in this study, as they would heavily increase the complexity of such a general analysis.

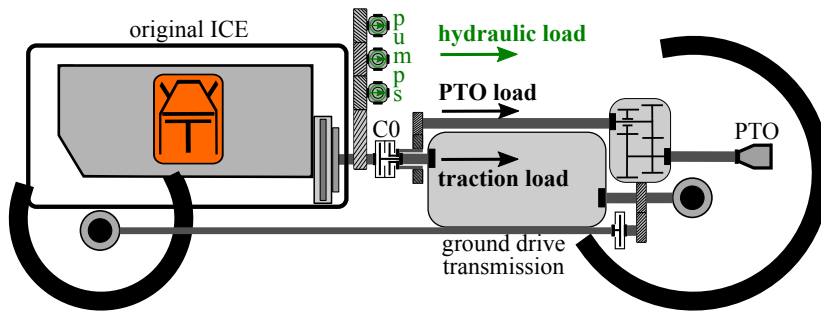


Figure 3.1: Outline of reference conventional powertrain.

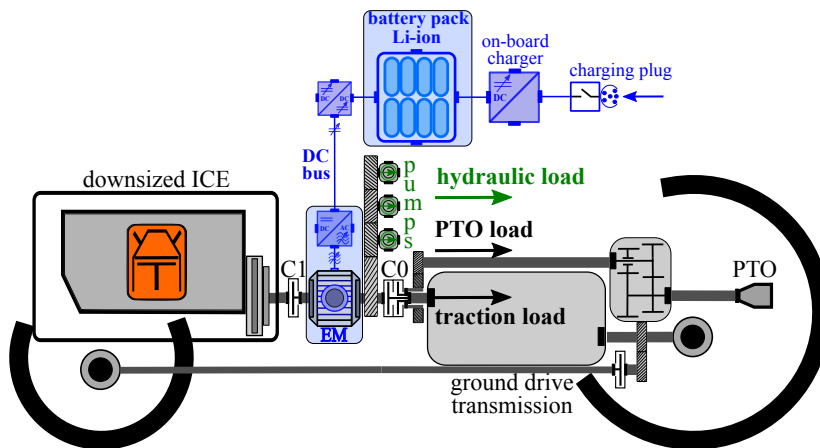


Figure 3.2: Outline of reference parallel hybrid electric powertrain.

## 3.2 Case studies and operating cycles

Farming vehicles cover a wide power range: they come from a few tens of kW for small family farming vehicles, to more than 400 kW for high-power row crop tractors, throughout medium-size specialized vehicles for orchards and vineyards and utility tractors. Moreover, tractors perform a great variety of



Table 3.1: Yearly time contribution and average power of each operation.

Operation	Average power		Yearly time fraction (%)
	(kW)	(pu)	
76 kW specialized tractor			
Weeder	35.6	0.47	14.3
Atomizer	42.1	0.55	14.3
Grape harvester	20.7	0.27	14.3
Plant lifting plow	11.0	0.14	28.6
Tying machine	5.3	0.07	28.5
175 kW medium-duty row crop tractor			
Heavy plowing	96.6	0.55	33.4
Medium plowing	82.8	0.47	35.6
Rotary harrow	114.7	0.66	17.8
Field transport and idling	30.1	0.17	13.2
210 kW heavy-duty row crop tractor			
Subsoiler	150.8	0.72	10.3
Cultivator	97.4	0.46	12.3
Heavy plowing	85.7	0.41	18.7
Tiller	145.5	0.69	17.8
Rotary harrow	122.7	0.58	20.3
Road transport	63.6	0.30	10.3
Idling	12.7	0.06	10.3

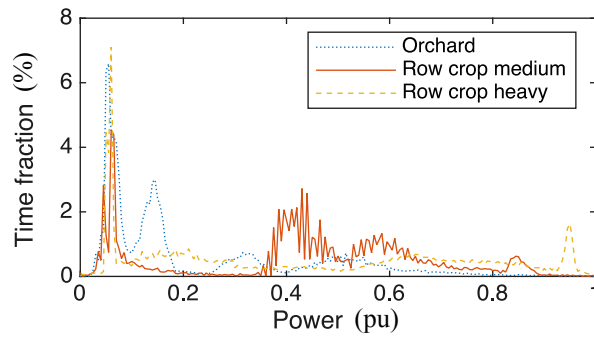
different operations. Since there is still a lack of standard duty cycles that fully represent the daily average operation of each tractor category and agricultural task, this work is based on actual field measurements [95, 96]. Three different case studies are considered, distinguished by power size and application:

- 76 kW specialized tractor for orchards and vineyards;
- 175 kW row crop tractor, medium duty;
- 210 kW row crop tractor, heavy duty.

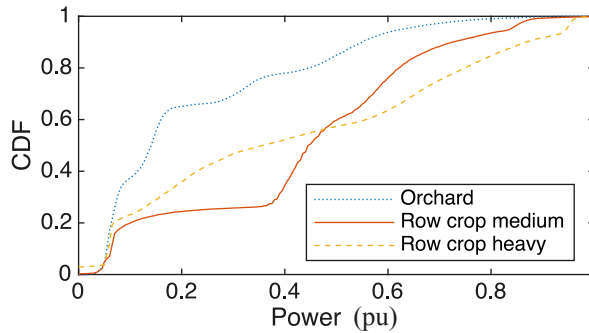
The simulations about the specialized and heavy-duty row crop tractors are carried out using working cycles directly from in-field measurements, whereas scaled duty cycles are derived from measured data to represent a medium-duty use of a row crop tractor.

Yearly time contributions and average power are reported in Tab. 3.1 for each case study and task. Average power is also expressed in per unit of the original ICE rating. In the analysis presented hereafter, working hours per

### 3. LIFE CYCLE COST ANALYSIS OF HYBRID ELECTRIC TRACTORS



(a) Operating time fraction at every power level.



(b) Cumulative distribution function.

Figure 3.3: Load distribution in the three case studies.

year are considered equal to 1000 h and 850 h for the specialized vehicle and the two row crop tractors, respectively [97].

Fig. 3.3 shows load distribution as a function of power for each of the aforementioned categories, where power values are in per unit of the associated rated power of the original non-hybrid tractor. In particular, Fig. 3.3a shows the fraction of operating time at each power level, while Fig. 3.3b reports the cumulative distribution function (CDF), which indicates the operating time fraction that can be performed with a power level smaller than or equal to the related abscissa power value. From the CDF curves, it can be seen that the specialized tractor for orchards and vineyards works approximately 75-80 % of the time at less than 40 % of its rated power. On the other hand, the same fraction of time on the medium-duty row crop tractor requires ~60 % of the rated power, whereas for the heavy-duty row crop this value exceeds 70 % of the rating. This preliminary observation, together with a literature review, suggests that the specialized tractor category will be more promising for powertrain electrification, compared to the two heavier categories, at least with the hybrid configuration considered in this study.

### 3.3 System modeling

A quasi-static backward-facing model is adopted to simulate both hybrid and conventional tractor. The simulation model is used to determine fuel and electrical energy consumption, as well as the specifications of the main components of the hybrid electric powertrain, namely battery pack, electric machine (EM) and drive power converter (PE), i.e. EM inverter. Input load data are obtained from field tests on conventional non-hybrid tractors, which makes them intrinsically reliable and allows model validation by fuel consumption comparisons between measured data and simulations of the conventional powertrain. Measurements are taken at ICE shaft, and engine control unit (ECU) data are acquired. Thus, loads are assumed to be applied directly at ICE shaft, without modeling driver behavior, vehicle dynamic and transmissions: all the transmission ratios and losses are already included in the load values.

The model is built in Simulink, and MATLAB is used for results post-processing, as well as for all iterative processes described hereafter (Section 3.4). However, any numerical tool that handles dynamic systems can be adopted. Simulations are performed using the automatically-selected variable-step solver of Simulink, with maximum step size equal to the sampling interval of field tests input data.

The scheme of the model is outlined in Fig. 3.4. The function of each block is exhaustively explained in the following.

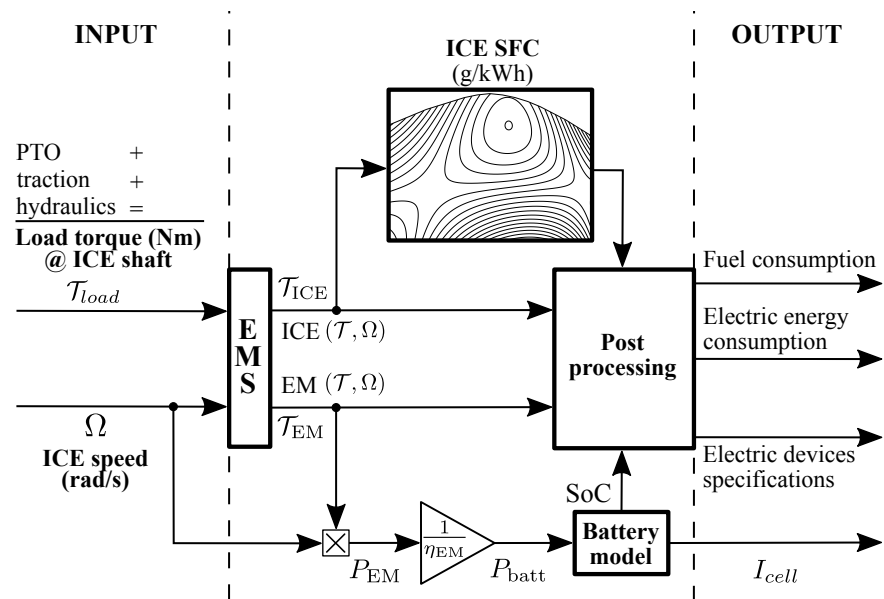


Figure 3.4: Scheme of the hybrid tractor model for LCC evaluation.

### 3.3.1 Energy management strategy

A rule-based energy management strategy (EMS) is chosen. The implemented rules are derived from [98]. However, contrary to previous works in literature, a speed-independent EM torque is used for battery charging, instead of setting it to achieve the maximum ICE efficiency for the given speed. Charging with the maximum efficiency torque at medium to high engine speed would lead to a higher battery current, easily exceeding battery limitations, unless a high-capacity storage is adopted.

When the load torque  $\mathcal{T}_{load}$  remains below a certain lower threshold  $\mathcal{T}_{Lim}$ , ICE operates at that lower limit, whereas EM acts as a generator to match the load torque. If the load is greater than  $\mathcal{T}_{Lim}$ , ICE supplies the entire load torque up to a certain upper limit curve ( $\mathcal{T}_{Lim}(\Omega)$ ). Above this higher speed-dependent curve, EM covers the difference between load and ICE torque (electric boosting). The upper threshold  $\mathcal{T}_{Lim}(\Omega)$  can correspond to the actual engine torque limit or ICE can be limited to a lower curve in order to use the energy stored in the battery to cover part of the load, in particular when a task rarely requires electric boosting.

Both torque thresholds are different for each operating cycle, and they are chosen in order to minimize the required battery capacity and, when desired, to maximize electric energy usage if a certain cycle is not particularly power intensive, while complying with battery C-rate limitations. Thresholds tuning is explained in Section 3.4.

In general, the optimal design for a rule-based EMS requires experience and knowledge of the whole load cycle. Thus, it might have some limitations when implemented in a real vehicle. However, the chosen strategy is deemed acceptable for this analysis thanks to its simplicity. EMS functionalities are summarized by (3.1), and a graphical explanation is provided in Fig. 3.5.

$$\mathcal{T}_{ICE} = \begin{cases} \mathcal{T}_{Lim}, & \text{if } \mathcal{T}_{load} \leq \mathcal{T}_{Lim} \\ \mathcal{T}_{load}, & \text{if } \mathcal{T}_{Lim} < \mathcal{T}_{load} \leq \mathcal{T}_{Lim}(\Omega) \\ \mathcal{T}_{Lim}(\Omega), & \text{if } \mathcal{T}_{load} > \mathcal{T}_{Lim}(\Omega) \end{cases} \quad (3.1)$$

$$\mathcal{T}_{EM} = \begin{cases} \mathcal{T}_{load} - \mathcal{T}_{Lim}, & \text{if } \mathcal{T}_{load} \leq \mathcal{T}_{Lim} \\ 0, & \text{if } \mathcal{T}_{Lim} < \mathcal{T}_{load} \leq \mathcal{T}_{Lim}(\Omega) \\ \mathcal{T}_{load} - \mathcal{T}_{Lim}(\Omega), & \text{if } \mathcal{T}_{load} > \mathcal{T}_{Lim}(\Omega) \end{cases}$$

### 3.3.2 ICE and electric drive modeling

The energy management algorithm determines the amount of torque  $\mathcal{T}_{ICE}$  provided by ICE, while engine speed is assumed equal to field measurements.

Downsized engines are considered in the hybrid electric tractor model to

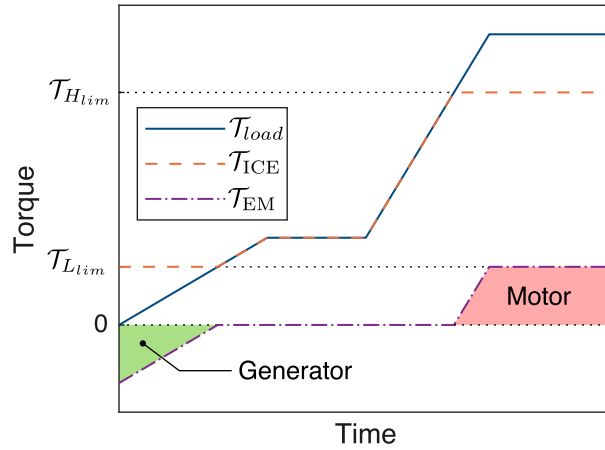


Figure 3.5: Rule-based EMS in a demo operating cycle. Constant upper threshold torque limit is shown for sake of simplicity.

exploit the potentialities of the chosen parallel architecture. For the two row crop tractors, various levels of ICE downsizing are included in the analysis. The torque limit curve of a the original base engine is scaled with a downsizing coefficient  $R$  to obtain a fine variation of ICE power ratings. At the same time, the operating cycles were kept constant to introduce a certain safety margin in terms of both performance and price. This setting choice favors the conventional non-hybrid variants, although load torque should decrease with ICE downsizing, as some of the parasitic losses (e.g. cooling fan) are included in the load torque input data.

On the specialized tractor, instead, a single 55 kW ICE is considered for the hybrid variant, as the new emissions regulations are less restrictive below 56 kW. Despite this approach may be controversial for emission reduction purposes, such expedient has been already adopted in several similar works [96, 98, 39]. Therefore, in the case of the specialized tractor, instead of varying ICE power rating, EM exploitation is changed while keeping the same battery size, as the objective is to minimize it. Three operating modes are considered:

- *hybrid 1* mode uses EM only in cycles where ICE needs boosting; this operating mode is used to determine the battery capacity following the iterative procedure described hereafter (Section 3.4);
- *hybrid 2* mode maximizes EM exploitation; electric assistance in medium duty cycles, e.g. atomizer and harvester; full electric mode (ICE off) during long-lasting periods in low-power duty cycles, e.g. plant lifting plow and tying machine, until the battery reaches a 20 % state of charge (SOC), which is a value consistent a 60 % discharge limitation from an 80 % initial SoC;

### 3. LIFE CYCLE COST ANALYSIS OF HYBRID ELECTRIC TRACTORS

- *hybrid mix* is intermediate case between *hybrid 1* and *hybrid 2* modes; full electric operation is limited in order to reduce the initial tractor cost compared to *hybrid 1*. As instance, operation with plant lifting plow is always performed with ICE on, as a higher power EM would be needed for full electric operation.

Fuel consumption estimation is based on engine torque and speed, using a specific fuel consumption (SFC) map, if available, or a polynomial approximating function, which is tuned to give a good match with consumption measurements of engine ECU during field tests. The estimation relative error averaged on all operations is lower than 4% in each case study, which can be considered a sufficient approximation for the purpose of this work.

For the 55 kW downsized ICE of the specialized hybrid electric tractor, an actual SFC map is used. On the contrary, SFC maps of row crop tractors downsized engines are obtained by scaling some polynomial approximating functions with the downsizing coefficient  $R$ , in the same way adopted for engine torque ratings. This approach is not completely accurate and some adjustment should be considered [99]. However, the combined magnitude of these adjustments usually does not exceed 5%. Moreover, the correction factors assume the highest values in the knock-constrained region, i.e. high load and low speed, which is not an issue for compression ignition engines. As will be seen later, ICE downsizing is not extreme on the two row crop tractors: an  $R$  lower than 0.8 is not worthwhile. As a consequence, the SFC estimation error is further limited even when no adjustments are considered. The simulation results obtained with this scaling approach are deemed accurate enough for this analysis, although no measured fuel consumption data are available for the hybrid tractor.

Electric machine (EM) torque  $\mathcal{T}_{EM}$  is determined as the difference between load and ICE torque, times the speed reduction ratio between engine and EM shafts, while EM speed is equal to ICE speed divided by the speed ratio. For simplicity, in this analysis the speed ratio is set equal to 1, i.e. a direct drive solution is chosen. A constant 0.85 efficiency ( $\eta_{EM}$ ) is assumed to account for the combined losses of EM and its drive inverter [100].

#### 3.3.3 Battery model

Battery model is based on the steady-state model proposed in [101]. Cell current is given by:

$$I_{cell} = \frac{U_{oc} - \sqrt{U_{oc}^2 - 4R_{cell}P_{cell}}}{2R_{cell}}, \quad (3.2)$$

where:

- $R_{cell}$  and  $U_{oc}$  are electric equivalent resistance and open-circuit voltage of a single cell, respectively; both are functions of the state of charge;

- $P_{cell}$  is the power supplied to a single cell, which is simply computed by dividing battery power by number of cells  $N_{cell}$ , assuming a perfectly balanced battery management action; battery power  $P_{batt}$  is obtained from EM mechanical power  $P_{EM}$  using electric drive efficiency  $\eta_{EM}$ ;

Battery current and power are assumed positive when the battery is charged. State of charge at time instant  $t$  is computed as:

$$\text{SoC}(t) = \text{SoC}_{t=0} + \int_0^t \frac{I_{cell}(\tau)}{\text{Cap}_{cell}} d\tau, \quad (3.3)$$

with  $\text{Cap}_{cell}$  being cell capacity (A h).

Although not completely accurate [102], total battery energy content (Wh) is estimated as:

$$E_{batt} = \text{SoC}_{t=t_{end}} \cdot U_r \cdot \text{Cap}_{cell} \cdot N_{cell}, \quad (3.4)$$

where  $U_r$  is rated cell voltage and  $\text{SoC}_{t=t_{end}}$  is state of charge at the end of the duty cycle. Cell capacity, and consequently battery size  $E_{batt}$ , are chosen through the iterative procedure that will be described later (Section 3.4).

SoC is constrained between an initial maximum value  $\text{SoC}_{t=0}$  equal to 80 % and a minimum lower limit of 20 %, leading to a 60 % maximum depth of discharge (DoD). It is worthwhile to remark that battery can finish a 8 h duty cycle with the minimum allowed SoC value, i.e. completely discharged, as battery recharging is considered available from external sources at the end of each working day, thanks to the plug-in configuration chosen in this analysis.

In addition, C-rate constraints have also key importance in the model. Limitations assumed for this study are reported in Tab. 3.2.

Table 3.2: C-rate constraints.

	Continuous	Transient peaks ( $\leq 10$ s)
Charge	1C	3C
Discharge	3C	6C

### 3.3.4 Post processing stage

In the post processing stage, overall consumption, CO<sub>2</sub> emissions and relevant specifications of the main electric components, namely EM, PE and battery, are retrieved.

Fuel consumption is computed integrating fuel rate over the entire duty cycle:

$$\text{FC} = \int_0^{t_{end}} \frac{P_{ICE}(\tau) \text{SFC}(\tau)}{\delta} d\tau, \quad (3.5)$$

### 3. LIFE CYCLE COST ANALYSIS OF HYBRID ELECTRIC TRACTORS

where  $P_{ICE}$  is engine power and  $\delta = 0.82 \text{ kg L}^{-1}$  is diesel fuel density at tractor operating temperature. In a similar way, electric energy usage is estimated as the time integral of battery power:

$$E = \int_0^{t_{end}} P_{batt}(\tau) d\tau \quad (3.6)$$

Emissions are derived from fuel and electric energy consumption. Battery manufacturing is also considered, being among the main causes of the vast majority of emissions difference between hybrid electric and conventional tractors.

CO<sub>2</sub> equivalent emissions are assumed to be proportional to fuel consumption (under the complete combustion hypothesis), electric energy consumption and battery capacity. Coefficients of proportionality used in this study are:

- 3.92 kgCO<sub>2</sub>/kg<sub>fuel</sub> for diesel fuel consumption;
- 0.33 kgCO<sub>2</sub>/kWh<sub>energy</sub> for electric energy consumption;
- 100 kgCO<sub>2</sub>/kWh<sub>battery</sub> for battery manufacturing.

These factors comprise emissions from the whole process, including extraction of raw materials, transportation, production, delivery to costumers, and, for diesel fuel, also the emissions originating from its combustion. The direct measurement of the emission factors is not possible. The adopted value are based on estimations reported in literature. The value for fuel-related emissions is derived from [103], considering the energy based allocation method and lower heating value of diesel equal to 43.1 MJ/kg. As regard electric energy emissions, the assumed value is derived from [104], considering the average between European mix emission factors for low voltage supply of 2016 and 2030. It is reasonable to take the average value because the assumed tractor life extends to a few years beyond 2030. Finally, in [105] a 61-106 kgCO<sub>2</sub>/kWh<sub>battery</sub> is reported for battery production. A value close to the upper limit is chosen, because the required battery capacity in this analysis is relatively low if compared to road battery electric vehicles, which often adopt batteries larger than 50 kWh.

Electric machine design rated torque specification is determined considering the thermal equivalent torque, as a design solution based on peak torque would lead to an oversized machine. A low-pass filter is used, adopting as time constant a supposed thermal time constant  $\tau_{tm}$  of the EM. Thermal equivalent torque  $\mathcal{T}_{theq}$  is computed by low-pass filtering the instantaneous EM torque  $\mathcal{T}_{EM}(t)$ :

$$\mathcal{T}_{theq} = \sqrt{\mathcal{L}^{-1} \left[ \frac{\tau_{th}}{\tau_{th}s + 1} \mathcal{L}[\mathcal{T}_{EM}(t)^2] \right]}. \quad (3.7)$$

Reasonable time constants for water cooled EMs are considered, ranging from 200 s for the specialized tractor, to 500 s for the most downsized row crop medium-duty tractor. Rated power for the EM is determined in the same way.



On the contrary, peak power is taken as design requirement for the inverter, because the thermal time constant of power electronics is usually far lower than EMs. Battery current and power ratings are retrieved from (3.2), while battery capacity is sized according the iterative process presented hereafter.

### 3.4 Battery sizing and energy management tuning

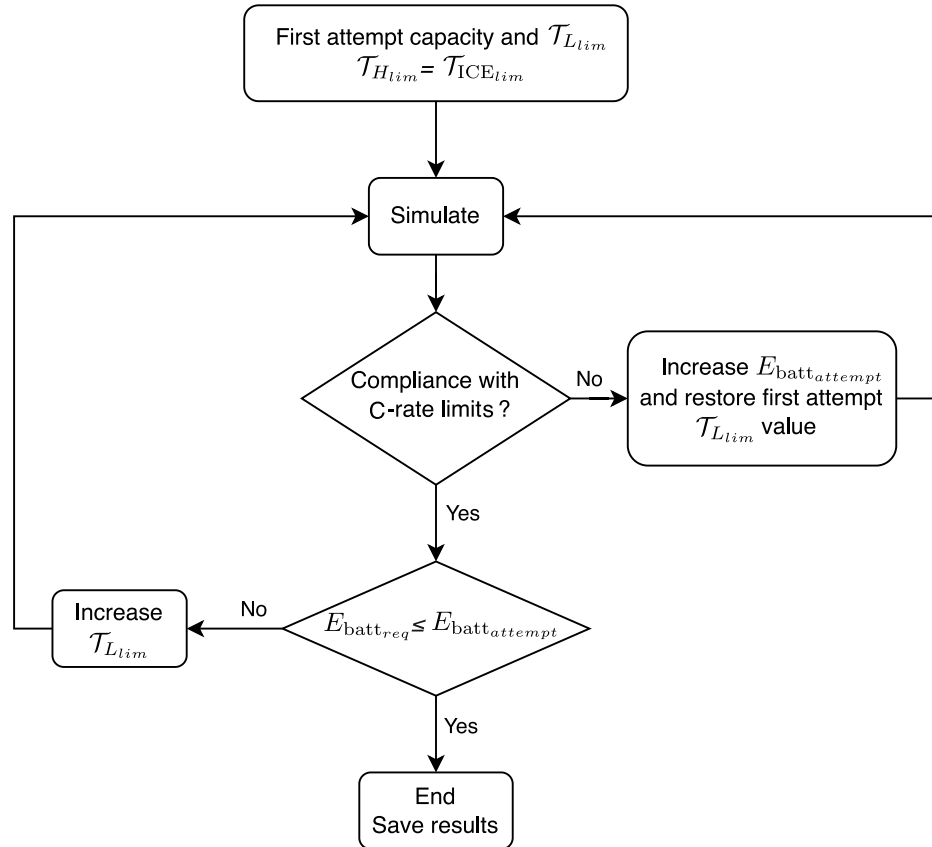


Figure 3.6: Battery capacity sizing iterative process.

In this section, battery sizing and energy management tuning is presented. In particular, detailed explanations are provided on how some model parameters are chosen, namely cell and battery capacity  $Cap_{cell}$ ,  $E_{batt}$ , and EMS lower and upper torque thresholds  $\mathcal{T}_{Llim}$ ,  $\mathcal{T}_{Hlim}(\Omega)$ .

The required battery capacity  $E_{batt\_req}$  for each load cycle is determined by multiplying the difference between the energy levels at the beginning and at the end of the cycle by the number of cycle repetitions necessary to achieve at least the minimum required daily operating time (i.e. 8 h), and adding the possible differences between maximum and initial energy levels, and between final and minimum energy levels. The obtained value is finally

### 3. LIFE CYCLE COST ANALYSIS OF HYBRID ELECTRIC TRACTORS

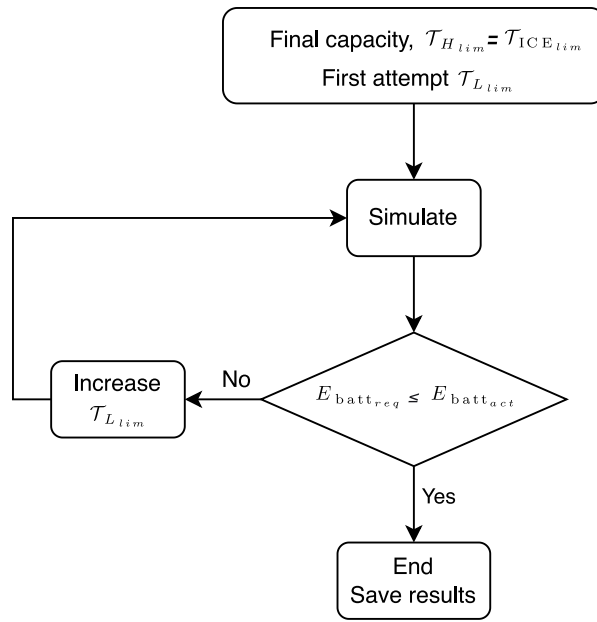


Figure 3.7: EMS tuning: lower torque threshold  $\mathcal{T}_{Lim}$ .

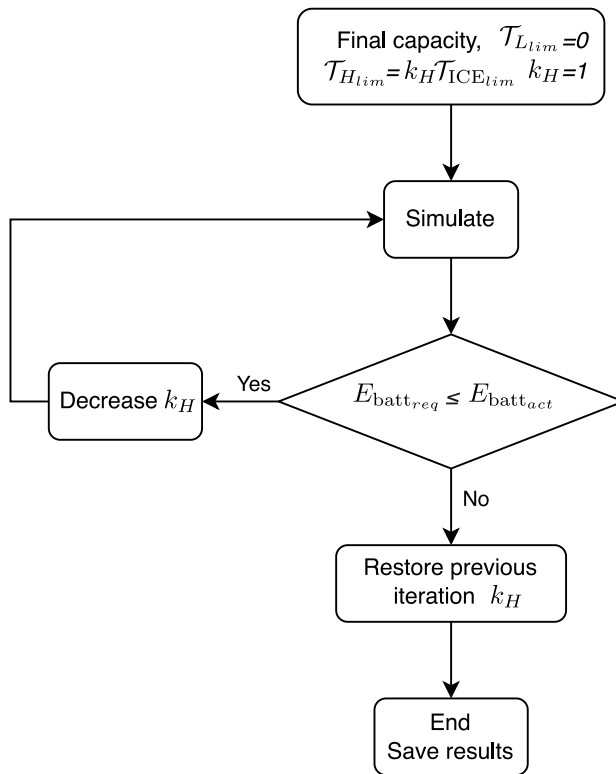


Figure 3.8: EMS tuning: upper torque threshold  $\mathcal{T}_{Hlim}$ .

divided by a certain depth of discharge (DoD) that is deemed acceptable. In this analysis, a conservative 60 % DoD is chosen in order to ensure a long battery life and to cope with the strong reliability requirements of agricultural industry [106]. Required battery capacity computation is summarized by the following equation:

$$E_{\text{batt}_{req}} = \left[ (E_i - E_f) \cdot \text{ceil} \left( \frac{t_{end}}{t_{min}} \right) + (E_{max} - E_i) + (E_f - E_{min}) \right] \cdot \frac{1}{\text{DoD}}, \quad (3.8)$$

where:

- $E_i$  and  $E_f$  are the battery energy levels respectively at the beginning and at the end of the operating cycle;
- $E_{max}$  and  $E_{min}$  are the maximum and minimum battery energy levels throughout the operating cycle, respectively;
- $t_{min}$  and  $t_{cycle}$  are the minimum required daily operating time and the single cycle duration, respectively.

The obtained capacity value depends on the energy management tuning, in particular on torque thresholds. The objective is to keep the battery capacity as low as possible for each downsized engine. Therefore, low attempt values for  $\mathcal{T}_{Llim}$  and battery capacity  $E_{\text{batt}_{attempt}}$  are used at first, while maintaining the upper limit  $\mathcal{T}_{Hlim}$  equal to the actual ICE torque limit curve  $\mathcal{T}_{ICElim}$ . Then, based on simulation results,  $\mathcal{T}_{Llim}$  and  $E_{\text{batt}_{attempt}}$  are adjusted according to the iterative process shown in Fig. 3.6. A higher  $\mathcal{T}_{Llim}$  threshold results in a more ICE-powered battery charging. The procedure is repeated until both battery capacity and C-rate requirements are fulfilled.

Once  $\mathcal{T}_{Llim}$  and capacity are determined for each load cycle, the final battery capacity  $E_{\text{batt}_{act}}$  is simply the maximum among values required by each cycle. Having set  $E_{\text{batt}_{act}}$ , the final value of EMS lower torque threshold  $\mathcal{T}_{Llim}$  can be determined. The process shown in Fig. 3.6 sets  $\mathcal{T}_{Llim}$  in order to minimize the battery capacity for each load cycle. However, except for the cycle that requires the maximum capacity, this approach leads to an unnecessary high lower torque threshold, which causes an increased fuel consumption. The process shown in Fig. 3.7 is used to determine the minimum possible  $\mathcal{T}_{Llim}$  value, maintaining the battery capacity required by a given cycle below or equal to the actual battery capacity  $E_{\text{batt}_{act}}$ . The lowest admissible value for EMS threshold  $\mathcal{T}_{Llim}$  is zero.

Finally, the EMS upper torque threshold curve  $\mathcal{T}_{Hlim}(\Omega)$  can be adjusted, maintaining  $E_{\text{batt}_{act}}$  and  $\mathcal{T}_{Llim}$  determined previously.  $\mathcal{T}_{Hlim}(\Omega)$  is obtained by multiplying the actual ICE torque limit curve by a coefficient  $k_H \leq 1$ . This factor can be lower than 1 only for the operating cycles that have  $\mathcal{T}_{Llim} = 0$ , otherwise a higher battery capacity or a higher  $\mathcal{T}_{Llim}$  would be needed. The

coefficient  $k_H$  is determined by gradually reducing it from 1, as shown in Fig. 3.8. Since row crop tractors operating cycles are very power-demanding compared to orchards and vineyards ones, lowering the amount of torque, and therefore power, that can be delivered by ICE results in a rapid increase of required battery capacity, however without significant operating cost savings. Thus,  $k_H$  is kept equal to 1 on the row crop tractors, i.e.  $\mathcal{T}_{H_{lim}}(\Omega) = \mathcal{T}_{ICE_{lim}}(\Omega)$ . This expedient contributes also in ensuring a long battery life by reducing its number of cycles.

## 3.5 Life cycle cost analysis

This work aims to provide a method to evaluate the economic feasibility of farming tractor electrification, and to determine the best engine downsizing, with a wide variety of variables. A life cycle cost (LCC) analysis is conducted to evaluate the economic convenience of a parallel hybrid electric tractor variant. LCC is the total present value of all the costs that occur during the life cycle of a product. In this study, only user costs are considered, whereas maintenance and disposal costs are ignored, as they are assumed to be equal for both hybrid electric and conventional powertrains, i.e. battery replacement is neglected. As discussed later, the best downsizing coefficient  $R$  results fairly close to 1 in both row crop tractors case studies, and also the fixed downscaling to 55 kW adopted in the specialized tractor do not lead to an excessive change of engine size. This outcome justifies the choice of constant maintenance costs. The LCC is computed as follows:

$$LCC = C_p + \sum_{t=0}^n \frac{C_t}{(1+d)^t} \quad (3.9)$$

where:

- $C_p$  is the initial investment cost (i.e. purchase);
- $C_t$  are all the relevant operating costs that occur during the analyzed period in the year  $t$ , fuel and electric energy consumption in this study;
- $t$  indicates the year when each operating cost  $C_t$  occurs. In general  $C_p$  could be treated exactly as all the future costs, but a separate term is introduced for clarity.
- $n$  is the period under study, in this case the service life; a general global engine life requirement lies between 6,000 and 12,000 hours, with high-power engines exhibiting longer rated lifetimes. In this work, a 10.000 h life is assumed, and years of life are computed dividing life in hours by the annual operating time;

- $d$  is the discount rate used to compute the present value of future costs. Literature reports discount rates ranging from 3.69 % [107] to 13.87 % [108], for German agriculture sector. An 8 % discount rate is chosen in this analysis.

The first term is indicated also as capital expenditure (Capex), while the second term given by the summation represents the overall operating costs (Opex) during the product life.

### 3.5.1 Powertrain components and energy pricing

In order to perform a LCC analysis, consumer prices of the various elements, as well as energy costs (fuel and electricity), need to be determined. All the components shared by both hybrid electric and conventional powertrains are ignored, and all prices are intended on consumer side. For all the considered powertrain main elements, a price range is taken into account, as prices cannot be exactly determined and could change most probably in the near future. Moreover, this choice allows the identification of those main components that have the highest impact on initial costs and overall LCC. It is important to consider a price range also for energy costs, in order to include possible country-related variations and future fluctuations.

### 3.5.2 Powertrain components costs

As regard capital expenditure, the following specific consumer-side costs are considered.

- *ICE*  
According to [15], for a high-technology 150 kW tractor, the engine represents about 19 % of the tractor cost. A survey of the market prices of 86 tractors with rated power ranging from 75 kW to over 200 kW is conducted. Assuming the 19 % fraction valid throughout all the power range, and performing a linear regression, the incremental price results approximately 290 €/kW. Since the percentage taken as reference is intended as a production cost, the obtained specific cost is rounded to 300 €/kW. This value is used as upper limit of ICE price range. Then, the price range is extended down to 50 €/kW. The latter limit is a very low value, and it is probably far from a real market price, however it is included to widen the payback time evaluation.
- *Battery*  
A price survey conducted in 2020 [109] reports a 137 \$/kWh volume-weighted average battery pack production price, so a 50 to 250 €/kWh price range is chosen to cover price reductions expected in the near future and the higher specific cost of power-oriented battery packs. Simulations show that the number of battery cycles does not reach excessive

### 3. LIFE CYCLE COST ANALYSIS OF HYBRID ELECTRIC TRACTORS

values, considering the adopted DoD. Mid-life battery pack replacement, thus, seems not necessary and battery cost can be accounted only once in LCC computation.

- *EM*

In 2017, the US DRIVE research center [110] stated that the production cost of a 100 kW peak-power EM lies in between 600 and 800 \$, which means 6–8 \$/kW peak). An older study [111] reported an approximate material cost range of 250–600 \$ for a 50 kW interior permanent magnet motor for automotive applications, depending on NdFeB price; and approximately 150 \$ for a 550 kW copper-rotor induction motor. For both motors, a 2.5 consumer price to material cost ratio was considered in the study. This results in 7.5–30 \$/kW peak power. Considering the lower production volumes of farming tractors compared to passenger vehicles, and the lower power of electric machines in a hybrid arrangement, as will be reported later in this work, a 15–60 €/kW price range is used.

- *PE (inverter and battery DC/DC regulator)*

In 2017, the US DRIVE research center reported a 1000 \$ production cost of a 100 kW peak-power electric drive for automotive applications, i.e. 10 \$/kW. Another work [112] presented a price range of approximately 800–8500 \$ for a 60 kW inverter (i.e. 13–142 \$/kW), where the higher values refer to an oversized system intended to improve reliability. In this study, a 15–60 €/kW range is chosen, taking into account the production volume and power aspects presented above regarding EM pricing.

Other additional devices and subsystems needed for powertrain electrification, e.g. additional clutches and cooling systems, as well as development costs, are ignored. Anyway, this approach is partially balanced by the fact that load cycles are unchanged despite ICE downsizing, resulting in slightly higher operating costs.

#### **Energy costs**

As regard operating costs, the following specific consumer-side energy prices are considered.

- *Agricultural diesel fuel*

In [113], prices around 0.9 €/L are used for agricultural diesel fuel. The range considered in this work is 0.7–1.3 €/L.

- *Electric energy*

Electric energy price is based on data published by the Italian authority ARERA [114] for low-voltage non-household consumers. Depending on the time band, electricity price, without VAT, ranges from approximately 0.155 to 0.18 €/kWh (September 2021). A price equal to 0.16 €/kWh is

chosen, as it is assumed that charging would happen mainly at night. The analysis is extended down to 0.1€/kWh and up to 0.28€/kWh.

### Standard specific prices

For each tractor category, a “*standard*” combination of components and energy specific prices is selected in a preliminary analysis. The selection is based on prices deemed most realistic at the time of writing. The following are assumed equal for the three tractor categories, unless explicitly indicated.

- ICE: 200 €/kW.
- Battery: 150 €/kWh.
- EM: 40 and 30 €/kW continuous rated power, for specialized and row crop tractors, respectively. A higher value is assumed for the specialized tractor due to the considerably lower EM rating, as will be shown later.
- PE: 30 €/kW peak power.
- Fuel: 0.9 €/L
- Electric energy: 0.16 €/kWh.

## 3.6 Results

Despite at the beginning this study was intended to cover a wide variation of ICE downsizing degree, preliminary simulations showed that a further reduction of ICE rated power requires a high battery capacity, exceeding 40 kWh, that in turn leads to high initial costs and could possibly not comply with packaging requirements [115]. On the contrary,  $R$  values very close to 1 are not investigated since all the hybrid electric powertrain components would be needed anyway, increasing tractor complexity and cost without resulting in significant operating costs savings. For the row crop medium tractor, a 0.8–0.92  $R$  range is analyzed taking three discrete values, while on the heavy duty tractor the analysis is limited to two values: 0.88 and 0.92. For the specialized tractor, a battery capacity comparable to the ones of the two larger tractors is obtained: this outcome is deemed acceptable, as ICE downsizing below 56 kW results in less restrictive emission regulations, so that some exhaust gas treatment devices can be removed, thus clearing more space onboard and limiting costs.

Tab. 3.3 reports relative variations on operational expenditure (Opex) for each hybrid tractor, compared to the conventional counterpart, with the aforementioned “*standard*” fuel and electric energy prices (Section 3.5.2). Negative values represent savings. The operational economy gain is far greater for the specialized tractor than for row crop tractors, in particular when compared

### 3. LIFE CYCLE COST ANALYSIS OF HYBRID ELECTRIC TRACTORS

to the heavier vehicle. This outcome is related to the operating cycles: operations become progressively more power-intensive moving from specialized to row crop heavy tractor, as presented in Section 3.2. Indeed, savings are higher when performing low-power tasks, as the original ICE operates in a low-efficiency region. Reducing engine size results in a better exploitation, moving the operating point to a higher efficiency region. Engine downsizing alone is responsible for approximately 15 % savings in low-power orchard and vineyard tasks (e.g. plant lifting plow and tying machine), as proven by results in *hybrid 1* mode, where full electric driving is completely avoided.

It is interesting to notice that in some load cycles, the operating costs of the hybrid variants are higher than their conventional counterparts (positive relative variations). This outcome is caused by the significant battery charging that is needed in some operations to ensure SoC constraints at the end of the minimum required daily working time. In these situations, ICE load point shifting to higher efficiency regions could not compensate for losses arising from double energy conversions.

The fractions of useful work that come from electric energy are reported in Tab. 3.4. From a comparison with Tab. 3.3, it is relevant to notice that no clear correlation exists between cost savings and fractions of useful work covered by electric energy. Indeed, if ICE is operated in a high-efficiency region (e.g. engine efficiency around 0.4), there is no huge difference between diesel and electric energy cost per unit of useful work. As a consequence, except for low-power cycles, where the original ICE works in low-efficiency regions, the vast majority of the savings comes from ICE load point shifting.

As regard initial investment cost, ICE and battery are the components with the highest influence on the purchase price of a hybrid tractor, as they represent the two major fractions of the capital expenditure (Capex) in Fig. 3.9.

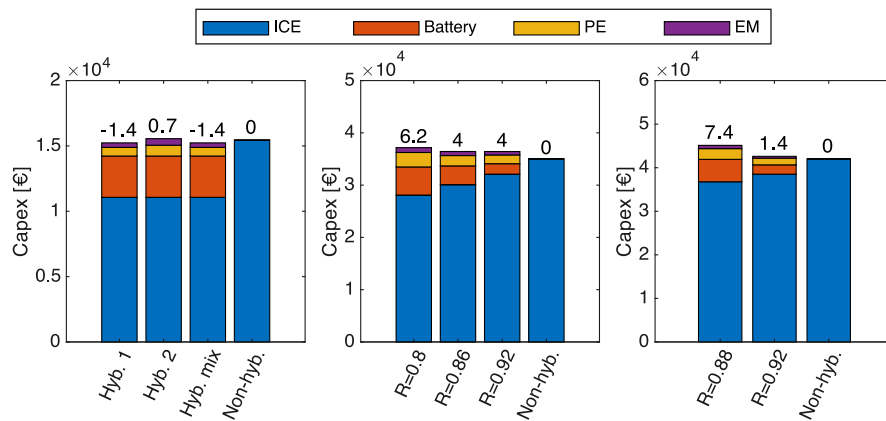


Figure 3.9: Capex of hybrid electric specialized, row crop medium and heavy tractors. Percentage variations with regard to conventional counterparts are shown above bars.



Table 3.3: Operating costs relative variation per cycle.

Operation	Opex difference (%)		
	Specialized tractor		
	Hyb. 1	Hyb. 2	Hyb. mix
Weeder	-3.31	-3.31	-3.31
Atomizer	-0.96	-2.17	-2.17
Grape harvester	-7.72	-8.43	-8.43
Plant lifting plow	-14.85	-17.99	-14.85
Tying machine	-16.06	-24.09	-24.09
<b>Average</b>	-6.88	-8.77	-8.14
	Row crop medium-duty use		
	$R = 0.8$	$R = 0.86$	$R = 0.92$
Heavy plowing	-1.56	-1.95	-1.74
Medium plowing	-5.33	-4.32	-3.30
Rotary harrow	-4.67	-3.98	-3.17
Field transport and idling	-1.42	0.35	2.57
<b>Average</b>	-3.60	-3.14	-2.41
	Row crop heavy-duty use		
	$R = 0.88$	$R = 0.92$	
Subsoiler		1.46	0.54
Cultivator		-0.11	-0.16
Heavy plowing		-0.99	-0.71
Tiller		-0.68	-0.48
Rotary harrow		-1.83	-1.25
Road transport		-1.73	-1.14
Idling		-3.00	-1.92
<b>Average</b>		-0.67	-0.54

Fig. 3.10 shows LCC composition and highlights the best engine downsizing or hybrid mode for the “standard” price combination. In the specialized tractor case, the best mode results *hybrid mix*, as the slightly higher operating costs savings achieved with *hybrid 2* are not enough to compensate for its higher purchase cost. Nevertheless, all the three hybrid modes achieve a lower LCC than the non-hybrid tractor. In row crop medium-duty case, the LCC benefit is always quite low for all the three  $R$  values.  $R = 0.86$  is the best downsizing degree for this tractor category, although LCC is very close to the one obtained with  $R = 0.8$ . In row crop heavy-duty case, the best  $R$  value is

### 3. LIFE CYCLE COST ANALYSIS OF HYBRID ELECTRIC TRACTORS

Table 3.4: Fractions of useful work performed using electric energy.

Operation	Work fraction (%)		
	Hyb. 1	Hyb. 2	Hyb. mix
Specialized tractor			
Weeder	4.09	4.09	4.09
Atomizer	0.05	2.77	2.77
Grape harvester	0	6.10	6.10
Plant lifting plow	0	12.16	0
Tying machine	0	25.56	25.56
Row crop medium-duty use			
	$R = 0.8$	$R = 0.86$	$R = 0.92$
Heavy plowing	2.03	1.35	0.71
Medium plowing	0	0	0
Rotary harrow	0.19	0.04	0.01
Field transport and idling	6.62	3.97	0.84
Row crop heavy-duty use			
	$R = 0.88$	$R = 0.92$	
Subsoiler		1.34	0.55
Cultivator		0	0
Heavy plowing		0.2	0.06
Tiller		1.43	0.60
Rotary harrow		0	0
Road transport		1.89	1.17
Idling		0	0

0.92. However, the benefit compared to the conventional non-hybrid variant is negligible. Initial cost increases significantly with a more downsized ICE ( $R = 0.88$ ), whereas annual savings do not raise appreciably, resulting in an overall LCC increase.

The effects of ICE and battery costs on LCC as a function of ICE downsizing ( $R$ ) are shown in Figs. 3.11, 3.12, for the two row crop tractors. The best downsizing coefficients are highlighted in the graphs. When ICE cost variation is considered (Figs. 3.11a, 3.12a), battery price is fixed to 150 €/kWh; on the contrary, ICE price is set to 200 €/kW, when battery cost variation is analyzed (Figs. 3.11b, 3.12b). EM and PE prices are kept equal to the “standard” values previously introduced (Section 3.5.2). As expected, the higher the ICE cost, the more convenient the ICE downsizing. This trend is clearly distinguishable on the medium-duty row crop tractor (Fig. 3.11a), whereas it is not so visible

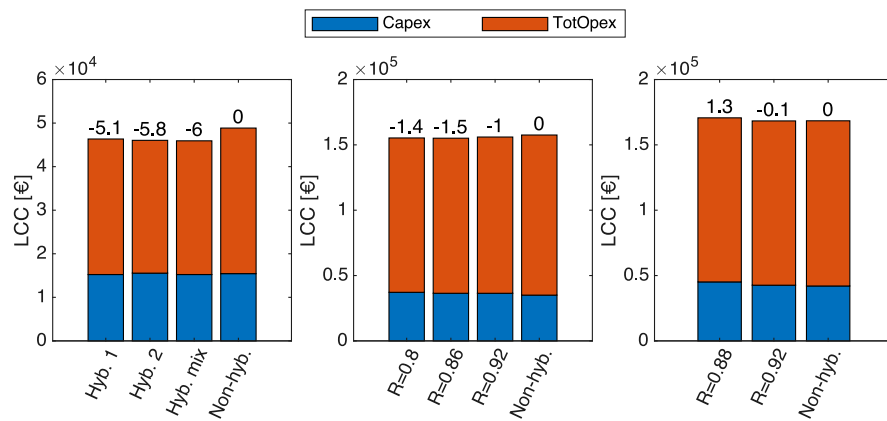


Figure 3.10: LCC of hybrid electric specialized, row crop medium and heavy tractors. Percentage variations with regard to conventional counterparts are shown above bars.

on the heavier tractor, as the less downsized hybrid variant remains always more convenient than the more downsized one (Fig. 3.12a). Only when a very high ICE cost is combined with a very low battery cost, the more downsized variant becomes more convenient. The opposite behavior is found when ICE cost is fixed and battery cost changes (Figs. 3.11b, 3.12b).

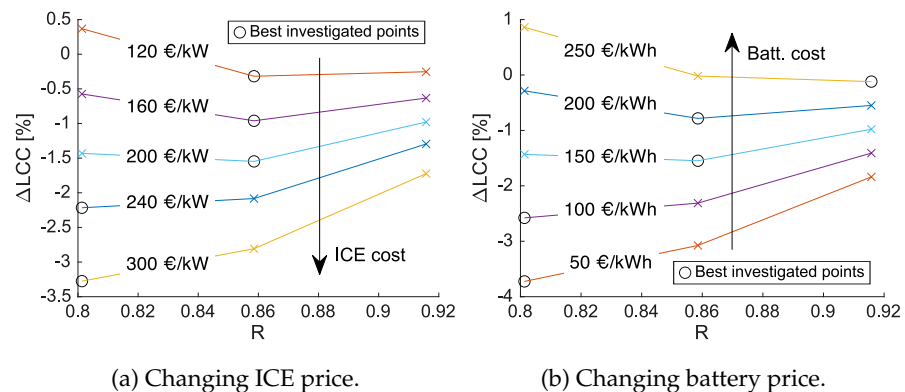


Figure 3.11: Medium-duty row crop tractor: LCC variation with engine downsizing factor.

In this work, payback time (PBT) refers to the minimum time after which a hybrid electric tractor becomes more convenient than its non-hybrid counterpart. It is computed varying the reference period  $n$  in (3.9). Figs. 3.13, 3.14 show PBT variation with ICE and battery price. For sake of clarity, only three battery prices are shown in the pictures: 100, 150, and 200 €/kWh. Results already take into account the best ICE downsizing or hybrid mode, respectively for row crop and specialized tractors. PBT trend is consistent with LCC

### 3. LIFE CYCLE COST ANALYSIS OF HYBRID ELECTRIC TRACTORS

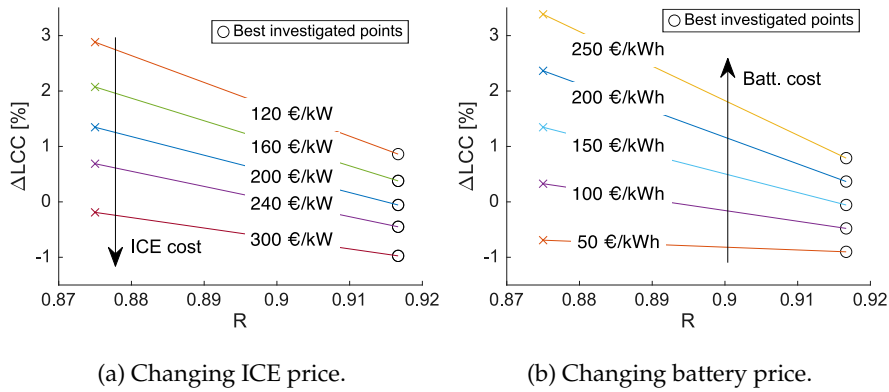


Figure 3.12: Heavy-duty row crop tractor: LCC variation with engine downsizing factor.

behavior: a lower ICE cost combined with a higher battery price leads to a higher penalty on purchase cost for hybrid variants, which is mostly not recoverable during tractor service life. This phenomenon affects especially the row crop heavy-duty vehicle, as shown in Fig. 3.14b. Since the annual savings are very low in this case, either the hybrid variant is already cheaper from the beginning, or the price penalty will not be recovered during service life, except for few improbable price combinations. Small dents in Fig. 3.14a are due to the changing optimal  $R$  value varying ICE cost.

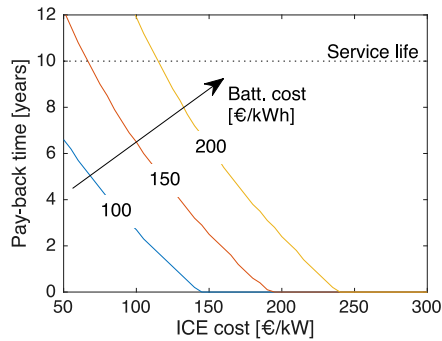


Figure 3.13: Payback time of specialized hybrid electric tractor as a function of ICE and battery price.

Figs. 3.15, 3.15 report LCC behavior varying diesel fuel and electric energy prices. Specific costs of powertrain main components are set to the "standard" values.

In the case of specialized tractor for orchards and vineyards, a lower diesel price and higher electric energy price favor hybrid modes that make less use of full electric driving (e.g. *hybrid 1*), as expected, and vice versa. Nonetheless, *hybrid 1* never becomes the most convenient mode, unless electric energy price

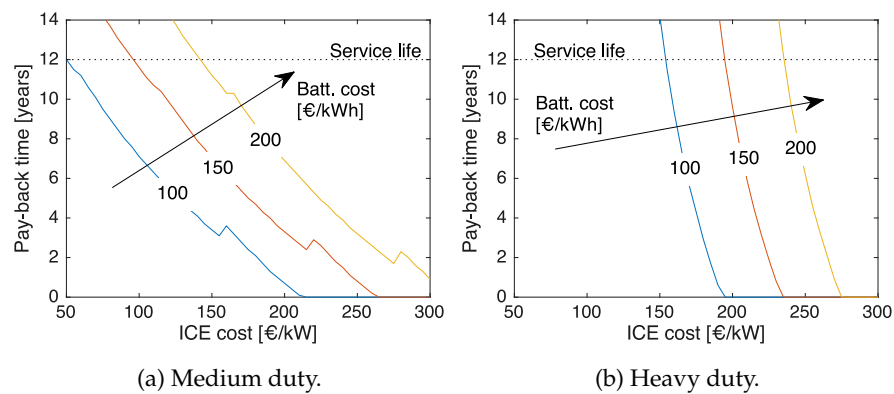


Figure 3.14: Payback time of row crop hybrid electric tractors as a function of ICE and battery price.

is implausibly high. Moreover, it emerges that the hybrid variant always show a considerably smaller LCC than the non-hybrid conventional counterpart.

Despite the same LCC trends can be identified on both row crop tractors, the advantage of hybrid variants is lower or does not even exist. A major aspect that appears from this analysis is that on the heavy duty row crop tractor the variant with the more downsized engine has a higher LCC than the conventional tractor, even combining the highest diesel price with the lowest electric energy price.

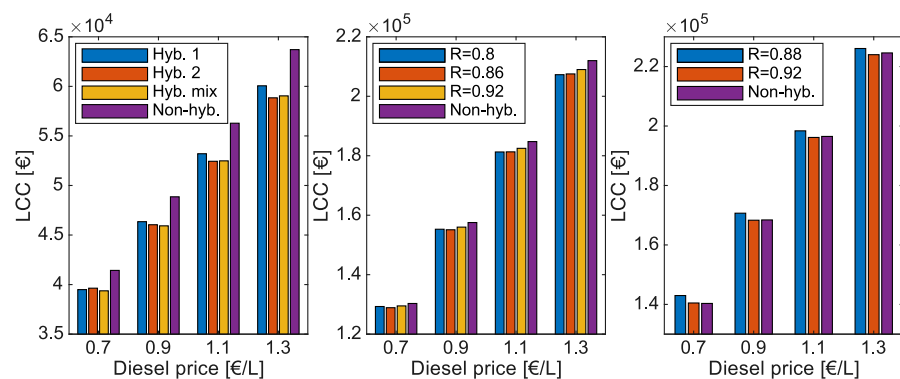


Figure 3.15: LCC behavior with varying diesel fuel price and fixed electric energy price (0.16 €/kWh).

Fig. 3.17 shows  $\text{CO}_2$  emissions in the three case studies. Emission reductions are consistent with operating cost savings (Tab. 3.3), except for the more downsized heavy duty row crop tractor. In this case, the increase of emissions from battery production and electric energy use, compared to  $R = 0.92$  variant, overcomes the  $\text{CO}_2$  reduction given by the lower fuel consumption.

### 3. LIFE CYCLE COST ANALYSIS OF HYBRID ELECTRIC TRACTORS

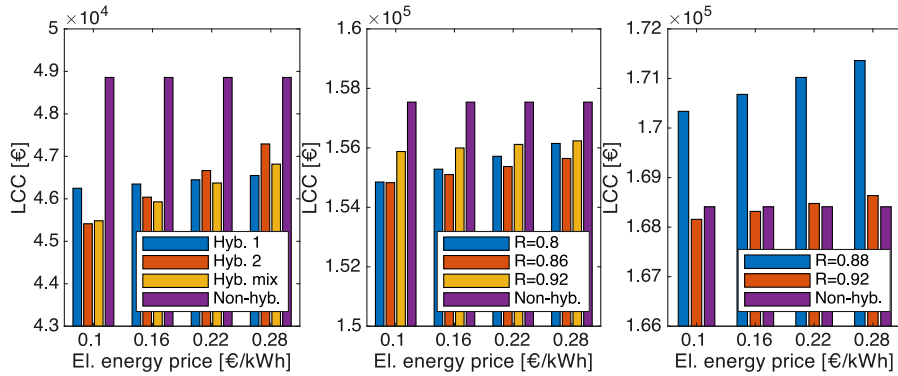


Figure 3.16: LCC behavior with varying electric energy price and fixed diesel fuel price (0.9 €/L).

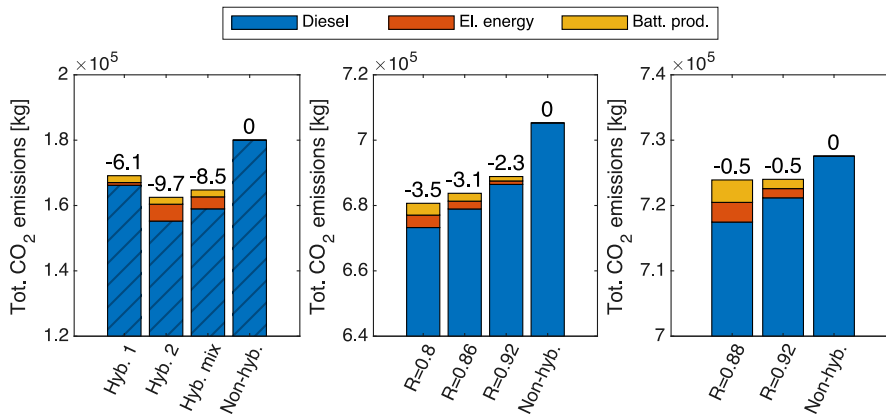


Figure 3.17: Total CO<sub>2</sub> emissions of hybrid electric specialized, row crop medium and heavy tractors. Percentage variations with regard to conventional counterparts are shown above bars.

#### 3.6.1 Main specifications and savings summary

Tab. 3.5 summarizes main electric system specifications and savings, computed with the “standard” price combination for each optimal arrangement of every case study. As expected, the specifications required for the specialized tractor in terms of EM torque and PE power are the least demanding, because of the less intensive load cycles, although engine downsizing is relatively high. On the contrary, battery size is comparable with row crop tractors, most probably due the different operations, i.e. limited possibility for ICE-powered battery charging. When comparing the two row crop tractors, it emerges that the medium-duty vehicle requires higher ratings, except for peak torque. Despite this outcome could initially appear counterintuitive, it is consistent with the lower  $R$  value, namely a more downsized ICE.

Initial cost of the specialized tractor is lower for the electrified version. This

result could be explained by the fact that the costs of additional devices needed for powertrain electrification, as well as development costs, are ignored. These aspects have a higher relative weight on a small tractor. Thus, this result is most probably too optimistic.

As regard LCC, savings with the specialized tractor are significant, even though not as relevant as in road vehicles. On the opposite, LCC reduction is considerably lower on the row crop medium tractor, and negligible on the heavy-duty one. This outcome is strictly related to the decrease of operational savings moving to tractors that perform more power-intensive tasks.

Table 3.5: Main electric specifications and summary of cost variations.

	Specialized tractor <i>hybrid mix</i>	Row crop medium $R = 0.86$	Row crop heavy $R = 0.86$
<hr/>			
EM torque (Nm)			
Overload peak	147	382	471
Continuous rating	63	157	118
<hr/>			
EM power (kW)			
Overload peak	22	66	51
Continuous rating	9	26	14
<hr/>			
Battery capacity (kWh)	21	24	14
<hr/>			
Capex			
Conventional (€)	15 442	35 018	42 022
Hybrid electric (€)	15 233	36 433	42 658
Relative variation (%)	-1.4	4.0	1.4
<hr/>			
Opex			
Conventional (€/year)	4980	16 258	16 771
Hybrid electric (€/year)	4574	15 747	16 681
Relative variation (%)	-8.2	-3.1	-0.5
<hr/>			
PBT (years)	0	3.3	9.6
<hr/>			





## 4 INVESTIGATION ON HARMONIC BALANCE METHOD

---

In this chapter, the harmonic balance technique is applied to a 2D non linear finite-element magnetic model with motion, coupled to a non linear circuit. The case study comprises a six-pole three-phase surface-mounted permanent magnet generator connected to a six-pulse full-wave diode bridge rectifier. Simulations are performed at fixed generator speed in two operating cases: with an open-circuit DC bus and supplying a load resistance. An exhaustive description of the case study is provided to allow an easy repeatability of this work.

Both time stepping and harmonic balance approaches are deeply discussed focusing on the model under study, along with relevant implementation details. Harmonic balance results are compared with benchmark time stepping outcomes in terms of voltage and current waveforms, progressively expanding the harmonic spectrum included in the simulations. The computational performance of the two approaches are compared in the end.

This work was carried out during my period abroad at Université Libre de Bruxelles, under the co-supervision of Prof. Johan Gyselinck and with the relevant contribution of Prof. Ruth V. Sabariego.

### 4.1 Introduction

Computing hardware have progressed impressively fast in the last two decades, and this trend is expected to keep growing in a short term perspective. Today computers far outperform their older counterparts of twenty years ago: CPUs can perform the same tasks ten times faster and memory storage devices have improved their capacity exponentially. Thanks to the increasing computational resources available for science and engineering, research on software and computational methods is more relevant than ever. The increasing computing power available in laboratories opens new possibilities every day, and a lot of scientists and engineers are trying to give answers on the best ways to exploit these new powerful resources. Indeed, today hardware allows the implementation of many simulation approaches whose requirements were prohibitive just less than ten years ago. Furthermore, code optimization and faster numerical techniques are still of key importance in improving R&D and design methodologies, thus reducing products time to market, especially in high-tech sectors and advanced applications.

Fast simulation techniques are of great interest, in particular when dealing with parametric sweep analyses and design optimization processes. Despite its higher memory requirement, the harmonic balance (HB) method can potentially decrease the computational cost of steady-state analyses of non linear systems with regard to the mainstream time stepping approach (TS), as it

#### 4. INVESTIGATION ON HARMONIC BALANCE METHOD

completely avoids initial transients [116]. Nonetheless, the application of this method to real-world engineering applications have not been widely investigated yet, and computational cost gains are not to be taken for granted. In particular, finite element HB simulation of rotating machinery coupled with non linear circuits has received little attention.

Steady-state simulations of non linear systems are mostly carried out in the time domain [117]. The straightforward implementation of TS schemes together with efficient algebraic sparse solvers makes this method the state-of-the-art general-purpose approach for the resolution of multi-physics non linear systems of partial differential equations (PDEs) [118, 119]. Since TS makes use of sparse matrices with a relatively small size, its memory requirements are affordable with common hardware. However, many time steps may be required to step first through the initial transient and then through a fundamental period at quasi steady state, especially in systems with a slow dynamic. Moreover, time step size may need to be particularly small to simulate zero-crossing events with a sufficient accuracy when dealing with non linear lumped elements, for instance power electronics components. Thus, the computational cost may increase significantly. Variable time step algorithms are usually implemented in these cases to improve performance without losing accuracy [120, 121].

On the contrary, frequency-domain approaches are not as widely adopted as TS methods. Single-frequency simulations using complex phasors representation are well-known [122]. Nevertheless, their applicability is limited to linear systems, where harmonic frequencies do not have any influence on one another [123]. This condition is never fulfilled when the system under analysis exhibits some sort of non linearity [124]. As an example, in non linear cases a source term acting only on the fundamental (first) frequency can affect all the rest of the harmonic spectrum. Harmonic balance is a more general frequency-domain approach that can handle these problems [125]. Memory requirements are always higher than TS, as HB relies on the solution of a single but larger algebraic system [126]: the higher the number of harmonics, the larger the system. Moreover, peculiar non linearities may require a high number of harmonic frequencies to reach a satisfying simulation accuracy [127], further increasing memory requirements [128]. On the other hand, HB provides directly a steady-state solution. Therefore, its application can potentially decrease the computational time [129], in particular for systems with slow dynamics, i.e. a relatively long initial transient.

The HB technique, firstly proposed only for circuit models [130, 131], has already been applied to 2D non linear finite-element (FE) analyses of rotating electric machines [132, 133] and stationary electromagnetic devices [134, 135]. However, to the best of the authors' knowledge, HB has never been tried on a system that couples a 2D non linear FE model with motion to a non linear circuit. The case study of this work comprises a synchronous generator with

iron saturation connected to a diode rectifier. A three-phase system is chosen to increase complexity. It is worth to mention that the chosen case study is a real-world engineering application. Open circuit and load conditions are simulated using both HB and TS approaches. Results and computational performance are compared and discussed.

This chapter is structured as follows: Section 4.2 describes the case study, how it is modeled and the PDEs general formulation; in Section 4.3 discrete algebraic equations (DAEs) of TS and HB methods are mathematically derived, showing also how non linearities and movement are handled; in Section 4.4 accuracy and performance of HB simulations are compared to benchmark TS results and the outcomes are discussed and commented; Section 4.5 summarizes the conclusions of this investigation.

## 4.2 Case study and modeling

The case study under analysis features a six-pole three-phase surface-mounted permanent magnet (SPM) generator connected to a six-pulse full-wave diode bridge rectifier. This electric generation arrangement is used in many areas: in automotive applications, it is common practice for low-voltage conventional electric systems, high-voltage electrification of engine auxiliaries and hybrid electric drivetrains; in power systems, it is the most simple front-end configuration for low-power wind turbines. In particular, the system under analysis is suitable for the electrical supply of auxiliaries of high-power diesel engines, with the generator connected to engine shaft through a speed reducer gearset. Relevant machine geometric and electric parameters are summarized in Table 4.1, together with continuous ratings. The phase resistance is estimated analytically, while the phase inductance is computed by means of magnetostatic FE analysis.

Figure 4.1 outlines the 2D FE machine model. Only a sixth of a planar section orthogonal to the machine axis is modeled: machine periodicity is exploited by implementing anti-periodic boundary conditions (BCs), as shown in Figure 4.1a. On the remaining boundary curves, the magnetic vector potential is set to 0 with classical Dirichlet BCs ( $a_z = 0$ ). Rotor movement inside stator is handled with the well-established moving band technique. Windings inside slots are modeled as stranded conductors, i.e. current density is uniform on each slot cross section area, skin and proximity effects are neglected. A full-pitch distributed configuration is adopted to increase the harmonic content of the airgap magnetomotive force, leading to a heavier computational load for the HB approach. Linear magnetic regions comprise air and the permanent magnet, which is simulated with a recoil line model identified by coercivity and remanence. Non linear iron of electrical steel fills the rest of the domain.

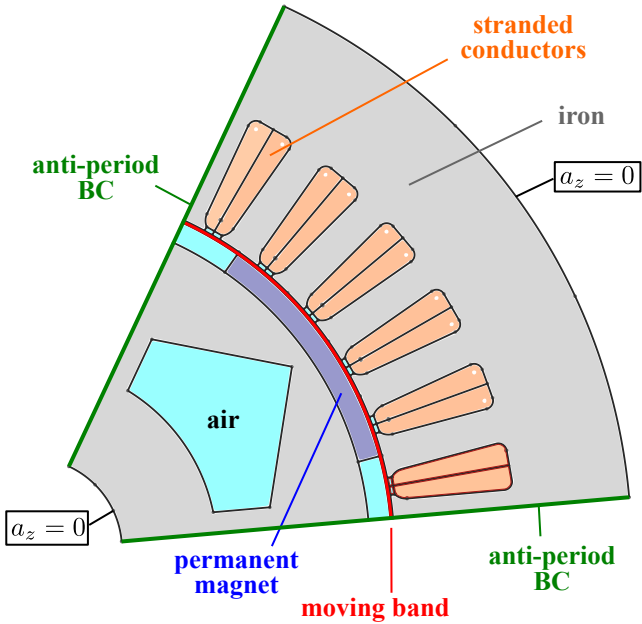
#### 4. INVESTIGATION ON HARMONIC BALANCE METHOD

Table 4.1: SPM generator parameters and continuous ratings.

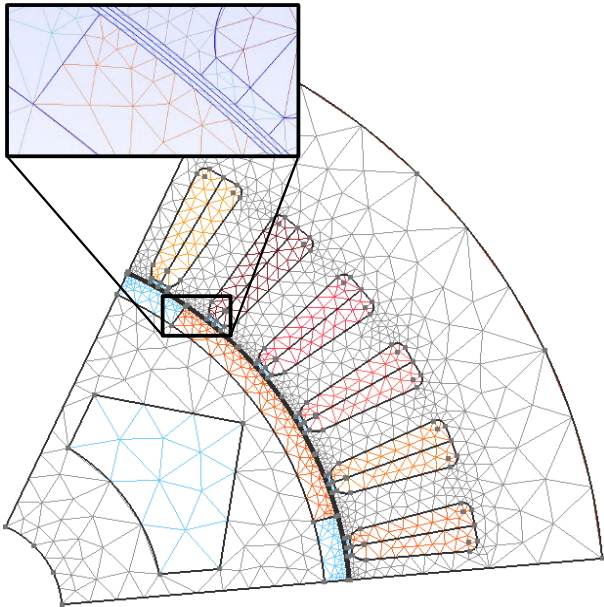
Parameter	Symbol	Value	Unit
<b>Continuous ratings</b>			
Power	$P$	12.5	kVA
Line to line voltage	$V$	400	V (rms)
Current	$I$	18	A (rms)
Frequency	$f_s$	300	Hz
Speed	$n_s$	6000	rpm
Braking torque	$\mathcal{T}$	20	Nm
<b>Geometrical parameters</b>			
Number of pole pairs	$p$	3	
Phases	$m$	3	
Airgap thickness	$g$	1.0	mm
Axial stack length	$L_{stk}$	100	mm
<b>Stator</b>			
Slots	$Q$	36	
Airgap diameter	$D_s$	103	mm
Outer core diameter	$D_e$	170	mm
Tooth width	$w_t$	5.0	mm
Slot height	$h_s$	17.3	mm
<b>Rotor</b>			
PM thickness	$t_m$	3.1	mm
PM angle	$\alpha_m$	40	deg
<b>Material properties</b>			
PM coercivity	$H_c$	818	kA/m
PM relative permeability	$\mu_{r_{pm}}$	1.07	
<b>Electric parameters</b>			
Phase resistance	$R_s$	0.15	$\Omega$
Synchronous inductance	$L_s$	1.5	mH
No-load flux linkage	$\Lambda_0$	0.19	Vs

The model is meshed using Gmsh [136]. The mesh comprises by 1677 nodes and 3473 triangular conforming elements. Stator and rotor boundary curves toward airgap moving band region are discretized with 82 nodes each. The meshed model is shown in Figure 4.1b. A zoom close to the airgap is also reported, with the moving band region not meshed initially.

The complete case study is outlined in Fig. 4.2: the 2D non linear FE model



(a) Machine model.



(b) Meshed model with a zoom on airgap.

Figure 4.1: 2D finite-element model of the SPM generator.

of the generator is coupled with a non linear circuit comprising a six-pulse full-wave diode bridge rectifier and a possible load resistance  $R_L$ , modeled

#### 4. INVESTIGATION ON HARMONIC BALANCE METHOD

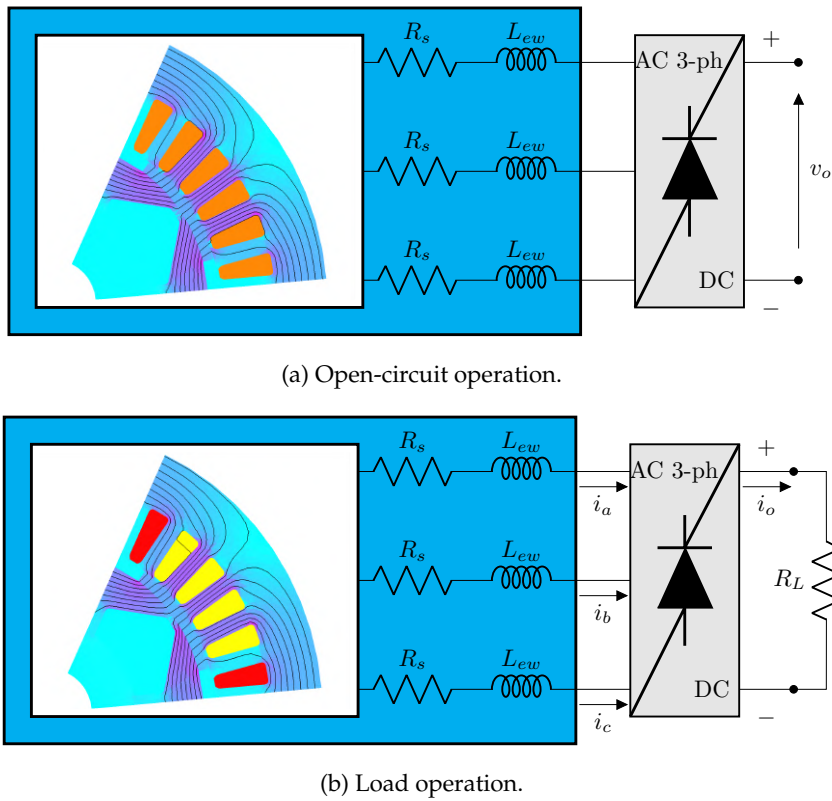
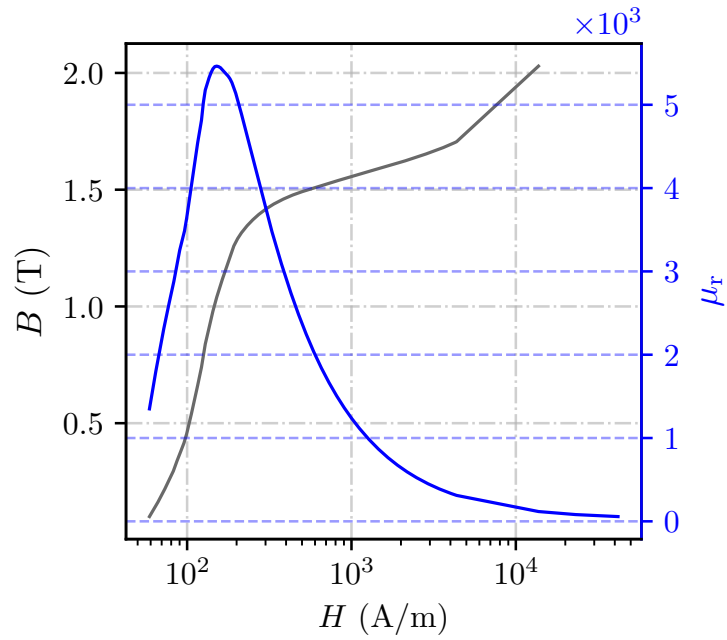
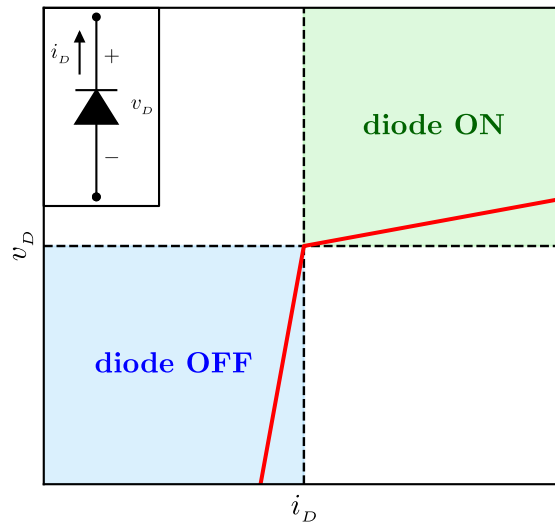


Figure 4.2: Case study outline.

with lumped circuit elements. Since the simulation comprises only two dimensions, the contribution of end winding  $L_{ew}$  to synchronous inductance should be considered. However, in this work end winding contribution is taken into account only for phase resistance, whereas 3D inductive effects are not considered, being their contribution negligible. Nonetheless, the comparison between TS and HB approaches remains valid, as the model used for all the simulations is the same. Analyses are carried out in two different operating conditions: at open circuit (Fig. 4.2a) and supplying a  $16 \Omega$  DC load resistance  $R_L$  (Fig. 4.2b). In both conditions the generator is rotating at a fixed speed of 6000 rpm, which corresponds to the rated value of the machine, thus leading to a 300 Hz fundamental frequency. It is worthwhile to notice that the machine phase resistances  $R_s$  are modeled with lumped elements too, while electromotive force generation and inductive effects are accounted by the finite-element model. No lumped inductances or capacitances are included in the coupled circuit.



(a) Single-quadrant BH curve and relative permeability of iron.



(b) VI characteristic of diodes.

Figure 4.3: Modeling of non linearities.

### 4.2.1 Non linearities

Two non linearities are present in the complete model of the case study under analysis: iron magnetic saturation in FE machine model and diodes non linear voltage-current (VI) characteristic in coupled lumped elements circuit. Models of non linearities are depicted in Fig. 4.3.

#### 4. INVESTIGATION ON HARMONIC BALANCE METHOD

Non linear magnetic behavior of electrical steel is simulated with a conventional single-quadrant  $BH$  curve. The characteristic used in the simulations is reported in Fig. 4.3a, together with the associated relative permeability curve.

$$B = \mu_r(H)\mu_0 H .$$

$B$  and  $H$  are the magnitudes of flux density and magnetic field vectors, respectively, while  $\mu_0 = 4\pi \cdot 10^{-7} \text{ H m}^{-1}$  is the air permeability and  $\mu_r$  is iron permeability. Hereafter, iron non linearity is treated in terms of magnetic reluctivity, as a more suitable approach in frame of the adopted formulation:

$$H = \nu_r(B)\nu_0 B ,$$

where the relative reluctivity is the defined as:

$$\nu_r = \frac{1}{\mu_r} ,$$

and  $\nu_0$  is air reluctivity. The iron is considered isotropic, even though the treatment explained hereafter can be extended to generic anisotropic electrical steel.

Diodes are modeled as non linear lumped resistances to approximate an ideal VI characteristic, as depicted in Fig. 4.3b. When the current through the diode  $i_D$  is positive, the element is conducting and its resistance  $R_D$  is quite low (ideally a short circuit), leading to a small voltage drop  $v_D$ . On the contrary, when the current is negative diode resistance is quite high (ideally an open circuit), thus voltage across the diode is high.

$$v_D = R_D(i_D)i_D .$$

$$R_D = \begin{cases} 0.1 \Omega & i_D \geq 0 \\ 10^4 \Omega & i_D < 0 \end{cases} .$$

#### 4.2.2 2D AV formulation

A 2D quasi-static formulation in the magnetic vector potential is adopted for the given model. The formulation is derived from magneto quasi-static Maxwell equations in differential local form and materials constitutive laws, coupled with lumped circuit elements characteristics and Kirchhoff laws. Boundary and interface conditions are also fundamental in the whole FE domain ( $\Omega$ ). However, for the sake of brevity they are not reported. The curl of the magnetic field  $\vec{h}$  is given by current density  $\vec{j}_s$  in stranded coil regions ( $\Omega_s$ ), considering also the coercive force field  $\vec{h}_c$  in permanent magnet subdomain ( $\Omega_{\text{pm}}$ ).

$$\left(\nabla \times \vec{h}\right)_{\Omega} - \left(\nabla \times \vec{h}_c\right)_{\Omega_{\text{pm}}} = \left(-\vec{j}_s\right)_{\Omega_s} . \quad (4.1)$$

Since machine winding are modeled as stranded conductors, the current density vector can be expressed as:

$$\vec{j}_s = k_{s_i} \vec{i}_s , \quad (4.2)$$



where  $\vec{i}_s$  is the current vector flowing through the winding and  $k_{s_i}$  is a coefficient defined as the ratio between the number of equivalent series turns and the cross section surface area of the winding coil, including slot fill factor:

$$k_{s_i} = k_{fill} \frac{N_{t_s}}{S_s} .$$

In stranded conductors, the curl of the electric field  $\vec{e}$  is given by the time variation of the magnetic flux density vector:

$$\left( \vec{\nabla} \times \vec{e} \right)_{\Omega_s} = \left( -\frac{\partial \vec{b}}{\partial t} \right)_{\Omega_s} . \quad (4.3)$$

Magnetic constitutive laws are generally non linear due to the presence of iron saturation in non linear regions ( $\Omega_{NL}$ ), even though many subdomains have a linear relation, as in air regions ( $\Omega_0$ ), machine slots ( $\Omega_s$ ) and permanent magnet ( $\Omega_{pm}$ ).

$$\left( \vec{h} \right)_{\Omega_{NL}} = \left( \nu_r(\vec{b}) \nu_0 \vec{b} \right)_{\Omega_{NL}} . \quad (4.4)$$

In the case study under analysis, iron reluctivity depends only on the magnitude of the flux density  $B = \|\vec{b}\|$ , being the material isotropic and neglecting any magnetic hysteresis phenomena.

Kirchhoff voltage law prescribes a null electric potential difference sum along every loop of the coupled circuit domain  $\Omega_c$ . Considering also diodes characteristic, load resistance and generator electromotive force (emf), Kirchhoff voltage law can be expressed as:

$$\left( (\text{emf})_{\Omega_s} - R(i)i - R_s i_s \right)_{\Omega_c} = 0 , \quad (4.5)$$

where  $i_s$  is the scalar current flowing through generator winding and the resistance term  $R$  is generally current-dependent due to the presence of diodes non linearity.

Magnetic vector potential  $\vec{a}$  and electric scalar potential  $u$  need to be defined to derive a suitable formulation for FE discretization. Flux density field is the curl of magnetic vector potential, while electric field is the gradient of electric scalar potential:

$$\begin{aligned} \vec{b} &= \vec{\nabla} \times \vec{a} \\ \vec{e} &= -\vec{\nabla} u \end{aligned} . \quad (4.6)$$

Since the FE model is planar (2D), magnetic field and flux density have only  $x$  and  $y$  in-plane components. As a consequence, magnetic vector potential, electric field and winding current have only  $z$  out-of-the-plane component. Therefore, they can be treated as scalar quantities.

The substitution of (4.2) and (4.4) in (4.1) and the introduction of magnetic vector potential lead to:

$$\vec{\nabla} \times \nu(B) \vec{\nabla} \times \vec{a} = -k_{s_i} \vec{i}_s . \quad (4.7)$$

#### 4. INVESTIGATION ON HARMONIC BALANCE METHOD

Accounting for (4.3) and introducing the magnetic vector and electric scalar potentials, (4.5) becomes:

$$k_{s_v} \frac{\partial}{\partial t} \int_{\Omega_s} \bar{a} dS_s - R(i)i - R_s i_s = 0, \quad (4.8)$$

where the first term on the left hand side represents generator emf, which is expressed using the coefficient  $k_{s_v}$  derived from stranded coil model as the product between number of series turns and stack axial length divided by cross section surface of winding coil:

$$k_{s_v} = \frac{N_{t_s} L_{stk}}{S_s}$$

Considering the planar dimensionality of the problem and fundamental identities of differential calculus, the general system of PDEs is finally derived from (4.7) and (4.8) as:

$$\begin{cases} \nabla \cdot (\nu(a_z) \bar{\nabla} a_z) = \bar{\nabla} \times \bar{h}_c - k_{s_i} i_{s_z} \\ k_{s_v} \int_{\Omega_s} \frac{\partial a_z}{\partial t} dS_s - R(i)i = R_s i_{s_z} \end{cases}. \quad (4.9)$$

Known terms are placed on the right hand sides. However, the only source term of the model is permanent magnet coercivity  $\bar{h}_c$ , whereas winding current  $i_{s_z}$  is coupled with the circuit domain. The unknowns are the  $z$  component of the magnetic vector potential in the FE domain and the current through each lumped element of the circuit domain, including generator winding. Since current values on circuit branches are the unknowns in this formulation, current loop method is adopted to solve circuit coupling, in both TS and HB resolution approaches.

### 4.3 Methodology

In this section, the time stepping and harmonic balance discrete algebraic equations (DAEs) are derived from the general PDEs in (4.9). The two resolution approaches are described, presenting also the handling of non linearities and movement. Both simulation methods are implemented in GetDP [137].

#### 4.3.1 Time stepping approach

Time stepping general DAEs are derived by weakening (4.9) with piece-wise linear basis functions, adopting a Galerkin approach. DAEs obtained with this procedure can be expressed as follows:

$$\begin{cases} \mathbf{S}(\mathbf{A}, t)\mathbf{A} = \mathbf{H}_c - \mathbf{K}_{s_i} \mathbf{I}_s \\ \mathbf{K}_{s_v} \frac{d\mathbf{A}}{dt} - \mathbf{R}(\mathbf{I})\mathbf{I} = \mathbf{R}_s \mathbf{I}_s \end{cases}. \quad (4.10)$$

Degrees of freedom vectors  $\mathbf{A}$  and  $\mathbf{I}$  contain  $n_n$  magnetic vector potential nodal approximations and  $n_c$  current values, respectively, where  $n_n$  is the number of mesh nodes and  $n_c$  are the branches of coupled circuit. The coupling with the external circuit is represented in weak discrete form by matrix  $\mathbf{K}_{s_v}$  and vector  $\mathbf{K}_{s_i}$ , that remind to the associated coefficients  $k_{s_v}$  and  $k_{s_i}$  in continuous PDEs of (4.9). Permanent magnet coercivity is contained in  $\mathbf{H}_c$  vector.

The stiffness matrix  $\mathcal{S}(\mathbf{A})$  can be expressed as the sum of three blocks: a linear part  $\mathcal{S}^{lin}$ , a non linear term due to iron saturation  $\mathcal{S}^{nl}$  and a time-dependent contribution given by the moving band region  $\mathcal{S}^{mb}$ :

$$\mathcal{S}(\mathbf{A}, t) = \mathcal{S}^{lin} + \mathcal{S}^{nl}(\mathbf{A}) + \mathcal{S}^{mb}(\theta(t)) . \quad (4.11)$$

The coefficients of the linear block  $\mathcal{S}^{lin}$  are given by the magnetic reluctivity of linear materials, such as air, permanent magnet and winding conductors, while differential reluctivity tensor  $\bar{\nu}^\partial$  is used for coefficients of  $\mathcal{S}^{nl}$ :

$$\bar{\nu}^\partial = \nu(B)\bar{\mathbf{1}} + 2\frac{d\nu}{dB^2}\bar{b}\bar{b} . \quad (4.12)$$

Thanks to this approach, the non linear block of the stiffness matrix can be correctly treated by a Newton-Raphson scheme during the resolution. Moving band gives a linear contribution that is recomputed for each rotor position.

The matrix  $R$  includes the linear load resistance and non linear diodes. A particular treatment is not needed in this case, as in TS approach diodes non linearity is not handled by Newton-Raphson scheme, because diode resistances depend only on the sign of the current.

DAEs in (4.10) can be condensed in a unique system as follows:

$$\mathbf{M}(\mathbf{X}(t))\mathbf{X}(t) + \mathbf{N}\frac{d\mathbf{X}}{dt} = \mathbf{F}(t) , \quad (4.13)$$

where matrix  $\mathbf{M}$  has a diagonal structure given by stiffness and resistance matrices, matrix  $\mathbf{N}$  contains circuit coupling terms, vector  $\mathbf{X}$  comprises all Dofs and vector  $\mathbf{F}$  the input sources.

A Theta method with fixed time step is implemented to solve the system. Time step is chosen equal to the following fraction of the fundamental period:

$$\Delta t = \frac{T}{360} = \frac{1}{360f_s} ,$$

thus resulting approximately in 0.01 ms over 3.3 ms of fundamental period. Three fundamental periods are simulated and the last one is taken as steady-state result.

### 4.3.2 Harmonic balance approach

The harmonic balance system is obtained by weakening (4.9) with harmonic basis functions, e.g. in a Galerkin approach. Harmonic basis functions are

#### 4. INVESTIGATION ON HARMONIC BALANCE METHOD

defined as:

$$\begin{aligned} \mathcal{H}(t) &= [h_0(t), h_1(t), \dots, h_{n_h}(t)] = \\ &= [1, 0, \cos(2\pi f_1 t), \sin(2\pi f_1 t), \dots, \cos(2\pi f_{n_f} t), \sin(2\pi f_{n_f} t)] , \end{aligned} \quad (4.14)$$

where  $n_f$  is the number of non-zero frequencies, while  $n_h$  is the number of harmonic basis function, which is given by:

$$n_h = 2(n_f + 1)$$

Zero-frequency basis functions are needed to handle permanent magnet source term and electric quantities on diodes and DC side.

HB system can be expressed as [138]:

$$\mathbf{M}^H \mathbf{X}^H = \mathbf{F}^H , \quad (4.15)$$

where the three matrix terms are expanded as follows:

$$\mathbf{M}^H = \begin{bmatrix} \mathbf{M} & 0 & \dots & \dots & 0 \\ 0 & \ddots & \ddots & \ddots & \vdots \\ \vdots & \ddots & \mathbf{M} & \ddots & \vdots \\ \vdots & \ddots & \ddots & \ddots & 0 \\ 0 & \dots & \dots & 0 & \mathbf{M} \end{bmatrix} + \begin{bmatrix} 0 & \ddots & \ddots & \ddots & \dots \\ \ddots & \ddots & \ddots & \ddots & \ddots \\ \ddots & 2\pi f_k \mathbf{N} & 0 & 2\pi f_k \mathbf{N} & \ddots \\ \ddots & \ddots & \ddots & \ddots & \ddots \\ \dots & \ddots & \ddots & \ddots & 0 \end{bmatrix} , \quad (4.16)$$

$$\mathbf{X}^H = \begin{bmatrix} \mathbf{A}^H_0 \\ \mathbf{I}^H_0 \\ \dots \\ \mathbf{A}^H_1 \\ \mathbf{I}^H_1 \\ \dots \\ \vdots \\ \dots \\ \mathbf{A}^H_{n_f} \\ \mathbf{I}^H_{n_f} \end{bmatrix} , \quad \mathbf{F}^H = \begin{bmatrix} H_c \\ 0 \\ \dots \\ -K_{s_i} \mathbf{I}^H_{s_1} \\ R_s \mathbf{I}^H_{s_1} \\ \dots \\ \vdots \\ \dots \\ -K_{s_i} \mathbf{I}^H_{s_{n_f}} \\ R_s \mathbf{I}^H_{s_{n_f}} \end{bmatrix} . \quad (4.17)$$

As it appears from previous expressions, damping time-dependent terms are no more present, as HB computes directly a steady-state solution. Matrix  $\mathbf{M}^H$  is made by the sum of two terms: a diagonal block matrix which is the repetition of TS matrix  $\mathbf{M}$ , and a second term which include TS matrix  $\mathbf{N}$  exploiting the orthonormality of harmonic basis functions. Thus, harmonic stiffness matrix and resistances are comprised in the first term of  $\mathbf{M}^H$ . Both iron and diode non linearities are treated with a Newton-Raphson scheme,

taking advantage of differential reluctivity and differential resistance, respectively:

$$\frac{\partial \bar{h}_k}{\partial b_l} = \frac{2}{T} \int_0^T h_k(t) h_l(t) \frac{\partial \bar{h}}{\partial b} dt, \quad (4.18)$$

$$\frac{\partial v_k}{\partial i_l} = \frac{2}{T} \int_0^T h_k(t) h_l(t) \frac{\partial v}{\partial i} dt, \quad (4.19)$$

with time integration performed numerically on a fundamental period with a given integration step. Since moving band is a linear region, its contribution is pre-assembled:

$$\mathbf{S}^{H_{mb}} = \frac{2}{T} \int_0^T \mathbf{S}^{mb}(\theta(t)) h_k h_l dt \quad (4.20)$$

Vectors  $\mathbf{X}^H$  and  $\mathbf{F}^H$  contain Dofs and known terms respectively, with the PM coercivity only on the zero-frequency component. The number of harmonic Dofs is  $n_n \times n_{h,r}$  and corresponds to matrix and vectors size. It is worth noticing that matrix dimension is  $n_h \times n_h$  higher than TS approach.

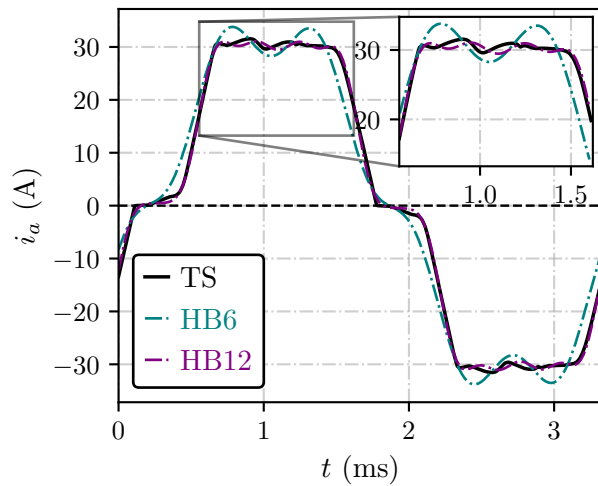
HB analyses are performed increasing progressively the harmonic spectrum considered in the simulation. The nomenclature  $HB_{n_h}$  indicates a HB analysis up to the  $n_{h_{th}}$  harmonic order in the figures and tables hereafter. It is important to state that the whole model domain is split, with a different set of frequencies considered for generator FE rotor and generator stator connected to circuit. In particular, only DC component (zero frequency) and harmonic orders multiple of six are considered in rotor subdomains, as predicted by theory of synchronous machines, while the full spectrum is included in stator and coupled circuit regions due to diodes non linear behavior. Normally, even harmonic orders can be neglected in synchronous machines stators. However, in the case study under analysis, stator is connected to a non linear circuit, whose non linearity requires the full spectrum. The two domains with a different set of harmonics are coupled at the nodes of moving band contour lines. A significant reduction of the computational cost can be achieved by neglecting frequencies that do not have any influence on certain subdomains.

## 4.4 Numerical results

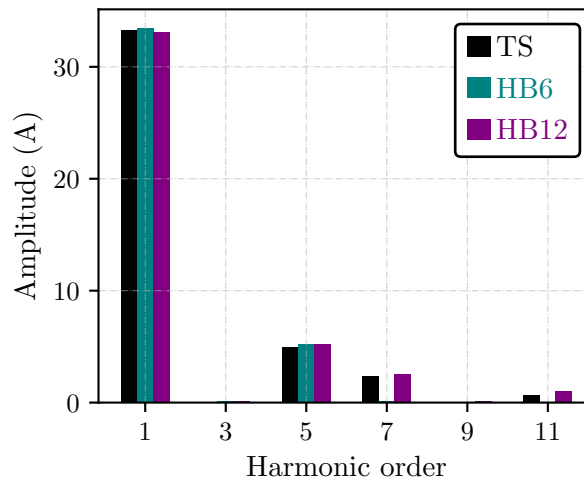
The TS and HB simulations of the considered case study are carried out in two operating conditions: supplying a resistance on DC side and at open circuit. HB analyses are extended up to 36 harmonic frequencies (plus the 0 Hz DC component).

The accuracy of HB simulations is assessed using TS steady-state results as benchmark. Figure 4.4 shows phase current on generator side during load operation. Waveforms are reported in both the time domain on a fundamental period (Figure 4.4a) and the harmonic spectrum (Figure 4.4b). For phase

#### 4. INVESTIGATION ON HARMONIC BALANCE METHOD



(a) Time-domain waveforms on a fundamental period.

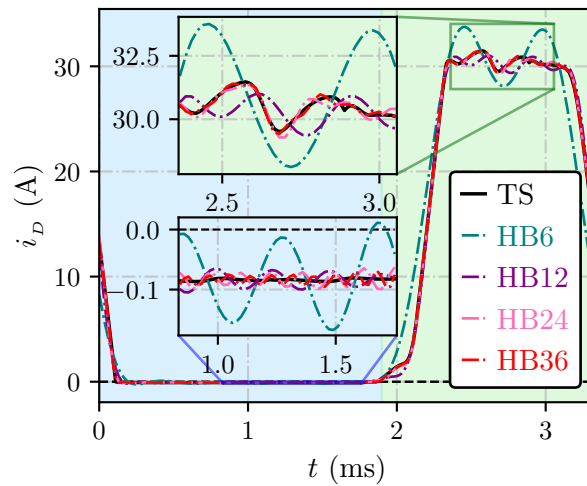


(b) Frequency-domain harmonic spectra.

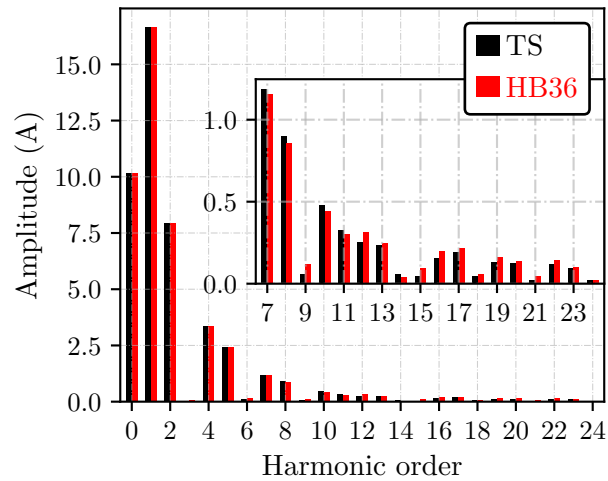
Figure 4.4: Load AC phase current.

current, there is a good agreement between HB results and TS outcomes just when frequencies up to 12th harmonic order are included in HB simulation, as shown in Figure 4.4a. Indeed, the HB12 results have relative errors on global RMS value and total harmonic distortion (THD) of 0.45 % and 5.89 %, respectively. Moreover, results are well in agreement with theory of balanced symmetric three-phase systems, because AC quantities do not exhibit even harmonic orders nor odd frequencies multiple of three, as it appears in Figure 4.4b.

The diodes behavior in rectifier load operation is depicted in Figure ??, where current through a diode and voltage across the same diode are reported.



(a) Current time-domain waveforms on a fundamental period.

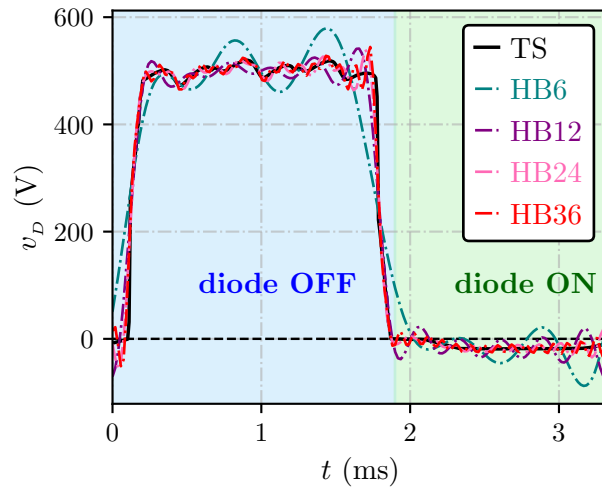


(b) Current frequency-domain harmonic spectra.

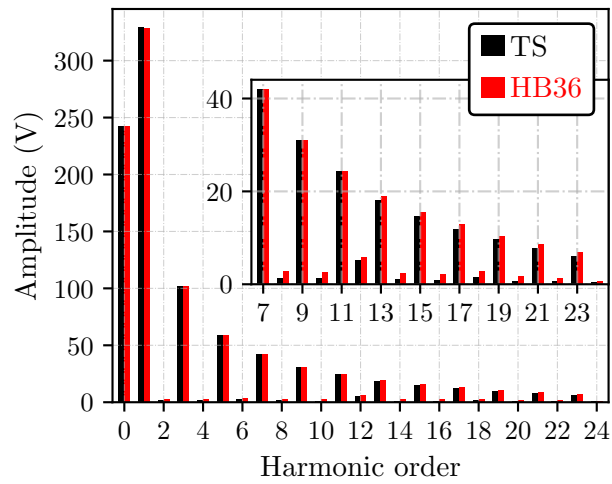
Figure 4.5: Load current through a diode.

Oscillations around theoretical quasi-square waveform can be observed in both the TS and HB results due to diode modeling. Current oscillations (see Figure 4.5a) are present both during conduction (diode ON) and when diode is reversed biased (diode OFF). During OFF state, relatively small current oscillations lead to significant voltage fluctuations (see Figure 4.6a), because of a quite high diode OFF resistance. Nevertheless, a good approximation of TS waveforms is achieved also in this case, even though harmonic frequencies included in HB simulation need to go up to the 36th order. Furthermore, it is important to notice that diode waveforms comprise the whole harmonic spectrum, considering current (Figure 4.5b) and voltage (Figure 4.6b) together,

#### 4. INVESTIGATION ON HARMONIC BALANCE METHOD



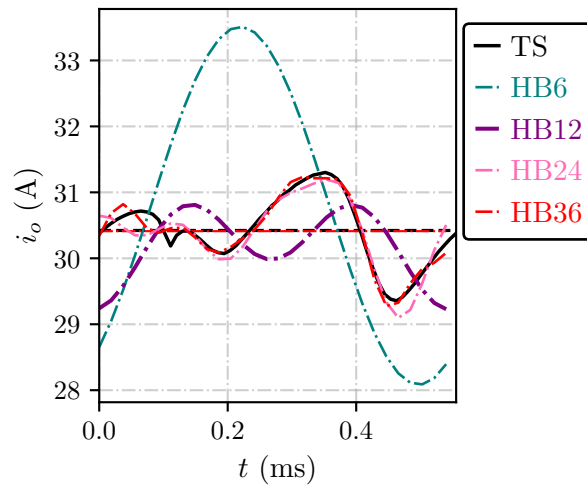
(a) Voltage time-domain waveforms on a fundamental period.



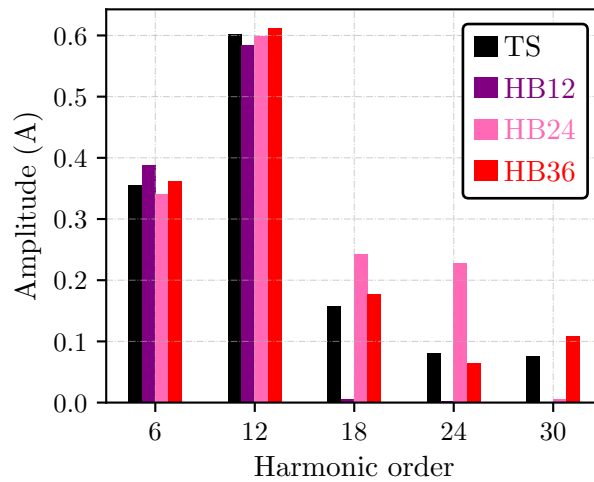
(b) Voltage frequency-domain harmonic spectra.

Figure 4.6: Load voltage across a diode.





(a) Time-domain waveforms on a ripple period.



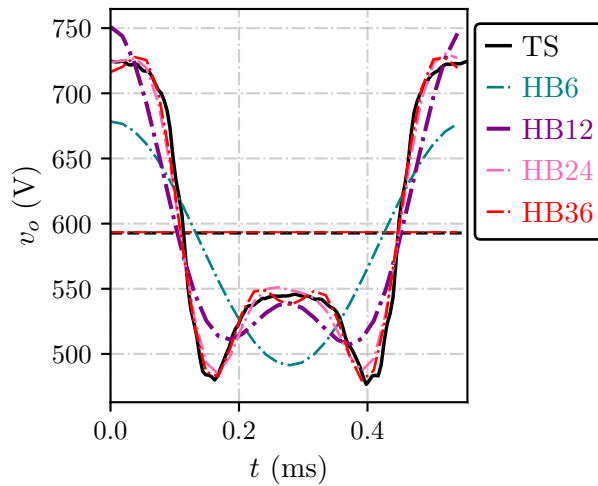
(b) Frequency-domain harmonic spectra.

Figure 4.7: Load DC output current.

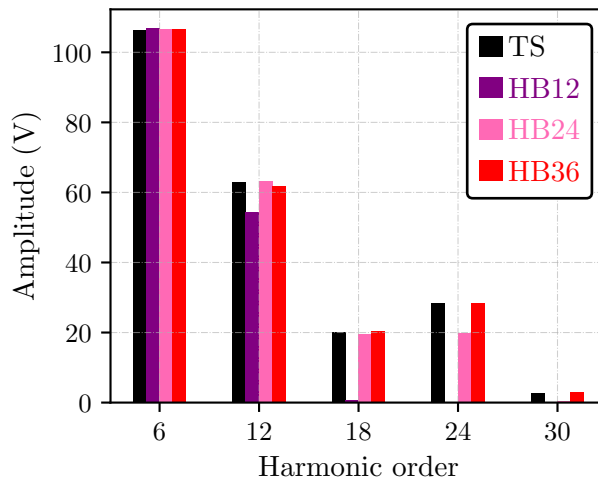
which is the reason why no harmonic can be neglected in the stator and coupled circuit.

Load current on DC output is shown in Figure 4.7. Note that TS results are not accurate in evaluating current commutation effects on DC quantities, mainly because of the fixed time step adopted in the TS approach. However, mean values are accurate and TS outcomes are still taken as reference. Also in this case, HB approximates TS waveform with a satisfying accuracy only when a relatively high number of frequencies are included in the simulation, as shown in Figure 4.7a. Relative errors on mean value (i.e. DC component) and THD are 0.03 % and 2.16 %, respectively. Moreover, Figure 4.7b proves

#### 4. INVESTIGATION ON HARMONIC BALANCE METHOD



(a) Time-domain waveforms on a ripple period.



(b) Frequency-domain harmonic spectra.

Figure 4.8: Open-circuit DC output voltage.

again that simulation outcomes are in agreement with theory, as DC load current has only a DC 0-frequency component (not shown in spectrum) and harmonic orders multiple of 6, which produce a ripple period six times lower than the fundamental one, as predicted by the analytical model of a six-pulse diode rectifier.

Similar comments can be made about Figure 4.8, where open-circuit DC voltage is shown both in time domain (Figure 4.8a) and frequency spectrum (Figure 4.8b). The accuracy of HB simulations is evaluated as relative errors on global average values, i.e. mean, RMS and THD, with respect to benchmark TS results. Outcomes are reported in Table 4.2 for AC phase and DC

Table 4.2: HB accuracy benchmarked with TS results.

HB sim.	Relative errors (%)					
	Load phase current		Load DC current		Open-circuit DC voltage	
	RMS	THD	Mean	THD	Mean	THD
HB6	0.39	6.28	1.20	178.24	1.20	106.81
HB12	0.45	5.89	0.78	18.12	0.78	34.49
HB18	0.41	0.81	0.32	11.35	0.30	14.75
HB24	0.13	0.22	0.17	8.28	0.17	7.63
HB30	0.06	0.17	0.09	4.18	0.08	3.41
HB36	0.02	0.14	0.03	2.16	0.03	1.99

Table 4.3: TS and HB computational performance.

Sim.	Iterations	CPU time (min)	Cumulative time (min)	Required RAM (GB)
TS	~5 ‡	41	41	0.2
HB6	11	2	2	2.5
HB12†	8	6	8	8.6
HB18†	8	11	19	18.5
HB24†	8	21	40	32.2
HB30†	7	30	70	46.1
HB36†	11	58	128	48.1

†Preconditioning starting from previous HB solution.

‡Per time step.

output current in load condition, and open-circuit DC voltage. It can be clearly seen that accuracy improves when expanding harmonic spectrum, as relative errors diminish with the increasing harmonic presence from HB6 to HB36. Furthermore, it can be noted that precision on mean and RMS values is always below 2%, whereas relative errors on THD are generally higher and many frequencies are needed to reach a satisfying accuracy, in particular for DC output quantities. Therefore, if the focus is on mean and RMS values, few harmonics may be enough to get sufficient precision, whereas when accuracy is required on the entire waveform, many frequencies must be included in HB simulation, especially for DC quantities.

Finally, the computational performance is compared between the TS and HB approaches in terms of simulation time and memory requirements. Results are reported in Table 4.3 and Figure 4.9 when simulating load operation.

#### 4. INVESTIGATION ON HARMONIC BALANCE METHOD

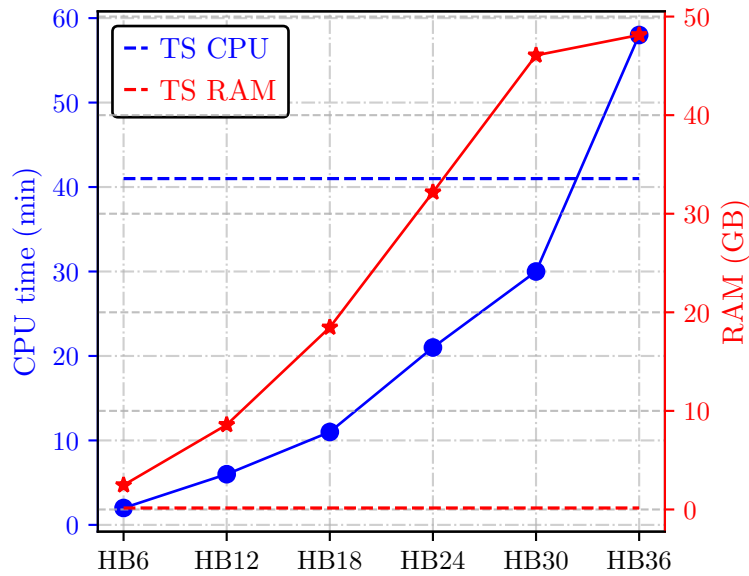


Figure 4.9: Graphical comparison between TS and HB computational performance on the case study under analysis.

Similar performance are observed in the open circuit condition.

As expected, HB always requires more RAM than TS, even with few frequencies included in the simulation, as the size of the matrices involved in the computation is higher. The requirement of 48.1 GB for HB36 may seem impressive. Nonetheless, today it can be handled even by common workstations: the simulations reported in this work have been performed with a desktop computer featuring a 3.6 GHz CPU and a 64 GB RAM. Matrices size causes also a slower convergence of Newton-Raphson algorithm. Indeed, the number of iterations required by HB simulations is always higher than a single TS analysis.

Nonetheless, the comparison of computational time is the most relevant for the purpose of this work. A significant reduction of the CPU time is achieved until HB30, considering each HB simulation alone. Hereto, HB30 takes about 11 min less than TS to run. However, HB simulations of the case study under analysis need a proper preconditioning to reach convergence. In this particular case study, the most effective preconditioning technique is to use previous solution as preconditioner for the next one, considering the harmonic orders of DC output quantities. In other words, the solution of HB6 is taken as preconditioner by HB12, and so on until HB36. As a consequence, the actual computational time of each HB simulation must include also the CPU time taken by all previous runs, i.e. the cumulative time, because all the previous HB simulations must be performed before the current one to achieve convergence. Therefore, an actual computational gain is obtained only up

to HB24, which requires just one minute less than TS. However, accuracy of HB24 is sufficient only in terms of mean and RMS values, whereas THD of DC quantities is still far from TS results. Further investigations on the most suitable preconditioning technique are needed.

The performance analysis in Table 4.2 and Figure 4.9 does not favor the HB approach. However, it is fair to point out that the application at hand exhibits relatively fast dynamics, i.e. a short transient, and it is therefore not the best test case to highlight the advantages of HB approach. Indeed, the electromagnetic time constant of the system, considering synchronous inductance and all resistances is about ten times lower than a fundamental period. As a consequence, TS needs to simulate only two periods to reach steady state. In addition, the choice of a fixed time step scheme further reduce TS CPU time, despite the less accurate approximation of DC quantities near diodes commutations. Moreover, the HB implementation adopted in this work is far from optimal with regard to the TS approach. A smarter implementation could make the difference, especially when combined with a more suitable diode model for HB handling, and an adapted solver and preconditioning. Further efforts are needed in this direction.

## 4.5 Comments

This work assesses the capabilities of harmonic balance approach in simulating a real-world engineering application, with respect to mainstream time stepping method. The case study comprises a 12.5 kVA SPM generator connected to a full-bridge diode rectifier. A three-phase system is chosen to increase problem complexity. The system is simulated both at load and open circuit.

The application of HB to a problem that includes movement and non linearities both in FE model and coupled circuit is extensively discussed, starting from continuous PDEs until final DAEs. Implementation details are also presented.

The accuracy of HB simulations is evaluated in comparison with TS results, progressively expanding the number of frequencies considered in the computation. HB can handle non linear problems with movement and circuit coupling with a satisfying precision, both in terms of mean and THD values.

However, TS outperforms HB in the given case study. Indeed, computational performance of HB are heavily affected by non linearities in lumped parameters, i.e. power electronics components like diodes. Moreover, effectiveness of HB strongly depends on an efficient implementation. Finally, the chosen application definitively favors TS, because of the relatively fast dynamic responsiveness. Systems with longer initial transients may benefit more effectively of HB approach.

Although, study of HB preconditioning techniques and solvers is still needed.



## 5 CONCLUSIONS

---

Electrification of off-road working vehicles is a hot research topic in industry and academia. Among others, agricultural machinery have some peculiarities that make the introduction of more electric drives in their drivetrains particularly challenging, if not unfeasible. Furthermore, methodologies for the design of the main electric components of these high-voltage electromechanical systems are not well assessed yet. About this point, fast computational procedures may have a significant impact in reducing development costs and product time to market.

The main contribution of this thesis consists in the development of a method to evaluate the technical and economic feasibility of hybrid electric tractors based on life cycle cost analysis. A comprehensive technology review is also reported, focusing on proposals for the introduction of more electric drives in agricultural tractor powertrains. Trends and perspectives are extensively discussed, highlighting the most promising and feasible solutions in terms of fuel consumption reductions, field efficiency and performance. Finally, potentialities of harmonic balance numerical method are investigated on an application related to the main topic of this thesis.

### 5.1 Key findings of the thesis

A life cycle cost analysis is applied to evaluate electrification feasibility of three tractors with different power size and operating cycles. A parallel hybrid electric configuration is taken as reference, and costs are compared to conventional counterparts. A wide variety of feasible prices for the main powertrain components is considered on the three different case studies. Engine down-sizing or electric drive exploitation is varied too, depending on the tractor category. It emerges that significant savings can be obtained from powertrain electrification of specialized tractors for orchard and vineyards, as they often perform low-power tasks, even though operating cost reductions are lower than for road vehicles, e.g. passenger cars and trucks. On row crop tractors, which perform more power-intensive operations, operating cost savings are insufficient to gain relevant reductions of life cycle cost, leading to payback time that may be not competitive, when adopting realistic price combinations for powertrain components. Therefore, parallel hybrid electric layouts are not suitable for this category of tractors, and electrification should probably regard only auxiliaries and implements, exploiting series and power split architectures.

The developed method allows the evaluate of a safety margin for which a hybrid tractor remains profitable, i.e. how much of a price variation is possible, for a certain cost source, without resulting inconvenient compared to the

## 5. CONCLUSIONS

non-hybrid conventional counterpart. Although a limited number of engine downsizing values received an extensive analysis, the proposed methodology is valid for future more exhaustive economical feasibility studies, focusing also on other powertrain structures, especially when uncertainty occurs on components and energy costs.

The capabilities of harmonic balance (HB) approach are assessed in simulating a real-world engineering application, with respect to mainstream time stepping (TS) method. The case study comprises a three-phase SPM generator connected to a full-bridge diode rectifier. The application of HB to a problem that includes movement and non linearities both in finite-element model and coupled circuit is extensively discussed, reporting also implementation details.

Accuracy of HB simulations is evaluated in comparison with TS results, progressively expanding the number of frequencies considered in the computation. HB can handle non linear problems with movement and circuit coupling with a satisfying precision, both in terms of mean and THD values. However, TS outperforms HB in the given case study. Indeed, computational performance of HB are heavily affected by non linearities in lumped parameters, i.e. power electronics components like diodes. Moreover, effectiveness of HB strongly depends on an efficient implementation. Finally, the chosen application definitively favors TS, because of the relatively fast dynamic responsiveness. Systems with longer initial transients may benefit more effectively of HB approach.

### 5.2 Future developments

This dissertation aims to provide solid fundamentals for engineers dealing with electrification of agricultural tractors. Despite the topics and results discussed throughout this thesis, many insights deserve a deeper analysis, and some new paths may be foreseen.

Feasibility studies on the profitability of hybrid electric tractors could be extended to other case studies and layouts. Energetic models could be greatly improved with the availability of a larger and more structured database of field measurements: system modeling of agricultural machinery would particularly benefit of such data. Energy management strategies and high-level control schemes are other aspects that have received little attention.

The development of electromechanical power take offs together with the introduction of electric drives on implements is emerging as a key milestone in the electrification of agricultural machinery, thanks to the potentialities of these systems in improving field efficiency and enabling new functionalities, especially when precision agriculture principle and a high level of automation are implemented. Electric interfaces between tractor and implements are still not standardized. Therefore, this topic is widely open to novel proposals.



Electrification of agricultural implements, in particular, deserves a deeper and more structured investigation. Moreover, low-level control algorithms deserve proper investigations, as high-voltage systems may feature many interconnections between different electric drives, posing instability and reliability issues. Furthermore, electromechanical ground drive transmissions remains interesting for research and development.

Design aspects of specific components should be further explored. The thermal behavior of electric machines and power converters is of paramount importance in systems with a high level of integration and significant overload requirements. In addition, environmental conditions of agriculture operations may be very challenging for electric components. Thus, performance in a harsh environment should be carefully assessed.

Finally, promising solutions and analytical results should be corroborated by experimental testing on whole tractors, entire powertrains, or single subsystems and components. In applied engineering research, working on practical development of relevant case studies gives more value to final outcomes, as every concept and result is proven on reality. In addition, practical experience eases the discovery of issues and problems that may arise in the application under study, thus opening unexplored paths toward knowledge and progress.



## LIST OF PUBLICATIONS

---

- **E. Scolaro**, L. Alberti and D. Barater, "Electric Drives for Hybrid Electric Agricultural Tractors," in *2021 IEEE Workshop on Electrical Machines Design, Control and Diagnosis (WEMDCD)*, Modena, Italy, 2021, pp. 331-336, doi: 10.1109/WEMDCD51469.2021.9425671.
- **E. Scolaro**, D. Troncon and L. Alberti, "Energy Management of a Dual-Motor Electric Vehicle Based on Particle Swarm Optimization," *2021 IEEE Vehicle Power and Propulsion Conference (VPPC)*, Gijon, Spain, 2021, pp. 1-6, doi: 10.1109/VPPC53923.2021.9699328.
- **E. Scolaro**, M. Beligoj, M. P. Estevez, L. Alberti, M. Renzi and M. Mattetti, "Electrification of Agricultural Machinery: A Review," in *IEEE Access*, vol. 9, pp. 164520-164541, 2021, doi: 10.1109/ACCESS.2021.3135037.
- M. Beligoj, **E. Scolaro**, L. Alberti, M. Renzi and M. Mattetti, "Feasibility Evaluation of Hybrid Electric Agricultural Tractors Based on Life Cycle Cost Analysis," in *IEEE Access*, vol. 10, pp. 28853-28867, 2022, doi: 10.1109/ACCESS.2022.3157635.
- Luigi Alberti; **Elia Scolaro**; Matteo Beligoj, "Feasibility Evaluation of Hybrid Electric Agricultural Tractors Based on Life Cycle Cost Analysis," in *Transportation Electrification: Breakthroughs in Electrified Vehicles, Aircraft, Rolling Stock, and Watercraft*, IEEE, 2023, pp.437-451, doi: 10.1002/9781119812357.ch20.
- G. Galati, **E. Scolaro**, D. Michieletto, M. Beligoj, L. Ortombina, "Motor Vehicle Challenge 2023: The Winning Multi-physical Energy Management Algorithm", *2023 IEEE Vehicle Power and Propulsion Conference (VPPC)*, Milan, Italy, 2023, *Submitted*.



## BIBLIOGRAPHY

---

- [1] F. Tubiello, *Greenhouse Gas Emissions Due to Agriculture*. (FAO) Food and Agriculture Organization of the United Nations, 01 2019.
- [2] F. Tubiello and G. Conchedda, "Emissions due to agriculture Global, regional and country trends," *FAO food and nutrition paper*, vol. 1, 03 2021.
- [3] P. K. Rai, "Impacts of particulate matter pollution on plants: Implications for environmental biomonitoring," *Ecotoxicology and Environmental Safety*, vol. 129, pp. 120–136, 2016.
- [4] A. Juostas and A. Janulevičius, "Evaluating working quality of tractors by their harmful impact on the environment," *Journal of environmental engineering and landscape management*, vol. 17, no. 2, pp. 106–113, 2009.
- [5] "EU: Nonroad Diesel Engines," 2017. Accessed January, 2021.
- [6] "United States: Nonroad Diesel Engines," 2016. Accessed January, 2021.
- [7] "Nonroad Compression-Ignition Engines: Exhaust Emission Standards," 2016. Accessed January, 2021.
- [8] G. P. Moreda, M. A. Muñoz-García, and P. Barreiro, "High voltage electrification of tractor and agricultural machinery – A review," *Energy Conversion and Management*, 2016.
- [9] A. Lajunen, P. Sainio, L. Laurila, J. Pippuri-Mäkeläinen, and K. Tammi, "Overview of Powertrain Electrification and Future Scenarios for Non-Road Mobile Machinery," *Energies*, 2018.
- [10] A. Hammar, "Prospects on Diffusion of Agriculture Hybrid Tractors Equipped with On Board High Voltage System," in *SAE 2015 Commercial Vehicle Engineering Congress*, 2015.
- [11] J. Karner, M. Baldinger, and B. Reichl, "Prospects of Hybrid Systems on Agricultural Machinery," *Journal on Agricultural Engineering (JAE)*, 2014.
- [12] M. Gonzalez-de-Soto, L. Emmi, C. Benavides, I. Garcia, and P. Gonzalez-de-Santos, "Reducing air pollution with hybrid-powered robotic tractors for precision agriculture," *Biosystems Engineering*, vol. 143, pp. 79 – 94, 2016.
- [13] L. Alberti and M. Mattetti, *Challenges and State of the Art in the Agricultural Machinery Electrification*, pp. 417–423. 2023.
- [14] L. Alberti and D. Troncon, *Electrification of Agricultural Machinery*, pp. 425–435. 2023.

## BIBLIOGRAPHY

- [15] K. T. Renius, *Fundamentals of Tractor Design*. Springer, 2019.
- [16] "Deutz agricultural diesel engines," 2023. Accessed September, 2023.
- [17] M. Saetti, M. Mattetti, M. Varani, N. Lenzini, and G. Molari, "On the power demands of accessories on an agricultural tractor," *Biosystems Engineering*, vol. 206, pp. 109–122, 2021.
- [18] R. M. Babu, S. Manikandan, and R. P. Nageshwara, "Electrical Operated Fan for Cooling System on Agricultural Tractors," in *SAE Technical Paper*, SAE International, 2019.
- [19] L. Slone and J. Birkel, "Advanced Electric Systems and Aerodynamics for Efficiency Improvements in Heavy Duty Trucks," tech. rep., 2007.
- [20] N. Staunton, V. Pickert, and R. Maughan, "Assessment of advanced thermal management systems for micro-hybrid trucks and heavy duty diesel vehicles," in *2008 IEEE Vehicle Power and Propulsion Conference*, 2008.
- [21] E. G. Ribeiro, A. P. de Andrade Filho, and J. L. de Carvalho Meira, "Electric water pump for engine cooling," in *SAE Technical Paper*, SAE International, 2007.
- [22] H.-C. Lin, Y.-T. Chang, G.-L. Tsai, D.-M. Wang, F.-C. Hsieh, and J.-F. Jiang, "Oil Coking Prevention Using Electric Water Pump for Turbo-Charge Spark-Ignition Engines," *Mathematical Problems in Engineering*, 2014.
- [23] D. Pessina and D. Facchinetti, "Gemelli diversi," *Macchine Agricole Luglio*, 2009.
- [24] A. Kalinichenko, V. Havrysh, and V. Hruban, "Heat Recovery Systems for Agricultural Vehicles: Utilization Ways and Their Efficiency," *Agriculture*, 2018.
- [25] M. A. Andwari, A. Pesyridis, V. Esfahanian, A. Salavati-Zadeh, A. Karvountzis, and V. Muralidharan, "A Comparative Study of the Effect of Turbocompounding and ORC Waste Heat Recovery Systems on the Performance of a Turbocharged Heavy-Duty Diesel Engine," *Energies*, vol. 10, p. 1087, 07 2017.
- [26] A. E. Teo, M. S. Chiong, M. Yang, A. Romagnoli, R. F. Martinez-Botas, and S. Rajoo, "Performance evaluation of low-pressure turbine, turbocompounding and air-Brayton cycle as engine waste heat recovery method," *Energy*, 2019.

- [27] D. T. Hountalas, C. O. Katsanos, and V. T. Lamaris, "Recovering Energy from the Diesel Engine Exhaust Using Mechanical and Electrical Turbocompounding," in *SAE Technical Paper*, SAE International, 2007.
- [28] D. Hountalas and G. Mavropoulos, *Potential for Improving HD Diesel Truck Engine Fuel Consumption Using Exhaust Heat Recovery Techniques*, ch. 17, pp. 313–340. 2010.
- [29] B. Singh, "Novel and Ruggedized Power Electronics for Off-Highway Vehicles," *IEEE Electrification Magazine*, 2014.
- [30] M. Kebriaei, A. H. Niasar, and B. Asaei, "Hybrid electric vehicles: An overview," in *2015 International Conference on Connected Vehicles and Expo (ICCVE)*, 2015.
- [31] O. M. Govardhan, "Fundamentals and Classification of Hybrid Electric Vehicles," *International Journal of Engineering and Techniques*, 2017.
- [32] A. Somà, "Trends and Hybridization Factor for Heavy-Duty Working Vehicles," in *Hybrid Electric Vehicles* (T. Donateo, ed.), ch. Chapter 1, IntechOpen, 2017.
- [33] S. Florentsev, D. Izosimov, L. Makarov, S. Baida, and A. Belousov, "Complete traction electric equipment sets of electro-mechanical drive trains for tractors," in *2010 IEEE Region 8 International Conference on Computational Technologies in Electrical and Electronics Engineering (SIBIRCON)*, 2010.
- [34] C. Jia, W. Qiao, and L. Qu, "Modeling and Control of Hybrid Electric Vehicles: A Case Study for Agricultural Tractors," in *2018 IEEE Vehicle Power and Propulsion Conference (VPPC)*, 2018.
- [35] C. Jia, W. Qiao, and L. Qu, "Numerical Methods for Optimal Control of Hybrid Electric Agricultural Tractors," in *2019 IEEE Transportation Electrification Conference and Expo (ITEC)*, 2019.
- [36] F. E. G. Mendes, D. I. Brandao, T. Maia, and J. C. Braz de Filho, "Off-Road Vehicle Hybridization Methodology Applied to a Tractor Backhoe Loader," in *2019 IEEE Transportation Electrification Conference and Expo (ITEC)*, 2019.
- [37] D. Troncon, L. Alberti, S. Bolognani, F. Bettella, and A. Gatto, "Electrification of agricultural machinery: a feasibility evaluation," in *Fourteenth International Conference on Ecological Vehicles and Renewable Energies (EVER)*, 2019.
- [38] J. Barthel, D. Gorges, M. Bell, and P. Munch, "Energy Management for Hybrid Electric Tractors Combining Load Point Shifting, Regeneration

## BIBLIOGRAPHY

- and Boost,” in *2014 IEEE Vehicle Power and Propulsion Conference (VPPC)*, 2014.
- [39] F. Mocera and A. Somà, “Analysis of a Parallel Hybrid Electric Tractor for Agricultural Applications,” *Energies*, 2020.
- [40] M. Bertoluzzo, P. Bolognesi, G. Buja, and P. Thakura, “Role and Technology of the Power Split Apparatus in Hybrid Electric Vehicles,” in *IECON 2007 - 33rd Annual Conference of the IEEE Industrial Electronics Society*, pp. 256–261, 2007.
- [41] C. Rossi, D. Pontara, C. Falcomer, M. Bertoldi, and R. Mandrioli, “A Hybrid–Electric Driveline for Agricultural Tractors Based on an e-CVT Power-Split Transmission,” *Energies*, vol. 14, no. 21, 2021.
- [42] S. Grammatico, A. Balluchi, and E. Cosoli, “A series-parallel hybrid electric powertrain for industrial vehicles,” in *2010 IEEE Vehicle Power and Propulsion Conference*, 2010.
- [43] R. R. Melo, F. L. Antunes, S. Daher, H. H. Vogt, D. Albiero, and F. L. Tofoli, “Conception of an electric propulsion system for a 9 kW electric tractor suitable for family farming,” *IET Electric Power Application*, 2019.
- [44] J. Engström and O. Lagnelöv, “An Autonomous Electric Powered Tractor—Simulation of All Operations on a Swedish Dairy Farm,” *Journal of Agricultural Science and Technology*, vol. 8, 03 2018.
- [45] “New Holland’s NH2 fuel cell powered tractor to enter service,” *Fuel Cells Bulletin*, 2012.
- [46] P. J. Tritschler, S. Bacha, E. Rullière, and G. Husson, “Energy management strategies for an embedded fuel cell system on agricultural vehicles,” in *The XIX International Conference on Electrical Machines - ICEM 2010*, 2010.
- [47] “X-Concept Fendt,” 2019. Accessed January, 2021.
- [48] “e100 Vario Fendt,” 2019. Accessed January, 2021.
- [49] “Landini Rex4 Electro,” 2021. Accessed January, 2021.
- [50] “Steyr Konzept - FPT Industrial,” 2021. Accessed January, 2021.
- [51] “Carraro electrified solutions,” 2020. Accessed January, 2021.
- [52] Joskin, “Hybrid Power for Agricultural Transport,” tech. rep., 2019.
- [53] M. Varani, M. Mattetti, and G. Molari, “Performance Evaluation of Electrically Driven Agricultural Implements Powered by an External Generator,” *Agronomy*, vol. 11, no. 8, 2021.



- [54] R. Hoy, R. Rohrer, A. Liska, J. Luck, L. Isom, D. Keshwani, R. Hoy, R. Rohrer, A. Liska, J. Luck, L. Isom, and D. Keshwani, "Agricultural Industry Advanced Vehicle Technology: Benchmark Study for Reduction in Petroleum Use," tech. rep., 2014.
- [55] F. Rahe and R. Resch, "Electrification of Agricultural Machinery From the Perspective of an Implement Manufacturer," 2017.
- [56] R. Bals, D. Jünemann, and A. Berghaus, "Partial Electrification of an Agricultural Implement," *ATV heavy duty worldwide - Electrification and Digitalization*, 2019.
- [57] K. Hahn, "High Voltage Electric Tractor-Implement Interface," 2008.
- [58] M. Winter and R. J. Brodd, "What Are Batteries, Fuel Cells, and Supercapacitors?," *Chem. Rev.*, 2004.
- [59] R. A. Dougal, S. Liu, and R. E. White, "Power and life extension of battery-ultracapacitor hybrids," *IEEE Transactions on Components and Packaging Technologies*, vol. 25, no. 1, pp. 120–131, 2002.
- [60] D. Shin, Y. Kim, J. Seo, N. Chang, Y. Wang, and M. Pedram, "Battery-supercapacitor hybrid system for high-rate pulsed load applications," in *2011 Design, Automation Test in Europe*, pp. 1–4, 2011.
- [61] H. Shareef, M. M. Islam, and A. Mohamed, "A review of the stage-of-the-art charging technologies, placement methodologies, and impacts of electric vehicles," *Renewable and Sustainable Energy Reviews*, vol. 64, pp. 403–420, 2016.
- [62] H. Tu, H. Feng, S. Srdic, and S. Lukic, "Extreme Fast Charging of Electric Vehicles: A Technology Overview," *IEEE Transactions on Transportation Electrification*, vol. 5, no. 4, pp. 861–878, 2019.
- [63] C. Suarez and W. Martinez, "Fast and Ultra-Fast Charging for Battery Electric Vehicles – A Review," in *2019 IEEE Energy Conversion Congress and Exposition (ECCE)*, pp. 569–575, 2019.
- [64] H. Mousazadeh, A. Keyhani, A. Javadi, H. Mobli, K. Abrinia, and A. Sharifi, "Life-cycle assessment of a Solar Assist Plug-in Hybrid electric Tractor (SAPHT) in comparison with a conventional tractor," *Energy Conversion and Management*, 2011.
- [65] H. H. Vogt, D. Albiero, and B. Schmuelling, "Electric tractor propelled by renewable energy for small-scale family farming," in *2018 Thirteenth International Conference on Ecological Vehicles and Renewable Energies (EVER)*, 2018.

## BIBLIOGRAPHY

- [66] N. Mohamed, F. Aymen, M. Alqarni, R. A. Turkey, B. Alamri, Z. M. Ali, and S. H. A. Aleem, "A new wireless charging system for electric vehicles using two receiver coils," *Ain Shams Engineering Journal*, 2021.
- [67] P. Moriarty and D. Honnery, "Prospects for hydrogen as a transport fuel," *International Journal of Hydrogen Energy*, vol. 44, no. 31, pp. 16029–16037, 2019.
- [68] Z. Binti Awang Mat, Madya, Y. B. Kar, S. Hasmady Bin Abu Hassan, and N. Azrina Binti Talik, "Proton exchange membrane (PEM) and solid oxide (SOFC) fuel cell based vehicles-a review," in *2017 2nd IEEE International Conference on Intelligent Transportation Engineering (ICITE)*, pp. 123–126, 2017.
- [69] D. M. Ali and S. Salman, "A Comprehensive Review of the Fuel Cells Technology and Hydrogen Economy," in *Proceedings of the 41st International Universities Power Engineering Conference*, vol. 1, pp. 98–102, 2006.
- [70] Q. Wang, J. Li, Y. Bu, L. Xu, Y. Ding, Z. Hu, R. Liu, Y. Xu, and Z. Qin, "Technical assessment and feasibility validation of liquid hydrogen storage and supply system for heavy-duty fuel cell truck," in *2020 4th CAA International Conference on Vehicular Control and Intelligence (CVCI)*, pp. 555–560, 2020.
- [71] A. T-Raissi, A. Banerjee, and K. Sheinkopf, "Metal hydride storage requirements for transportation applications," in *IECEC 96. Proceedings of the 31st Intersociety Energy Conversion Engineering Conference*, vol. 4, pp. 2280–2285 vol.4, 1996.
- [72] G. Berardi, S. Nategh, N. Bianchi, and Y. Thioliere, "A Comparison Between Random and Hairpin Winding in E-mobility Applications," in *IECON 2020 The 46th Annual Conference of the IEEE Industrial Electronics Society*, pp. 815–820, 2020.
- [73] L. Alberti and D. Troncon, "Design of Electric Motors and Power Drive Systems According to Efficiency Standards," *IEEE Transactions on Industrial Electronics*, vol. 68, no. 10, pp. 9287–9296, 2021.
- [74] S. Zhitkova, M. Felden, D. Franck, and K. Hameyer, "Design of an electrical motor with wide speed range for the in-wheel drive in a heavy duty off-road vehicle," in *2014 International Conference on Electrical Machines (ICEM)*, 2014.
- [75] D. Troncon and L. Alberti, "Case of Study of the Electrification of a Tractor: Electric Motor Performance Requirements and Design," *Energies*, 2020.

- [76] W. Xu, J. Zhu, Y. Guo, S. Wang, Y. Wang, and Z. Shi, "Survey on electrical machines in electrical vehicles," in *2009 International Conference on Applied Superconductivity and Electromagnetic Devices*, pp. 167–170, 2009.
- [77] S. Zhitkova and K. Hameyer, "Realization of a wide speed range for an agricultural tractor," in *2016 XXII International Conference on Electrical Machines (ICEM)*, 2016.
- [78] I. Boldea, L. N. Tutelea, L. Parsa, and D. Dorrell, "Automotive Electric Propulsion Systems With Reduced or No Permanent Magnets: An Overview," *IEEE Transactions on Industrial Electronics*, vol. 61, no. 10, pp. 5696–5711, 2014.
- [79] S. Estenlund, M. Alaküla, and A. Reinap, "PM-less machine topologies for EV traction: A literature review," in *2016 International Conference on Electrical Systems for Aircraft, Railway, Ship Propulsion and Road Vehicles International Transportation Electrification Conference (ESARS-ITEC)*, pp. 1–6, 2016.
- [80] S. Amin, S. Khan, and S. S. Hussain Bukhari, "A Comprehensive Review on Axial Flux Machines and Its Applications," in *2019 2nd International Conference on Computing, Mathematics and Engineering Technologies (iCoMET)*, pp. 1–7, 2019.
- [81] F. C. Mushid and D. G. Dorrell, "Review of axial flux induction motor for automotive applications," in *2017 IEEE Workshop on Electrical Machines Design, Control and Diagnosis (WEMDCD)*, pp. 146–151, 2017.
- [82] D. J. Patterson, J. L. Colton, B. Mularcik, B. J. Kennedy, S. Camilleri, and R. Rohoza, "A comparison of radial and axial flux structures in electrical machines," in *2009 IEEE International Electric Machines and Drives Conference*, pp. 1029–1035, 2009.
- [83] A. Cavagnino, M. Lazzari, F. Profumo, and A. Tenconi, "A comparison between the axial flux and the radial flux structures for PM synchronous motors," *IEEE Transactions on Industry Applications*, vol. 38, no. 6, pp. 1517–1524, 2002.
- [84] Y. Yang, N. Schofield, and A. Emadi, "Integrated Electromechanical Double-Rotor Compound Hybrid Transmissions for Hybrid Electric Vehicles," *IEEE Transactions on Vehicular Technology*, vol. 65, no. 6, pp. 4687–4699, 2016.
- [85] A. Flah, I. A. Khan, A. Agarwal, L. Sbita, and M. G. Simoes, "Field-oriented control strategy for double-stator single-rotor and double-rotor single-stator permanent magnet machine: Design and operation," *Computers and Electrical Engineering*, vol. 90, p. 106953, 2021.

## BIBLIOGRAPHY

- [86] L. Cinti, D. Michieletto, N. Bianchi, and M. Bertoluzzo, "A Comparison between Hybrid Excitation and Interior Permanent Magnet Motors," in *2021 IEEE Workshop on Electrical Machines Design, Control and Diagnosis (WEMDCD)*, pp. 10–15, 2021.
- [87] F. Giulii Capponi, G. De Donato, G. Borocci, and F. Caricchi, "Axial-Flux Hybrid-Excitation Synchronous Machine: Analysis, Design, and Experimental Evaluation," *IEEE Transactions on Industry Applications*, vol. 50, no. 5, pp. 3173–3184, 2014.
- [88] A. Pelizari and I. E. Chabu, "FEM analysis of a non-conventional axial flux hybrid excitation motor under flux weakening operation for electric vehicle purpose," in *2015 International Conference on Electrical Systems for Aircraft, Railway, Ship Propulsion and Road Vehicles (ESARS)*, pp. 1–6, 2015.
- [89] D. Lusignani, D. Barater, G. Franceschini, G. Buticchi, M. Galea, and C. Gerada, "A high-speed electric drive for the more electric engine," in *2015 IEEE Energy Conversion Congress and Exposition (ECCE)*, pp. 4004–4011, 2015.
- [90] E. Gurpinar, D. De, A. Castellazzi, D. Barater, G. Buticchi, and G. Franceschini, "Performance analysis of SiC MOSFET based 3-level ANPC grid-connected inverter with novel modulation scheme," in *2014 IEEE 15th Workshop on Control and Modeling for Power Electronics (COMPEL)*, pp. 1–7, 2014.
- [91] Z. Zeng, Z. Li, and S. M. Goetz, "A High Performance Interleaved Discontinuous PWM Strategy for Two Paralleled Three-Phase Inverter," *IEEE Transactions on Power Electronics*, vol. 35, no. 12, pp. 13042–13052, 2020.
- [92] F. Savi, D. Barater, M. D. Nardo, M. Degano, C. Gerada, P. Wheeler, and G. Buticchi, "High-Speed Electric Drives: A Step Towards System Design," *IEEE Open Journal of the Industrial Electronics Society*, vol. 1, pp. 10–21, 2020.
- [93] X. Han, D. Jiang, T. Zou, R. Qu, and K. Yang, "Two-Segment Three-Phase PMSM Drive With Carrier Phase-Shift PWM for Torque Ripple and Vibration Reduction," *IEEE Transactions on Power Electronics*, vol. 34, no. 1, pp. 588–599, 2019.
- [94] L. Zhang, X. Hu, Z. Wang, J. Ruan, C. Ma, Z. Song, D. G. Dorrell, and M. G. Pecht, "Hybrid electrochemical energy storage systems: An overview for smart grid and electrified vehicle applications," *Renewable and Sustainable Energy Reviews*, vol. 139, p. 110581, 2021.

- [95] M. Mattetti, M. Maraldi, N. Lenzini, S. Fiorati, E. Sereni, and G. Molari, "Outlining the mission profile of agricultural tractors through CAN-BUS data analytics," *Computers and Electronics in Agriculture*, vol. 184, p. 106078, 2021.
- [96] D. Troncon, L. Alberti, and M. Matteti, "A Feasibility Study for Agriculture Tractors Electrification: Duty Cycles Simulation and Consumption Comparison," in *IEEE Transportation Electrification Conference and Expo (ITEC)*, 2019.
- [97] M. Mattetti, M. Maraldi, E. Sedoni, and G. Molari, "Optimal criteria for durability test of stepped transmissions of agricultural tractors," *Biosystems Engineering*, vol. 178, pp. 145–155, 2019.
- [98] M. Dalboni, P. Santarelli, P. Patroncini, A. Soldati, C. Concari, and D. Lusignani, "Electrification of a Compact Agricultural Tractor: A Successful Case Study," in *2019 IEEE Transportation Electrification Conference and Expo (ITEC)*, 2019.
- [99] P. Dekraker, J. Kargul, A. Moskalik, K. Newman, M. Doorlag, and D. Barba, "Fleet-level modeling of real world factors influencing greenhouse gas emission simulation in ALPHA," *SAE International Journal of Fuels and Lubricants*, vol. 10, pp. 217–235, mar 2017.
- [100] D. Barater, G. Buticchi, C. Concari, G. Franceschini, E. Gurpinar, D. De, and A. Castellazzi, "Performance analysis of unitl-h6 inverter with sic mosfets," in *2014 International Power Electronics Conference (IPEC-Hiroshima 2014 - ECCE ASIA)*, pp. 433–439, 2014.
- [101] E. Schaltz, "Electrical vehicle design and modeling," in *Electric Vehicles* (S. Soylu, ed.), ch. 1, Rijeka: IntechOpen, 2011.
- [102] R. Hickey and T. M. Jahns, "Direct comparison of state-of-charge and state-of-energy metrics for li-ion battery energy storage," in *2019 IEEE Energy Conversion Congress and Exposition (ECCE)*, pp. 2466–2470, 2019.
- [103] C. Moretti, A. Moro, R. Edwards, M. V. Rocco, and E. Colombo, "Analysis of standard and innovative methods for allocating upstream and refinery ghg emissions to oil products," *Applied Energy*, vol. 206, pp. 372–381, 2017.
- [104] M. Prussi, M. Yugo, L. De Prada, M. Padella, R. Edwards, and L. Lonza, *JEC well-to-tank report v5*. Publications Office of the European Union, 2020.
- [105] E. Emilsson and L. Dahllöf, "Lithium-ion vehicle battery production status 2019 on energy use, co 2 emissions, use of metals, products environmental footprint, and recycling," tech. rep., Nov. 2019.

## BIBLIOGRAPHY

- [106] J. Flint, D. Zhang, and P. Xu, "Preliminary Market Analysis for a New Hybrid Electric Farm Tractor," in *Proceedings of the 2014 International Conference on Global Economy, Commerce and Service Science*, 2014.
- [107] M. Wolbert-Haverkamp and O. Musshoff, "Is short rotation coppice economically interesting? an application to germany," *Agroforestry Systems*, vol. 88, no. 3, pp. 413–426, 2014.
- [108] O. Musshoff, "Growing short rotation coppice on agricultural land in germany: A real options approach," *Biomass and Bioenergy*, vol. 41, pp. 73–85, 2012.
- [109] H. Gao and J. Xue, "Modeling and economic assessment of electric transformation of agricultural tractors fueled with diesel," *Sustainable Energy Technologies and Assessments*, 2020.
- [110] "Electrical and electronics technical team roadmap," tech. rep., Oct. 2017.
- [111] J. Goss, M. Popescu, and D. Staton, "A comparison of an interior permanent magnet and copper rotor induction motor in a hybrid electric vehicle application," in *2013 International Electric Machines Drives Conference*, pp. 220–225, 2013.
- [112] D. K. Murugesan and I. Manickam, "Reliability and cost analysis of different power inverter topologies in electric vehicles," in *2015 IEEE Transportation Electrification Conference and Expo (ITEC)*, pp. 1–4, 2015.
- [113] G. Molari, M. Mattetti, N. Lenzini, and S. Fiorati, "An updated methodology to analyse the idling of agricultural tractors," *Biosystems Engineering*, vol. 187, pp. 160–170, 2019.
- [114] "Prezzi e tariffe." [arera.it](http://arera.it), Accessed August, 2021.
- [115] H. Löbberding, S. Wessel, C. Offermanns, M. Kehrler, J. Rother, H. Heimes, and A. Kampker, "From Cell to Battery System in BEVs: Analysis of System Packing Efficiency and Cell Types," *World Electric Vehicle Journal*, vol. 11, no. 4, 2020.
- [116] J. Gyselinck, P. Dular, C. Geuzaine, and W. Legros, "Harmonic-balance finite-element modeling of electromagnetic devices: a novel approach," *IEEE Transactions on Magnetics*, vol. 38, no. 2, pp. 521–524, 2002.
- [117] I. Wolff, "Finite difference time-domain simulation of electromagnetic fields and microwave circuits," *International Journal of Numerical Modelling: Electronic Networks, Devices and Fields*, vol. 5, no. 3, pp. 163–182, 1992.

- [118] M.-L. Henkel, F. Kasolis, S. Schöps, and M. Clemens, "A comparative study on electromagnetic quasistatic time-domain field calculations," *International Journal of Numerical Modelling: Electronic Networks, Devices and Fields*, vol. 36, no. 3, p. e3049, 2023.
- [119] D. Kuzmin, M. Möller, and S. Turek, "Multidimensional FEM-FCT schemes for arbitrary time stepping," *International Journal for Numerical Methods in Fluids*, vol. 42, no. 3, pp. 265–295, 2003.
- [120] Y. Kano, K. Watanabe, T. Kosaka, and N. Matsui, "A new modeling approach for circuit-field-coupled time-stepping electromagnetic analysis of saturated interior permanent magnet synchronous motors," *Electrical Engineering in Japan*, vol. 174, no. 1, pp. 49–58, 2011.
- [121] X. Cui, F. Yang, and M. Gao, "Improved local time-stepping algorithm for leap-frog discontinuous Galerkin time-domain method," *IET Microwaves, Antennas & Propagation*, vol. 12, no. 6, pp. 963–971, 2018.
- [122] K. Yamazaki, "Stray load loss analysis of induction motors due to harmonic electromagnetic fields of stator and rotor," *European Transactions on Electrical Power*, vol. 15, no. 3, pp. 299–310, 2005.
- [123] R. V. Sabariego and J. Gyselinck, "Eddy-Current-Effect Homogenization of Windings in Harmonic-Balance Finite-Element Models," *IEEE Transactions on Magnetics*, vol. 53, no. 6, pp. 1–4, 2017.
- [124] R. V. Sabariego, K. Niyomsatian, and J. Gyselinck, "Eddy-Current-Effect Homogenization of Windings in Harmonic-Balance Finite-Element Models Coupled to Nonlinear Circuits," *IEEE Transactions on Magnetics*, vol. 54, no. 3, pp. 1–4, 2018.
- [125] J. Lu, S. Yamada, and K. Bessho, "Harmonic balance finite element method taking account of external circuits and motion," *IEEE Transactions on Magnetics*, vol. 27, no. 5, pp. 4024–4027, 1991.
- [126] S. Yamada and K. Bessho, "Harmonic field calculation by the combination of finite element analysis and harmonic balance method," *IEEE Transactions on Magnetics*, vol. 24, no. 6, pp. 2588–2590, 1988.
- [127] I. S. Petukhov, "Harmonic Balance Method and Convergence of the 2-D Nonlinear Eddy Current Problem," 2019 IEEE 39th International Conference on Electronics and Nanotechnology (ELNANO), pp. 185–190, 2019.
- [128] W. Yao, J.-M. Jin, and P. T. Krein, "A 3D finite element analysis of large-scale nonlinear dynamic electromagnetic problems by harmonic balancing and domain decomposition," *International Journal of Numerical*

## BIBLIOGRAPHY

- Modelling: Electronic Networks, Devices and Fields*, vol. 29, no. 2, pp. 166–180, 2016.
- [129] X. Zhao, Y. Cao, and J. Lu, “Computation and Analysis of Power System Connected to Distributed Generation Based on Harmonic Balance Method,” 2020 International Conference on Smart Grids and Energy Systems (SGES), pp. 7–11, 2020.
- [130] C. Dalle, “Harmonic balance method applied to the numerical electrical physical modelling of two-terminal, non-linear microwave circuits in the frequency domain,” *International Journal of Numerical Modelling: Electronic Networks, Devices and Fields*, vol. 7, no. 4, pp. 253–265, 1994.
- [131] X. Zhao, J. Lu, and A. Seagir, “Harmonic Balance Method and Its Application in Electrical Power and Renewable Energy Systems,” 2021 IEEE PES Innovative Smart Grid Technologies - Asia (ISGT Asia), pp. 1–5, 2021.
- [132] J. Gyselinck, L. Vandeveldel, P. Dular, C. Geuzaine, and W. Legros, “A general method for the frequency domain FE modeling of rotating electromagnetic devices,” *IEEE Transactions on Magnetics*, vol. 39, no. 3, pp. 1147–1150, 2003.
- [133] J. Gyselinck, P. Dular, L. Vandeveldel, J. Melkebeek, A. M. Oliveira, and P. Kuo-Peng, “Two-dimensional harmonic balance finite element modelling of electrical machines taking motion into account,” *COMPEL: The International Journal for Computation and Mathematics in Electrical and Electronic Engineering*, vol. 22, pp. 1021–1036, 12 2003.
- [134] J. Lu and X. Chui, “Harmonic Analysis of HVDC Transformer using Harmonic Balance - Finite Element Method (HB-FEM),” 2007 International Symposium on Electromagnetic Compatibility, pp. 92–95, 2007.
- [135] J. H. Wang, X. F. Wang, and Y. H. Song, “Study of parameters of a tripler using the finite element method of harmonic balance,” *IEEE Transactions on Power Delivery*, vol. 20, no. 2, pp. 789–794, 2005.
- [136] C. Geuzaine and J.-F. Remacle, “Gmsh: A 3-D finite element mesh generator with built-in pre- and post-processing facilities,” *International Journal for Numerical Methods in Engineering*, vol. 79, no. 11, pp. 1309–1331, 2009.
- [137] P. Dular, C. Geuzaine, F. Henrotte, and W. Legros, “A general environment for the treatment of discrete problems and its application to the finite element method,” *IEEE Transactions on Magnetics*, vol. 34, no. 5, pp. 3395–3398, 1998.



## BIBLIOGRAPHY

- [138] S. Yamada, K. Bessho, and J. Lu, "Harmonic balance finite element method applied to nonlinear AC magnetic analysis," *IEEE Transactions on Magnetics*, vol. 25, no. 4, pp. 2971–2973, 1989.



## ACKNOWLEDGEMENT

---

This thesis is the end of a journey started eight years ago at University of Padova, the final chapter of a very important part of my life. Many people helped me during these years, and to thank all of them would require another chapter, which I definitely don't want to write. So, if you were with me even during a small period of my studies, and you are not mentioned below, or you don't feel properly thanked, please, consider your support valued and your friendship reciprocated: thanks for your valuable time with me.

The biggest thanks goes to my parents, Sabina and Andrea, whose invaluable support cannot be measured by common means, whose efforts I will never stop trying to deserve and give back. A huge thanks to my sister Sara, who gave me precious advice for my personal growth through her experience, and spent many hours helping me improve my English. Thanks to all my relatives that supported me during these years.

Thanks to all my friends, with whom I made amazing adventures and spent many joyful beers-and-cheers nights: my long-life friends, *La Compagnia dell'Olmo*, Mattia, Filippo, Elia, Federico, Matteo; my high school friends Edoardo, Lorenzo, Riccardo, Carlo, Damiano, Benedetta, Valentina; all my new friends, *The Wonderful People*, who are too many and too nice to be listed here; my mountain friends, Marco, Fabio and Silvia, with whom I have spent many weekends into the wild to recharge my mind energies (escaping engineering burn-out). Thanks to Chiara, who helped me through one of the toughest periods of my life and made me discover joy and love.

Thanks to all my colleagues from EDLab and Belgium, who have been very important for my professional and personal growth: my supervisor Luigi, who gave me life-changing opportunities, valuable professional advice and good time out of work; Nicola, for his precious tips; Ludovico, for his commitment to research, teaching and team-building, which I consider an example for younger researchers; Mosé, for his outstanding technical experience and funny monologues; Diego, for his precious help during my master thesis and first year of PhD; Matteo, with whom I worked together in many projects; Daniele, for his insights and critical thinking; Luca, Chiara and Alice for all the coffee breaks, happy moments together and fights; Ruth and Johan, for their precious supervision of my research and teaching activities during my period abroad, and their kindness out of the work sphere; Elma, who has been a very kind friend as well as a formidable colleague when I was in Bruxelles.

Last but not least, a special thanks to my friend and colleague Giuseppe, with whom I shared a big part of this long experience, studying and working hard together, facing challenges, enjoying travels, being each other's wingman. Thanks for this eight-year journey together.